METAL NANOPARTICLE MODIFIED POLYSULFONE MEMBRANE FOR WATER TREATMENT

By

LISEBO PHELANE

A thesis submitted in fulfilment of the requirements for the degree of Magister Scientiae in the Department of Chemistry, University of Western Cape.

Supervisor: Prof Priscilla Baker

May, 2013

KEYWORDS

Polysulfone (PSF)

Fouling

Hydrophilicity

Hydrophobicity

Silver nanoparticles (AgNPs)

Cobalt nanoparticles (CoNPs)

Nickel nanoparticles (NiNPs)

Organic acids

Cyclic Voltammetry (CV)

Square Wave Voltammetry (SWV)

Electrochemical Impedance Spectroscopy (EIS)

Coercivitity

Hexagonal closed packed (hcp)

Face center cubic (fcc)

ABSTRACT

Membrane separation processes have been widely applied in the treatment of wastewater with polysulfone (PSF) polymer membrane being the most frequently used in ultrafiltration of wastewater due to its chemical and structural stability and mechanical robustness. The disadvantage to these membranes is their hydrophobicity which leads to membrane fouling caused by organic pollutants in water. Many studies have been conducted to increase the hydrophilic properties of the polysulfone membrane surface. Most recently metal oxide nanoparticles have been introduced to the polymer matrix in order to reduce membrane fouling and increase its hydrophilicity with measurable success. Natural organic matters are the one of the major fouling agents during ultrafiltration, reverse osmosis and microfiltration. Two organic acids (Tannic Acid and Alginic Acid) were selected to test the fouling behaviour of nanometallic synthesised polysulfone membranes

For this study, polysulfone casting suspension was prepared by dissolving polysulfone beads in N,N-dimethly acetamide. Three metallic nanoparticles of Silver, Cobalt and Nickel were selected to improve the hydrophilicity of the polysulfone membrane. The metal nanoparticles were prepared using the chemical reduction method. Cobalt nanoparticles were synthesized by dissolving the cobalt chloride salt in deionized water and reduced with sodium borohydride at room temperature. The nickel chloride salt was dissolved in ethanol and reduced with sodium borohydride under magnetic stirrer. Silver nanoparticles were prepared by dissolving the silver nitrate in deionised water and heated to boil, the sodium citrate was added to reduced the silver nitrate. These nanoparticles were then integrated into the polysulfone polymer matrix to form the metal nanoparticle polysulfone nanocomposites. This study focused on four prepared polysulfone nanocomposite membrane; 1 unmodified polysulfone (PSF), 2 polysulfone modified with cobalt nanoparticles (PSF/Co), 3 polysulfone

modified with nickel nanoparticles (PSF/Ni) and 4 polysulfone modified with silver nanoparticles (PSF/Ag).

The prepared metallic nanoparticles were characterized using the microscopic techniques such as the high-resolution transmission electron microscope (HR-TEM), scanning electron microscope (SEM), and energy diffractive x-ray (EDX). The prepared polysulfone nanocomposites were characterized using the SEM technique and for electrochemical characterisation of the prepared polysulfone nanocomposite the following techniques were used; cyclic voltammetry (CV), square wave voltammetry (SWV) and electrochemical impedance spectroscopy (EIS). The contact angle technique was also used to study the hydrophilicity of the prepared polysulfone membranes. The fouling behaviour of the polysulfone and metal nanoparticle modified polysulfone was evaluated for voltammetry and impedance data.

SEM, TEM and EDS were used to confirm the size of the metal nanoparticles to be in the nanometer range. The SEM images of the modified polysulfone thin film showed porous structures compared to unmodified polysulfone. The polysulfone modified with cobalt nanoparticles (PSF/Co) was found to be the most hydrophilic nanocomposite because it measured the lowest contact angle value of 31.7°. The polysulfone modified with cobalt nanoparticles showed highest sensitivity for both the tannic acid ($3.06x10^{-5}$) and alginic acid ($4.46x10^{-5}$) as indicated by the slopes of the calibration curve. However, the polysulfone modified with nickel nanoparticles (PSF/Ni) showed better performance for the quantitative detection of alginic acid and tannic acid. The PSF/Ni showed the longest cut-off time than other modified polysulfone and the unmodified polysulfone showed the least cut-off time.

DECLARATION

I declare that *Metal nanoparticle modified Polysulfone membrane for water treatment* is my own work, that it has not been submitted for any degree or examination in any other university, and that all sources I have used or quoted have been indicated and acknowledged by means of complete references.

Lisebo Phelane May 2013

Signed……..

ACKNOWLEDGEMENTS

Firstly, I would like to thank God Almighty for his love, strength, patience and wisdom; He has given me to be able to complete this work

To my supervisors, Professor Priscilla G.L Baker and Professor Emmanuel Iwuoha, a big thank you for the opportunity you gave me, your excellent supervision, support and encouragement during the course of this work.

To the researchers in SensorLab, I thank you for welcoming me, helping me academically and your support throughout.

To my family, my father Thabang Phelane, mother Tlalane Phelane, Ntsoaki Phelane, Mamorena Phelane, Nthabiseng Phelane, Mamokete Phelane and Thabiso Phelane. I would like to take this opportunity to thank you for your love, support, care, upbringing and prayers.

Lastly to my baby boy Reitumetse Mokete Phelane, a big thanks.

DEDICATION

This project is dedicated to

My son

Mokete Reitumetse Phelane

And

My late grandmother

Lawukazi Mketsu Phelane

TABLE OF CONTENTS

Title page *i*

Keywords *ii*

Abstract *iii*

Declaration *v*

Acknowledgement *vi*

Dedication *vii*

Table of content *viii*

List of figures *xii*

List of tables *xvii*

Abbreviation *xviii*

Chapter 1

1.1 Metal modified Polysulfone 4

1.2 Water Treatment Membranes 6

1.3 Fouling caused by Natural Organic Matter 8

1.4 Model Organic Acid 9

1.5 Aims and Objectives of the study 19

1.6 Conceptual Diagram 21

1.7 Thesis scope 22

Chapter 2

2.1 Cyclic Voltammetry 23

2.2 Electrochemical Impedance Spectroscopy 25

2.3 Contact Angle 27

2.4 Electron microscopy 29

2.4.1Transmission Electron Microscopy 29

2.4.2 Scanning Electron Microscopy 30

2.5 Atomic Force microscopy 32

2.6 RAMAN 35

2.7 Instrumentation 37

2.7.1 Electrochemical measurement 37

2.7.2 Scanning Electron Microscopy 37

2.7.3 Transmission Electron Microscopy 38

2.7.4 Contact Angle Instruments 38

2.7.5 Raman Spectroscopy 38

2.7.6 Atomic Force Microscopy 38

2.8 Reagents and Materials 39

Chapter 3

3.1 Preparation of Polysulfone thin film 40

3.2 Synthesis of Nanoparticles 41

3.2.1Synthesis of Co nanoparticles 41

3.2.2 Synthesis of Ni nanoparticles 45

3.2.3 Synthesis of Ag nanoparticles 49

3.3 Preparation of nanocomposite thin film 53

3.3.1 Preparation of nanocomposite film (Co, Ni, Ag) 53

3.4 Characterisation of the prepared thin films 53

3.4.1 Scanning Electron Microscopy 53

3.5 Atomic Force Microscopy 60

3.6 RAMAN Results 60

3.7 Electrochemical Characterisation 63

3.7.1 Cyclic Voltammetry 63

Chapter 4

4.1 Cyclic Voltammetry 66

4.2 Square Wave Voltammetry 67

4.3 Calibration curves 82

Chapter 5

5.1 Electrochemical impedance spectroscopy 89

Chapter 6

6.1 Conclusion 102

6.2 Future Work 104

References 105

LIST OF FIGURES

FIGURE	TITLE	Page
1.1	Chemical structure of humic acid	10
1.2	Chemical structure of tannic acid	14
1.3	Chemical structure of alginic acid	17
2.1	Electrochemical cell with the electrode	24
2.2	CV showing the voltage vs the current	25
2.3	Randles equivalent circuit used for data fitting	27
2.4	Contact angle formed when water droplet meets the solid surface	27
2.5	A schematic representation of TEM	30
2.6	A schematic representation of SEM.	28
2.7	A schematic representation of contact mode AFM	31
2.8	A schematic representation of non-contact mode AFM	34
2.9	A schematic of the Stokes and Anti-Stokes shift	37
3.1	SEM image of the polysulfone	40
3.2	EDS spectra of the polysulfone	41
3.3	UV-vis spectra of Co nanoparticle	42
3.4	HR-TEM image of the Co nanoparticles.	43

3.5	EDX spectrum of the Co nanoparticles	44
3.6	SEM image Co nanoparticles	45
3.7	UV-vis of Ni nanoparticles	46
3.8	HR-TEM of the Nickel nanoparticles	47
3.9	EDX spectrum of Ni nanoparticles	48
3.10	SEM image of Ni nanoparticle	49
3.11	UV-VIS of AgNPs	50
3.12	HR-TEM image of the Ag nanoparticles	51
3.13	EDX spectrum of the Ag nanoparticles	52
3.14	SEM image of Ag nanoparticles	52
3.15	SEM image of the Polysulfone with Cobalt nanoparticles	54
3.16	EDS spectrum of PSF modified with Co nanoparticles	55
3.17	SEM image of Polysulfone with Ni nanoparticles	55
3.18	EDS spectrum of Polysulfone with Ni nanoparticles	56
3.19	SEM image of PSF modified with Ag nanoparticles	56
3.20	EDX spectrum of PSF modified with Ag nanoparticles	57
3.21	Raman spectrum for PSF	60
3.22	Raman spectrum of PSF/Co	61
3.23	Raman spectrum of PSF/Ni	62

3.24	Raman spectrum of PSF/Ag	62
3.25	CV of PSF unmodified membrane, modified polysulfone with metal nanoparticles and the Bare Pt electrode	64
4.1	Reaction Mechanism of polyphenols with Pt electrode	66
4.2	CV of a bare Pt electrode (black) overlayed with Pt/PSF modified electrode (red).	67
4.3	CV of Bare Pt at different scan rates (A). (B)CV of Pt/PSF modified electrode at different scan rate.	68
4.4	Concentration dependant SWV of PSF in the presence of alginic acid , (a) oxidation SWV and (b) reduction SWV.	70
4.5	Concentration dependant SWV of PSF in the presence of tannic acid (a) oxidation SWV and (b) reduction SWV	71
4.6	Concentration dependant SWV of PSF/Co in the presence of tannic acid (a) oxidation SWV and (b) reduction SWV	73
4.7	Concentration dependant SWV of PSF/Co in the presence of alginic acid, (a) oxidation SWV and (b) reduction SWV	74
4.8	Concentration dependant SWV of PSF/Ni in the presence of alginic acid	75
4.9	Concentration dependant SWV of PSF/Ni in the presence of tannic acid, (a) oxidation SWV and (b) reduction SWV	77

4.10	Concentration dependant SWV of PSF/Ag in the presence of tannic acid, (a) oxidation SWV and (b) reduction SWV.	78
4.11	Concentration dependant SWV of PSF/Ag in the presence of alginic acid	80
4.12	Calibration curves (A) Pt/PSF at different concentrations of tannic acid, (B) Pt/PSF at different concentration of alginic acid	83
4.13	Calibration Curves; (a) Pt/PSF/Ag, (b) Pt/PSF/Co (c) Pt/PSF/Ni in the presence of tannic acid.	84
4.14	Calibration Curves; (a) Pt/PSF/Ag (b) Pt/PSF/Co (c) Pt/PSF/Ni in the presence of alginic acid	86
5.1	Fixed frequency EIS studies for Pt/PSF in the presence of 0.11 M alginic acid and 0.11 M tannic acid	90
5.2	Fixed frequency EIS studies for PSF/Co in the presence of 0.11 M alginic acid and 0.11 M tannic acid	92
5.3	Fixed frequency EIS studies for PSF/Ni in the presence of 0.11 M alginic acid and 0.11 M tannic acid	93
5.4	Randles circuit	96
5.5	EIS plot of (A) PSF,(B) PSF/Co,(C) PSF/Ni and (D) PSF/Ag in the presence of tannic acid	96
5.6	EIS plot of (A) PSF, (B) PSF/Co, (C) PSF/Ni and (D) PSF/Ag in the presence of alginic acid	97

5.7	Rct plot of alginic acid at the thin films	98
5.8	Rct plot of tannic acid at the thin films	99
5.9	Caps plot of PSF, PSF/Co, PSF/Ni and PSF/Ag in the presence of (A) alginic acid and (B) tannic acid	100
5.10	Phase angle plot of PSF, PSF/Co, PSF/Ni and PSF/Ag in the presence of (A) alginic acid and (B) tannic acid	101

LIST OF TABLES

TABLE	TITLE	Page
Table 3.1	table of particle size, pore size of the modified membrane and lattice constant of the nanoparticle	58
Table 3.2	Contact angle measurements of the polysulfone membrane unmodified and the modified polysulfones with the standard deviation.	59
Table3.3	Table of results showing the diffusion coefficient and the Formal potential	65
Table 4.1	Diffusion Coefficients of PSF, PSF/Co, PSF/Ni and PSF/Ag in alginic acid and tannic acid.	81
Table4.2	Dynamic linear range of tannic acid and alginic acid at PSF, PSF/Co, PSF/Ag and PSF/Ni	87
Table5.1	Table of result of polysulfone thin films prepared in the presence of alginic acid and tannic acid	95

ABBREVIATIONS

AFM	Atomic force microscopy
Al_2O_3	Aluminium oxide
ATP	Adenosine triphosphate
Ca	Calcium
CA	Cellulose acetate
CAP	Cellulose acetate phthalate
CNT	Carbon nanotube
CTAB	Cetyl trimethyl ammonium bromide
CV	Cyclic voltammetry
DBP	Dibutyl phthalate
DDA	Dodecylamine
DNA	Deoxyribonucleic acid
EDS	Energy dispersive spectroscopy
EIS	Electrochemical impedance spectroscopy
Fcc	face center cube
Fe	Iron

FTIR	Fourier transform infrared spectroscopy
HA	Humic acid
Hcp	Hexagonal centre cubic
Mg	Magnesium
NMP	1-methyl-2-pyrolidone
NOM	Natural organic acid
NTA	Nitrilo triacetic acid
PES	Polyethersulfone
PMHS	Polymethyl hydrosiloxane
PSF	Polysulfone
PVA	Polyvinyl alcohol
PVP	Polyvinyl pyrolidone
SEM	Scanning electron microscopy
SPS	Sulfonated polysulfone
SPSB	Blended sulfonated polysulfone
SWV	Square wave voltammetry
TA	Tannic acid
TiO_2	Titanium oxide
ZrO_3	Zirconium oxide

Chapter 1

This chapter gives an introduction and the literature on polysulfone and metal modified polysulfone membranes

Water pollution is one of the major environmental problems in the world. Many techniques are used for the treatment of polluted water; methods such as the precipitation by chemical agent, the adsorption on activated carbon, the ion-exchange on resins and the membrane processes (ultra- and nanofiltration, reverse osmosis and electro membrane processes) are used. A membrane is a thin layer of semi-permeable material that separates substances when a force is applied across the membrane. Membrane processes are increasingly used for removal of bacteria, microorganisms, particulates, and natural organic material, which can impart colour, tastes, and odours to water and react with disinfectants to form disinfection by-products. There are different membrane processes namely microfiltration (MF), ultrafiltration (UF), nanofiltration (NF), and reverse osmosis (RO). Nanofiltration is a membrane filtration process for the removal of disinfection by-product precursors such as natural organic matter and heavy metals with the pore size of 0.001 micron. Ultrafiltration technique uses membranes with the pore sizes in the range of 0.1 to 0.001 micron and is used for the removal of high molecular-weight substances, and organic polymeric molecules. Microfiltration uses membranes with a pore size of approximately 0.03 to 10 microns.

A major challenge to these operations is the membrane fouling by proteins and other biomolecules in the feed stream. There are many factors contributing to fouling such as surface properties, hydrodynamic conditions, ionic strength and solute concentration. The extent of adsorption depends on the types of solute macromolecules. Fouling results in flux decline, which increases the energy demand for filtration. Fouling can occur in two ways:

cake fouling is generally reversible by water flushing or back washing and fouling due to the adsorption of foulants is essentially irreversible and can only be counteracted to a certain extent by aggressive chemical cleaning (Asatekin A., Kangb S, *et al, 2005*). Membranes are cleaned to remove foulants adsorbed however when cleaning becomes ineffective then the membrane must be replaced (Goosen A, Sablani S, Ai-Hinai H, *et al,2004)*. Membranes that resist fouling are the most important solution leading to more feasible ultrafiltration membrane process and more affordable clean water (Asatekin A., Kangb S, *et al, 2005*).

Polysulfone is one of the most frequently used polymers in the production of ultrafiltration and microfiltration membranes due to its properties (Castro Vidaurre E., Achete C.*et al, 2002)*. The properties of polysulfone are thermal high resistance, good mechanical and chemical stabilities and its film-forming properties (Summers G., Ndawuni M *et al, 2001)*. Polysulfone membranes are often used as sublayers in composite membrane for reverse osmosis, gas separation and pervaporation. However, the hydrophobic nature of polysulfone is prone to membrane fouling which shortens membrane life (Aryanti *et al, 2013*). Modification of the membrane may be done to improve its hydrophilicity. Hydrophilicity is the tendency of a surface to become wet or to absorb water. The technique of modification normally involves the use of hydrophilic polymers or copolymers, blending of hydrophilic or change polymers with hydrophobic polymers, grafting of polymers and the surface modification of the membrane itself (Chowdhury *et al., 2001)*.

In 2006 Chenamsetty and fellow researchers modified the sulfonated polysulfone by ion-beam irradiation. The charge modified the surface morphology of the membrane and also decreases the negative charge of the membrane. Using FTIR and AFM, it was concluded that fouling of the modified membrane was significant less severe than that of virgin membrane. Ion-beam irradiation was observed to be an effective membrane modification technique (Chenamsetty R. *et a.l, 2006)*.

In 2004 Zhao, modified the PSF membrane using DNA and prepared the porous PSF beads using a liquid-liquid phase separation technique. The hydrophilicity of the membrane modified increased and that the DNA-immobilized PSF beads have the potential to be used in environmental applications. The surface of polysulfone membrane was changed from hydrophobic to hydrophilic by oxygen plasma treatment. Thus, oxygen plasma treatment of polysulfone reduced the fouling and increased the flux of polysulfone membrane in the waste treatment because of the hydrophilicity of oxygen plasma treated membrane and charge repulsion between the oxygen plasma treated membrane and the gelatin molecules (Kim *et al.,* 2002).).

Another study focused on infusing PSF with carbon nanotube, with PVA as a barrier layer. From the results that were obtained (Iyuke *et al., 2013*); the SEM image of the PSF without the CNT addition showed to be highly porous with pores less than 10 microns. The image of the PSF with CNT showed some changes to the way the structure appeared before the addition. The pores of the membrane were seen to be more numerous and more finely dispersed. In 2013, Aryati and colleagues investigated the influence of the concentration of acetone as non-solvent on polysulfone membrane performance. The aim of the study was to obtain high selectivity and low fouling of polysulfone ultrafiltration membrane. The membrane was prepared by dissolving polysulfone in N, N - dimethyl acetamide mixed with polyethylene glycol (PEG) and different concentrations of acetone. It was found that addition of both PEG and acetone into membrane solution improved membrane performance. The increase of PEG concentration contributed to the increase of membrane hydrophilicity (Aryati *et al., 2013*).

Two types of sulfonated polysulfone membrane were applied for ultrafiltration removal of humic substances and metal ion admixtures from aqueous solutions. The membranes were formed from 20% polymer solution by phase inversion of sulfonated polysulfone (SPS20)

and its blend with polysulfone (SPSB/50) was prepared. It was found that ultrafiltration membranes made of polysulfone can be used effectively in the removal of humic substances from water. The increase of sulfone group content in polymeric matrix limited the occurrence of fouling, which contributed to the increase of effectiveness of the process (Kabsch-Korbutowicz *et al, 1994*). A was study was done focusing on modifying the polysulfone with polyaniline (Alam *et al., 2012*). The aim of the study was to investigate the improvements in modified membrane. Polyaniline was synthesized by chemical polymerization of aniline. Modified polysulfone with polyaniline nanocomposites was synthesized by solution blending with NMP. It was found that polyaniline increased the separation characteristics and also altered the membrane morphology and surface roughness. Therefore, the inclusion of polyaniline nanoparticles in the polysulfone showed a significant effect on hydrophilic property which induced the improvement of permeability characteristic of polysulfone membrane (Alam *et al., 2012*)

1.1 Metal Modified Polysulfone

Blending the PSF with metal nanoparticles has attracted many research studies due to the advantage offered. The membrane filtration research studies focused on the following metals TiO_2, Al_2O_3 and ZrO_2 for waste water treatment. Studies have been conducted focusing on TiO_2 for water treatment, a study that was done by Li *et al* (2005), showed that water flux through a polyethersulfone-TiO_2 the membrane was enhanced (Kim *et al,2010*). Most recent investigation for water filtration focused on Al_2O_3/PES and ZrO_3/PES membranes (Maximous *et al, 2010*). Zirconia (ZrO_3) membranes are known to be chemically more stable than titania (TiO_2) and alumina (Al_2O_3) membranes and that they are more suitable for liquid phase inversion applications. The membrane strength of PES casting suspension was enhanced by the addition of zirconia nanoparticles.

In 2005, T-H Bae, did a study which focused on three different polymer, polysulfone (PSF), polyvinylidenefluoride (PVDF) and polyacrylonitrile (PAN), were membrane material. The aim of the study was to investigate the fouling mitigation effect of TiO_2 immobilized UF membranes during the activated sludge filtration. Two types of TiO_2 immobilized ultrafiltration membranes (TiO_2 entrapped and deposited membranes) were prepared and applied to the polymers in order to evaluate their fouling mitigation effect. Addition of the TiO_2 changed membranes characteristic the membrane were more porous and showed lower flux decline compared to neat polymeric membrane. Fouling mitigation effect increased with nanoparticle content. Membrane fouling was reduced by TiO_2 nanoparticles regardless of polymeric materials used (T-H Bae, T-M Tak *et al., 2005*). A study was done investigating four different nanoparticles (TiO_2, SiO_2, ZnO and ZrO_2) were dispersed in a polyethersulfone (PES) casting solution. Different membranes were prepared: a pure PES membrane and four PES membranes that were modified with four different nanoparticles (TiO_2, SiO_2, ZnO, and ZrO_2). The composite membranes were then prepared from this casting solution via the phase inversion method. A study was done investigating four different nanoparticles (TiO_2, SiO_2, ZnO and ZrO_2) were dispersed in a polyethersulfone (PES) casting solution. Different membranes were prepared: a pure PES membrane and four PES membranes that were modified with four different nanoparticles (TiO_2, SiO_2, ZnO, and ZrO_2). The composite membranes were then prepared from this casting solution via the phase inversion method. The porosity in all the modified membranes was smaller than the pure PES membrane. Of the modified membranes, SiO_2 exhibited the smallest porosity, whereas ZrO_2 exhibited the largest, however SiO_2 fouled the least. The pure PES membrane had the greatest contact angle indicating that it was the most hydrophobic. This suggests that the modification with nanoparticles successfully did improve membrane hydrophilicity. From the flux decline, PES took the least amount of time to foul which indicates that the pure PES membrane fouled the

most easily. Surprisingly, ZnO took the second least amount of time to reach the third phase of flux reduction, therefore it fouled the second most easily. Both SiO_2 and TiO_2 both took the longest time to reach phase three (400 minutes), which indicates that they had they had the best anti-fouling performance. The SiO_2 membrane performed best in this experiment, because of its high initial pure water flux, high rejection rate, and superior antifouling performance (Sheppard, 2013).

Different characterization methods were used to characterize the nanocomposites. SEM was one of the tools used to indicate pore size, membrane thickness and surface morphology. The contact angle measurements were done to investigate the hydrophilic properties of the membrane. Evaluating the SEM results for the metal nanocomposite membranes indicated highly porous and asymmetric sponge-like structures. The morphology of the surface of the membrane showed an increase in the number of pores after modification with metal nanoparticles. The modification of the polymeric casting suspension with the metal nanoparticles increased the membrane porosity and also improved the membrane hydrophilicity (Richards H, 2012).

1.2 Water Treatment Membranes

Cellulose (CA) is a commonly used polymer for nanofiltration and reverse osmosis membranes. The properties of CA are; it is cheap, represent relatively good resistance against chlorinated agents. Cellulose membranes show significant hydrophilic property due to the active hydroxyls in each repeating structure of cellulose molecule (Li *et al, 2006*). Cellulose acetate and regenerated cellulose membranes have been widely applied in ultrafiltration, microfiltration and dialysis.

In 2010 Madaeni S.S, did a study on nano-silver embedded cellulose acetate membrane that was prepared using electro-less plating. The membranes were characterized using various

techniques, like SEM, EDS and contact angle. The SEM images showed the deposition of silver nanoparticles on the membrane pores and the EDS analyses proved the presence of silver nanoparticles in the modified membrane. The contact angle was measured for both the unmodified CA and modified CA. Increasing silver concentration leaded to an improvement in contact angle (Madaeni S.S, Akbarzadch T *et al., 2010*).

Saljoughi E and Mohammadi T. (2009), in their study they looked at the effect of parameters that were used and different asymmetric CA membranes were prepared from CA/PVP/NMP via immersion precipitation in coagulation water bath. The SEM images of the prepared membrane with increasing PVP concentration from 0 – 3 wt% caused the formation of macrovoids and more porous structures however, further increasing PVP from 3 – 6 wt% resulted in suppression of macrovoids and formation of denser structures (Saljoughi E. *et al., 2009).*

In 2013 Guezguez and fellow researchers coated the cellulose acetate with a mixture of polymethylhydrosiloxane (PMHS) and polydimethylsiloxane (PDMS) in order to improve water permeability. The contact angle decreased with decreasing PDMS concentration. The membranes that were coated with 30/70 concentration retained the smallest contact angle, showing that the membrane was the most hydrophilic. The pure water flux was used to determine membrane performance. The water flux decreased when membranes were covered by a thin layer of PMHS. Water fluxes are enhanced when the surface of CA membranes were coated by a mixture of PMHS-PDMS (Guezguez *et al., 2013*).

Polyethersulfone (PES) is a high-performance thermoplastic, with good mechanical properties, excellent thermal and chemical stability. PES has become the material of choice for membrane applications. The disadvantage of the PES is its hydrophobic nature. The PES was sulphonated to improve its hydrophilicity. Guan reported the findings of the sulphonated

PES studies. The contact angle of the unmodified PES was 75.9° but the contact angle decreased with the amount of sulphonation. When the degree of sulphonation 41.22% the contact angle was the smallest 36.6°, indicating that the hydrophilicity of the PES was improved (Guan *et al., 2005).*

The PES was blended with the cellulose acetate phthalate (CAP) to improve the hydrophilicity of the PES (Rahimpour A., Madaeni *et al, 2007*). Since the CAP is a hydrophilic polymer which is able to improve the hydrophobicity of the prepared membrane. In this work, CAP was added to the casting suspension in the presence of polyvinylpyrrolidone as pore former. The contact angle was measured to evaluate the changes in the hydrophilicity of the PES after blending with CAP. The contact angle when the composition of PES (60 wt %) and CAP was (40 wt %) the contact angle was 50.7°.

1.3 Fouling caused by Natural Organic Matter (NOM)

Membrane filtration processes are vulnerable to fouling. Natural organic matter are the major fouling agents during the membrane filtration processes. Organic matter consist of a wide range of compounds ranging from low to high molecular weight compounds and dissolved organic carbon. Compounds such as polysaccharides, proteins, humic and fulvic acid and organic acids are examples of the organic matter. Polysaccharides are produced during biological waste water treatment and they are part of the soluble microbial products. Alginic acid is a type of a polysaccharide produced by bacteria and algae, is made up of manuronic and guluronic acids. Studies investigating the properties of alginic acid because of the role played by alginic acid bioflocculation, however no studies available that describes the role of alginic acid in the reverse osmosis membrane fouling. Humic and fulvic acid represents the major part of dissolved organic matter in aquatic environments. They result from degradation of biological and chemical residues of plants and animals. The fouling tendency of humic

acid is due to their ability to bind to multivalent salts. Membrane fouling caused by humic acid is influenced by the characteristics of the humic substances and membrane, and the chemical composition of the feed water. Since humic acid is a major class of NOM, researchers always uses it as a model compound for membrane performance in water treatment.

1.4 Model Organic Acids

Humic Acid

Humic Acid is a major component of humic substances, which are the major organic constituents of soil, many upland streams and ocean water. Humic acids are colloids and they behave as clays even though the nomenclature suggest that they are acids and form true salts. When the cation exchange sites on the humic molecule are filled predominantly with hydrogen ions, the material is considered to be an acid and is named accordingly. It has no effect on pH because the acid is insoluble in water but is soluble at higher pH values. It is not a single acid rather a complex mixture of many different acids containing carboxyl and phenolate groups so that the mixture behaves functionally as a dibasic acid. There are several subclasses of humic acids, (tannins, lignins, fulvic acids). Soil humic acids are mainly derived from the biochemical degradation of plant and animal residues and from microbial synthetic activity and constitute a significant fraction of the soil organic matter. The presence of carboxylate and phenolate groups gives the humic acid the ability to from complexes with ions such as Mg^{2+}, Ca^{2+} and Fe. Humic acid has the average chemical formula $C_{187}H_{186}O_{89}N_9S_1$.

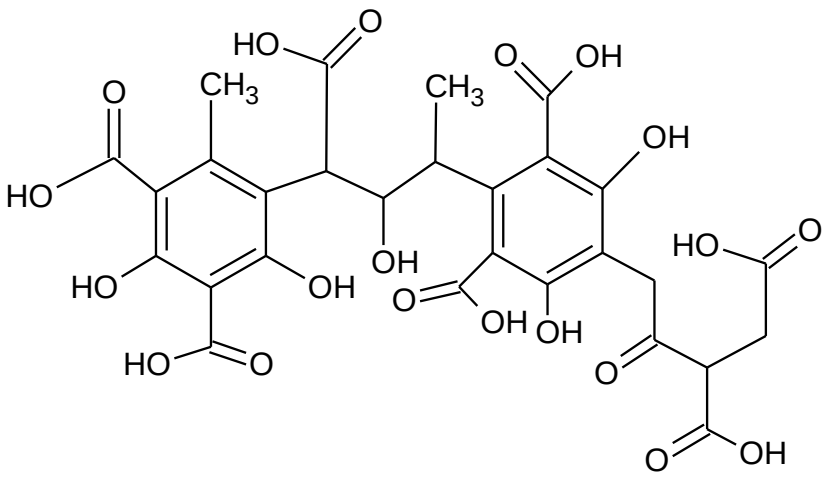

Fig 1.1: chemical structure of humic acid

There is an increase in use of humic acid for their beneficial impact on the growth and cultivation of crops, flowers, and particularly in organically deficient soil. Humic acid is not a fertilizer as it does not directly provide the nutrients to plants but is a compliment to fertilizer. In many instances humic acid will reduce the need for fertilization due to the soil and plants ability to make better use of it. Fertilization can be eliminated totally if sufficient organic material is present and the soil can become self sustaining through microbial processes and humus protection (Stevenson *et al, 1994*). When applied to clay, humic acid can help break up compacted soils, allowing for enhanced water penetration and better root zone growth and development. When applied to sandy soils, humic acid adds essential organic materials necessary for water retention thus improving root growth and enhancing the sandy soils ability to retain and not leach out vital plant nutrients. Due to its ubiquity in the environment and its polyelectrolytic nature, HA is an important colloid and sorbent phase controlling the speciation and fate of many organic and inorganic pollutants in surface aquatic and groundwater systems (Weber *et al, 1988*)

Dissolved HA often interferes with water treatment processes and significantly affects the quality of the final portable water product (Reckhow *et al., 1990*). For example, relatively

high concentrations of HA in source water can cause formation of trihalogenated methanes that are possible carcinogens. One of the main concerns is the environmental problem caused by the presence of HA in waters. Due to the above mention problems the removal of HA from water is necessary and some techniques have been used successfully. The coagulation of HA by aluminum sulphate has been studied, and it is also used in treatment plants to remove humid substances from water (Odegaard *et al.,1999*). Other techniques were used to remove HA such as natural adsorbents and cationic polymers. However, only few studies have dealt with the removal of HA using the cationic quaternary ammonium compound cetyl trimethyl ammonium bromide (CTAB). A technique was proposed to remove humic substances from water that combined the use of CTAB and a polymeric synthetic adsorbent in a column (Adou *et al. 2001*).

In 2007 Brum, studied two different cationic surfactants which were used to precipitate low dosage (20 ppm) of HA and their effect has been investigated. A column flotation was designed to generate small bubbles and remove efficiently HA from water. The study showed the difference in the adsorption of the surfactants used to precipitate HA and revealed a higher adsorption of CTAB compared to that of dodecylamine (DDA). The concentration of precipitant collector required to achieve maximum removal increases with the pH. However after exceeding the precipitant collectors optimum concentration, the removal tends to zero in the system HA/CTAB (Brum *et al., 2007*).

A study was done which aimed to elucidate the heterogeneous structural and compositional characteristics of HA with different apparent molecular sizes (Li *et al. 2004*). The size or apparent molecular weight of HA is an important property correlated well with the reactivities of HA in both natural and engineered environmental systems. Molecular sizes of HA are shown to affect formation of harmful disinfection by-products in water chlorination

process (Reckhow *et al., 1990*). The BHA sample was fractionated into eight fractions using a cross-flow ultrafiltration technique. The results obtained from the study showed that the humic acid extracted from Pahokee peat was composed of macromolecules with a range of molecular weights and chemical compositions. They could be fractionated by ultrafiltration into subsamples, each having relatively less heterogeneous properties. As the molecular cutoff of the ultrafiltration fractionated HA fraction increased, the apparent Mw increased accordingly.

Research was done to investigate the efficiency of ultrafiltration membranes in the removal of humic acid from river waters. The water that had been deionised and distilled (milliQ water) was used as the background water to which humic acid was added. Pressure, membrane pore size and initial humic acid concentration was varied during the experimental stages to investigate their effects on humic acid removal efficiency and which combination would provide the best removal of HA. All three membranes were capable of removing humic acid from an initial concentration of 15 mg/L to acceptable levels. The ultrafiltration membranes, of MWCO 10 kDa, 5 kDa and 3 kDa, are capable of removing humic acid from the model feed solutions to levels below those required. The 3 kDa and 5 kDa membranes experienced severe fouling possibly due to the adsorption of humic acid molecules on the surface and inside the membrane pores. The 10 kDa membrane provided highest permeate flux with minimum fouling and was capable of reducing an initial humic acid concentration of 15 mg/L to below the maximum allowable level of 1.17 mg/L. This was concluded to be the optimal membrane size as it provides best humic acid removal and operability (Lowe *et al., 2008*).

Tannic Acid

Tannic acid represents a class of carbohydrates (Kweon *et el, 2005*). Tannic Acid is one type of tannin that has a fairly weak acidity. It is usually yellow, white or a light brown powder. It tends to dissolve easily in water. Tannic acid is a complex organic acid found in most plants. It is a derivative of the simple sugar glucose ($C_6H_{12}O_6$) in which five hydroxyl groups (OH) has been replaced by large complex side chains known as digalloyl groups. The name comes from the fact that the compound is used in the process known as tanning. It transforms the proteins in raw animal hides into forms that resist the natural process of decomposition, converting the hides into leather. It belongs to a large class of chemical compounds known as tannins that have the common chemical property of being able to precipitate proteins. Tannic acid is not a true acid because it does not contain the carboxyl group (COOH) present in all organic acids; instead it is a polyphenol, a compound with many phenol (C_5H_5OH) groups. As a watersoluble polyphenolic compounds, TA has been demonstrated to be toxic to aquatic organism, such as algae, phytoplankton, fish and invertebrates. Moreover, TA will react with chlorine during water treatment and sterilization and produce carcinogenic disinfection by-products (DBPs), which cause cancer and affect the health of human beings very seriously.

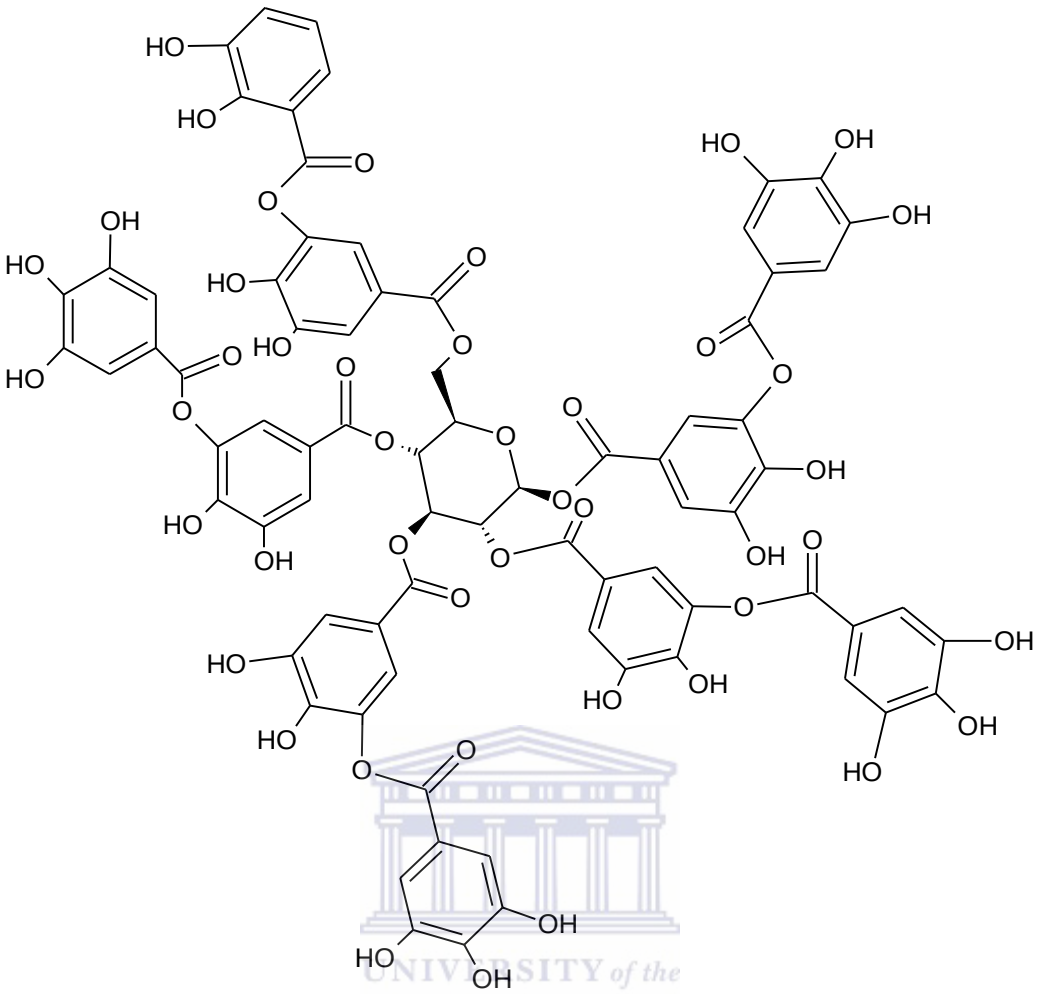

Fig 1.2: chemical structure of tannic acid

Tannic acids help eliminate diarrhea, reduce swelling of hemorrhoids, loosen catarrh in the respiratory system, and control various kinds of internal bleeding. Externally, tannins are beneficial in rubs for aching muscles and joints, in salves for open, slow-healing sores, and as antiseptics. Plants high in tannic acid have been used to treat cancers, but tannic acid itself has been found to be carcinogenic under certain conditions. In very small amounts, tannic acid is approved for food use and is added to many commercial foods. Since the astringency of tannic acid involves the precipitation of protein, the addition of protein (such as milk or cream) to a tannin-rich tea would bind the tannin, rendering it biologically inert.

Phosphorus, mainly in the form of phosphoric anion, widely exists in municipal and industrial wastewater effluents and is the primary cause of eutrophication in aqueous environments. The current technologies to remove phosphorus include chemical precipitation, physical and biological methods. A study was done in order to examine the feasibility of using tannic acid as coagulant aid during phosphorus removal process. Precipitation with ferric chloride as the coagulant and tannic acid as the coagulant aid were examined by using wastewater from different sources (Zhou *et al., 2008*). Tannic acid was chosen as the coagulant aid for this study. Hydrolysable tannin, tannic acid contains a number of adjacent hydroxyphenyl groups, which are suitable ligands to combine with heavy metal ions, such as chromium, cobalt, and iron to form polyphenol– metal complexes (Yamaguchi *et al., 1992*). It was concluded from the results obtained that during the coagulation/flocculation processes for different types of wastewater, tannic acid addition can accelerate the settling speed of the flocs, reduce the residual Fe (III) to eliminate the yellow colour caused by Fe (III), and slightly increase the phosphorus removal efficiency.

Many of methods for removing tannic acid have been reported, including electrochemical method, coagulation, ultrafiltration, biodegradation, and sorption. Among these methods, sorption has been found to be one of the cheapest and efficient methods for removing tannic acid from water. Currently, new practices have been focused on the use clay minerals as an alternative to replace the conventional sorbents, based on both the environmental and economic points of view. A study was done to study the removal of tannic acid from aqueous solution by chitosan-coated attapulgite. Attapulgite is a crystalline hydrated magnesium silicate with a fibrous morphology. It has been intensively used as sorbents for removing heavy metal ions and organic contaminants owing to its large specific surface area and cation exchange capacity (Deng *et al., 2012*). The natural attapulgite was firstly treated by 5% HCl,

and then the acid-treated attapulgite (ATP) was modified with chitosan with different mass ratios of acid-treated attapulgite and chitosan. The sorption capacities of tannic acid onto the made ATPs were compared, and the optimum sorbent was applied to removing tannic acid from aqueous solution. The results showed that chitosan was successfully grafted onto ATP, and the ATP modified by chitosan possessed excellent sorptive property for tannic acid in aqueous solution. Tannic acid sorption is strongly dependent on solution pH, coexisting cations, and temperature. The results implied that optimum sorbent is a promising sorbent for sorptive removal of tannic acid from water treatment (Deng *et al. 2012*).

Alginic Acid

Alginic acd is a type of a polysaccharide which plays a major role in membrane filtration. Alginic acid is a naturally occurring hydrophilic colloidal polysaccharide obtained from the various species of brown seaweed. It is a linear copolymer consisting mainly of residues of b -1,4-linked D-mannuronic acid and a -1,4-linked L-glucuronic acid. These monomers are often arranged in homopolymeric blocks separated by regions approximating an alternating sequence of the two acid monomers. In extracted form it absorbs water quickly; it is capable of absorbing 200-300 times its own weight in water. Its colour ranges from white to yellowish-brown. Alginic acid is also called algin or alginate. Alginic acid is a biopolymer carrying carboxyl groups capable of forming complexes with metal ion. Potassium alginate is a chemical compound that is the potassium salt of alginic acid. It is an extract of seaweed. Its empirical chemical formula is $KC_6H_7O_6$. Another type of alginic acid is sodium alginate, the sodium salt of alginic acid. Its empirical formula is $NaC_6H_7O_6$. Sodium alginate is a gum, extracted from the cell walls of brown algae.

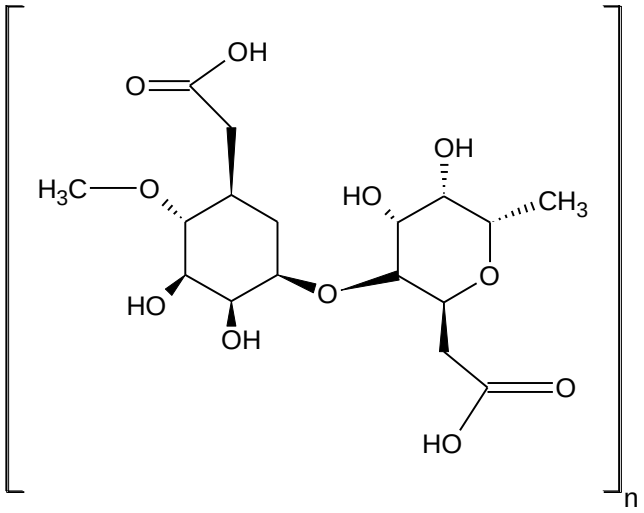

Fig 1.3: chemical structure of alginic acid

Due to its major property which is the ability to absorb water quickly, alginate can be changed through a lyophilization process to a new structure that has the ability to expand. It is used in the weight loss industry as an appetite suppressant. A major application for sodium alginate is in reactive dye printing, as thickener for reactive dyestuffs in textile screen-printing and carpet jet-printing. Potassium alginate is widely used in foods as a stabilizer, thickener, and emulsifier. The ability of alginic acid and its salts to stop bleeding is widely used in the treatment of erosial and helcoid diseases of the gastrointestinal tract. When taking in alginates render a mild antacid action, when interrelating with hydrochloric acid of gastric juice they form a gel which covers the mucous membrane as gastric dressing thus preventing it from further influence of hydrochloric acid and pepsine and stopping the bleeding. Alginates have a positive effect on the liver, pancreas and kidney functions. The use of alginic acid in the form of calcium salt strengthens the sorbing properties of the drug in respect of heavy metals and radioisotopes and thus avoiding the negative impact on the balance of calcium salts in the body.

Many studies have been carried out about the application of alginic acid to the aqueous phase separation of heavy metals, and the possibility of alginic acid for the adsorbent material has been suggested. A study was conducted to apply alginic acid efficiently to wastewater treatment system; it was immobilized by novel PVA–boric acid method using glutaraldehyde to reduce the hydration of the immobilized bead. And, the characteristics of metal removal and recovery using the immobilized alginic acid bead with PVA were also investigated. From the result, it was concluded that the immobilized alginic acid bead can be applied to wastewater treatment system. Especially, it can be used in lead ion-rich wastewater (Jeon *et al., 2002).*

Jeon et al 2001, did a study and the objective of the study was to apply to the plating wastewater for water reuse, and heavy and precious metal recovery using carboxylated alginic acid bead. The application to the actual plating wastewater, the biosorbent was immobilized by PVA-Boric acid method (Jeon *et al., 1981*). The carboxylated alginic acid immobilized with polyvinyl alcohol was used to reuse water and to recover heavy metals efficiently in the Panwall-plating complex wastewater; which is classified as acid-alkaline, chelating, and chromic wastewater. Since the bead did not swell and has enough strength to sustain its weight, channeling of flow and the increase of pressure drop were not observed through the column operation. To remove heavy metals efficiently, pre-treatment methods such as pH manipulation and oxidation reaction between sodium hypochlorite and wastewater was applied. The results reflect the difference of affinity for carboxylated alginic acid bead between copper and nickel ion. The removal efficiency of chromium (3+) was increased to about 21% in chromic wastewater in the batch process. The results show the possibility for reuse as industrial water and ease in recovering heavy metals of the effluent (Jeon *et al., 2001*).

Jeon et al, 2005, studied the effects of ionic strength and organic materials on copper ion which exists abundantly in most of real industrial wastewaters uptake capacity and desorption characteristics using NTA as desorbing agent for carboxylated alginic acid. Biosorption is the representative name of the phenomenon of removing heavy metals in water by microorganisms or their metabolic products by various mechanisms. In order of adsorption and desorption cycles, the lead uptake capacity on carboxylated alginic acid was relatively maintained through cycles. Consequently, it could be concluded that carboxylated alginic acid could be used economically in real process such as plating and electroplating wastewater treatment systems (Jeon *et al,. 2005*).

1.5 Aim and Objectives of the study

The aim of the study is to develop metal nanoparticles modified polysulfone membrane to minimize the fouling behaviour of polysulfone membrane for use in water treatment process.

Objectives of the study:

- Chemical synthesis and preparation of metal nanoparticles modified polysulfone films at an electrochemical transducer interface
- Synthesis of metal nanoparticles (Silver, Cobalt and Nickel)
- Studying the morphology of the thin film materials and its relation to hydrophilicity as measure by contact angle
- Characterisation of the thin film materials with voltammetry, impedance spectroscopy and Raman spectroscopy

- Evaluating the performance of the thin films in the presence of selected organic pollutants which are alginic acid and tannic acid

1.6 Conceptual diagram

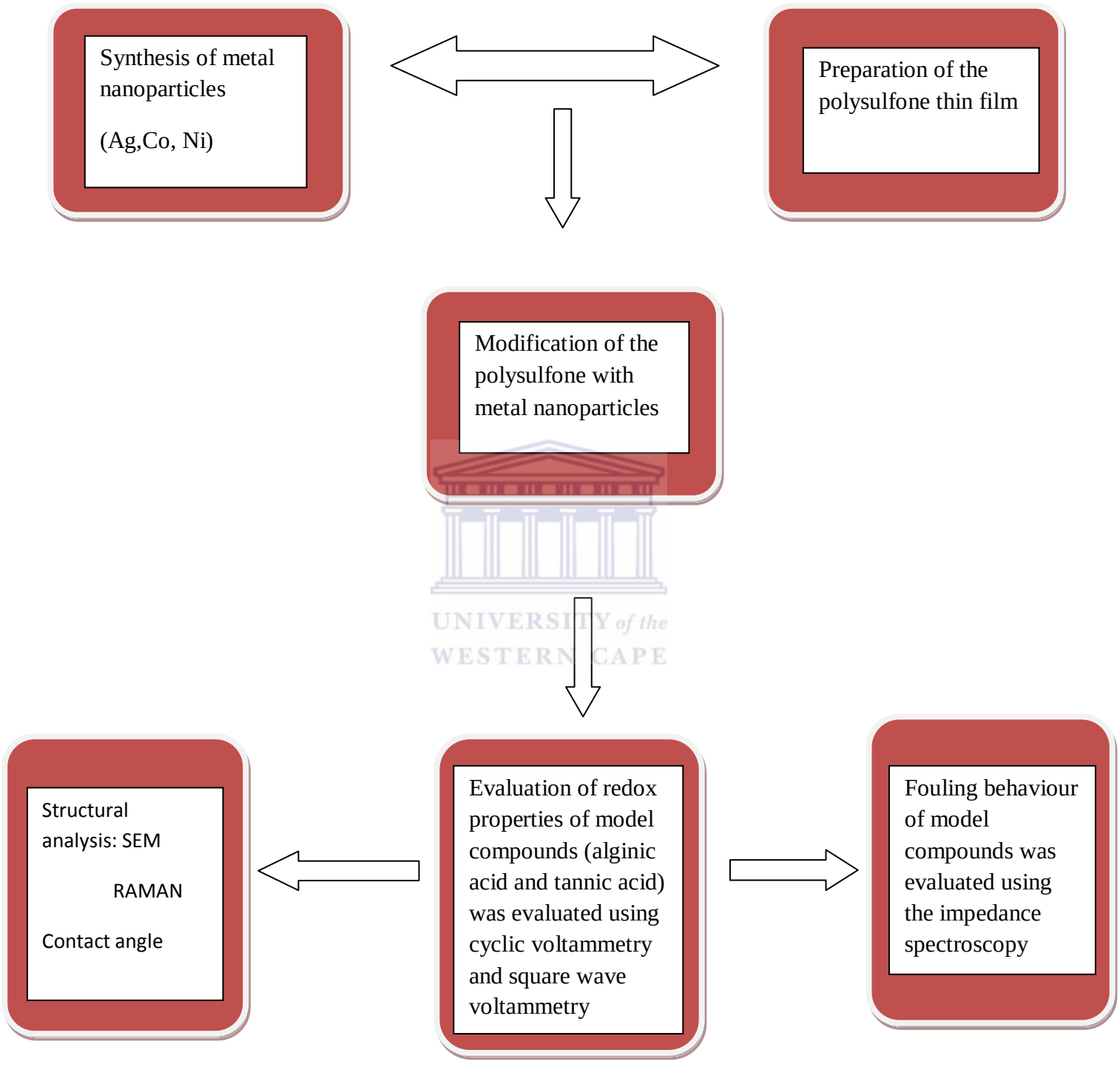

1.7 Thesis scope

The thesis is divided into 6 chapters:

- Chapter 1 provides the background to the study and introduction of Polysulfone membranes and its use in water treatment. The model organic acid compounds (tannic acid and alginic acid) are also introduced in the context of organic pollutants in waste water.

- Chapter 2 presents the principles of operation and application of instrumentation to characterise materials and analyse standard organic compounds in aqueous solutes

- Chapter 3 discusses the preparation as strategy for PSF and metal nanoparticles prepared as thin films

- Chapter 4 presents the interpretation of the electrochemical evaluation of data obtained by CV, SWV

- Chapter 5 presents the EIS studies to evaluate the fouling behaviour of the model organic acids (tannic acid and alginic acid) at the thin films prepared

- Chapter 6 draws the general conclusion in terms of improved performance of the membrane after modification as evaluated in standard laboratory experiments.

Chapter 2

The methods and instruments that were used for the characterisation the prepared polysulfone thin films are discussed in this chapter.

The methods that were used for metal nanoparticles modified polysulfone membrane for water treatment study were; atomic force microscopy (AFM), scanning electron microscopy (SEM) and transmission electron microscopy all representing microscopic techniques. This allowed us to study the morphology and the elemental analyses of the prepared materials. Electrochemical techniques that were used are cyclic voltammetry (CV), square wave voltammetry (SWV) and electrochemical impedance spectroscopy (EIS). The Raman spectroscopy was also used to evaluate the vibrational modes of the thin films prepared

2.1 Cyclic Voltammetry

Cyclic voltammetry is a technique for studying the electrochemical behaviour of a system. Major information can be extracted from cyclic voltammetric experiment such as thermodynamics of redox reactions, kinetics of heterogeneous electron transfer reaction, coupled chemical reactions or adsorption processes.

The technique cyclic voltammetry is based on cycling the potential applied to a stationery electrode immersed in an inert solution and measuring the resulting current. The output is captured as a voltammogram where current is plotted as a function of the applied potential. The time necessary for a particular scan depends upon the scan rate and the potential window to be traversed. The electrochemical cell used consists of three electrodes immersed in an electrolyte. An electrolyte is the boundary at which dissolved substrates may pick up or lose electrons. An electrolyte is needed to supply electrical conductivity between the electrodes.

The working electrode is the electrode at which the electrochemical phenomena (reduction or oxidation) being studied are taking place. The reference electrode provides a constant potential that can be taken as the reference standard for the potential applied at the working electrode. The commonly used reference electrodes are the silver-silver chloride (Ag/AgCl) and the Calomel electrode (Hg/HgCl/KCl). The third electrode is the counter electrode or auxiliary which serves as a collector in the cell, so that current can pass (fig 2.1).

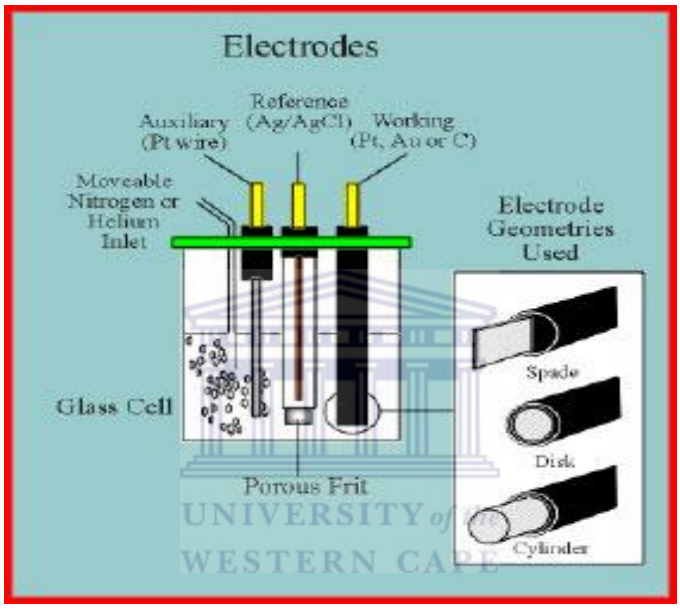

Fig 2.1: electrochemical cell with electrodes (*www.chem.ucla.edu*)

A typical one electron redox exchange may be represented as follows:

$$O + n\,e \longleftrightarrow R$$

In the forward scan, R is electrochemically generated from O and the cathodic current peak is produced, whereas in the reverse scan R is oxidized back to O and the anodic current peak is formed.

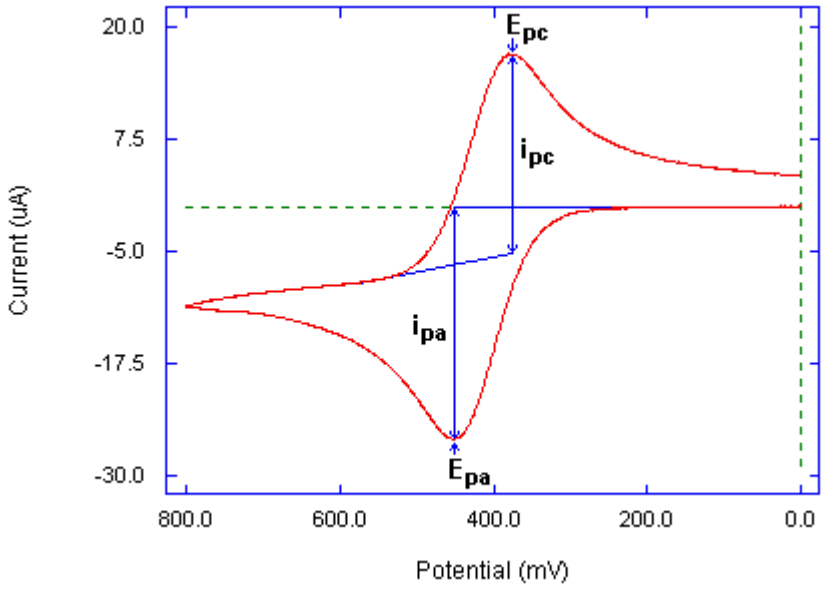

Fig 2.2: CV showing the voltage vs the current

Peak potentials (Ep^c and Ep^a) and the peak currents (ip^c and ip^a) are there two sets of essential parameters which characterize a redox couple. For a reversible redox reaction the oxidized and reduced forms are in equilibrium at the electrode surface. The cathodic and anodic peaks are separated by a potential of approximately 59/n mV, where n is the number of electrons transferred.

$$E = Epa + Epc / 2 = 59 / n$$

When reversible peaks are present the thermodynamic information in the form of half cell potential $E^0_{1/2}$ can be determined. In a semi-reversible reaction the ipa/ipc is less than or greater than 1 and is possible to determine more kinetic information

In the case of irreversible peaks, their thermodynamic $E^0_{1/2}$ cannot be determined with cyclic voltammetry. The couple could be irreversible because of a following chemical process; another reason for irreversibility could be a physical process such as precipitation.

2.2 Electrochemical Impedance Studies

EIS involves measurements and analysis of materials in which ionic conduction strongly dominates. EIS investigates the system response to the application of a periodic small amplitude ac signal. These measurements are carried out at different ac frequencies. Analysis of the system response contains information about the interface, its structure and reactions taking place.

In impedance spectroscopy, a small sinusoidal voltage is placed on the sample over a wide range of frequency, from 10^5 to 10^{-3} Hz, it is therefore an alternating current (AC) technique. The controlling computer system measures the degree of the current induced by the potential and in addition the phase angle between potential and current maxima

For DC conditions $V = iR$

For AC conditions $V = iZ$

Where Z is the impedance of the system.

From Ohms Law for AC conditions the impedance can be calculated by setting the input potential and measuring the induced current. When the phase angle, θ, between the voltage applied and the current induced is zero, then a pure resistance is present. In the case where a phase angle of 90^o is measured between the voltage and current at the same frequency a pure capacitance is present. Angles between these values can mean a combination of a capacitor and resistance are present.

Impedance data is commonly analysed by fitting it to an equivalent circuit model. The circuit that is usually used in the Randles equivalent circuit which is composed of different elements such as resistors, and inductors joined in series or in parallel, to represent solution resistance, interfacial capacitance and charge transfer processes (Fernandez-Sanchez, 2005)

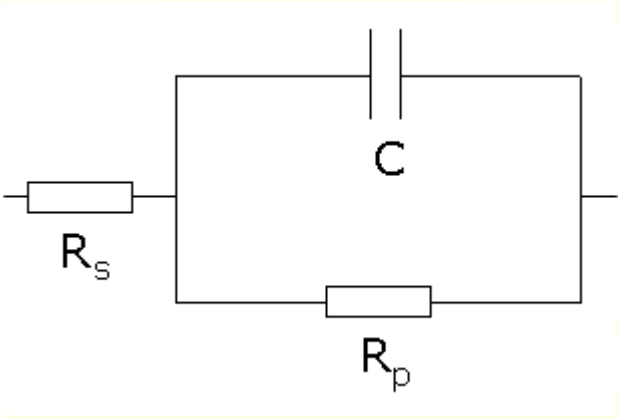

Fig2.3: Randles equivalent circuit used for data fitting

2.3 Contact Angle

The contact angle is the angle at which a liquid/vapour interface meets a solid surface. The method is illustrated with a small liquid droplet resting on a flat solid surface. The drop formed at the solid surface is quantified using the Young's Relation. A given system of solid, liquid, and vapour at a given temperature and pressure has a unique contact angle. The contact angle is commonly used in membrane material science to describe the relative hydrophobicity / hydrophilicity of a membrane surface.

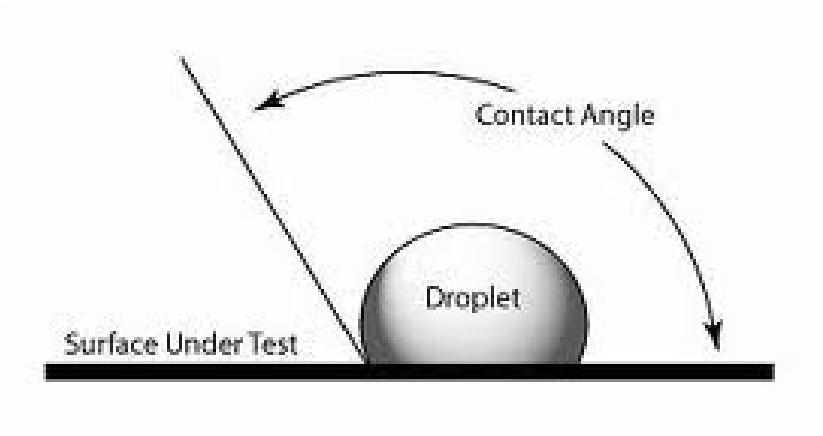

Fig 2.4: *contact angle formed when water droplet meets the solid surface*

There are different ways of measuring a drop. Contact angle can be measured on static drop, the drop formed before measurement and has a constant volume during the measurement. Dynamic drop is measured on increasing drops known as advancing angles and those measured on reducing drops as retreating angles. When a drop is deposited on a flat solid surface, the contact angle, θ, is the angle formed by a liquid at the three phase boundary where the liquid, vapour, and solid meet.

$$\gamma_{SL} = \gamma_{SL} + \gamma_{LV} \cos\theta$$

Where

γ_{SL} = Interfacial tension between the solid and gas

γ_{SL} = interfacial tension between the solid and liquid

γ_{LV} = interfacial tension between the liquid and vapour

The information can be obtained from contact angle measurement:

- The affinity of a liquid to a solid surface; if water is used to measure the contact angle can deduce the hydrophobic or hydrophilic character of the surface.
- If several reference liquids are used, the surface energy of the solid can be calculated discriminating between polar and dispersive components.
- The measure of the hysteresis between advancing angle and recessing angle give information on non-homogeneity of the surface.

Another way of describing contact angle is to use cohesion and adhesion. Cohesion is the force between the liquid molecules which hold the liquid together, while the adhesion is the force between the liquid molecules and the solid molecules. Contact angle is a quantitative

measure that demonstrates the ratio of cohesion vs. adhesion. If the contact angle is near zero, the liquid droplet spreads completely on the solid surface, adhesive forces are dominating. If the contact angle is very high, which means that the liquid droplet bead up on the solid surface, mean that cohesive forces are dominating.

2.4 Electron Microscopy

Electron microscopes are instruments that use a beam of highly energetic electrons to analyse objects on a very fine scale. This analysis can yield information about the morphology (shape and size of the particles making up the sample material), topography (surface features of a sample), composition (the elements and compounds that the sample is made up of and the relative amounts of them) and the crystallographic information (how the atoms are arranged in the sample). The electron microscopes were developed because of the limitations of light microscopes which are limited by the lights up to 500x and 1000x magnification and a resolution of 0.2 micrometers. The Transmission Electron Microscope was the first type of electron microscope to be developed and is patterned on the light transmission microscope except that a focused beam of electrons is used instead of light to see through the specimen

2.4.1 Transmission Electron Microscopy

Transmission electron microscopy (TEM) is a microscopy technique which uses a beam of electrons transmitted through an ultra thin specimen, interacting with the specimen as it passes through. The formation of an image is possible from the interaction of the electrons transmitted through the specimen; the image is magnified and focused onto an imaging device, on a layer of photographic film, or to be detected by a sensor such as a CCD camera. TEMs are capable of imaging at higher resolution than light microscopes, owing to the small de Broglie wavelength of electrons. The main use of this technique is to examine the specimen structure, composition or properties in submicroscopic details so that this

microscopy technique is significantly involved in numerous fields such as biological components, chemistry, materials science or electronics. At smaller magnifications TEM image contrast is due to absorption of electrons in the material, due to the thickness and composition of the material. At higher magnifications complex wave interactions modulate the intensity of the image, requiring expert analysis of observed images. Alternate modes of use allow for the TEM to observe modulations in chemical identity, crystal orientation, electronic structure and sample induced electron phase shift as well as the regular absorption based imaging.

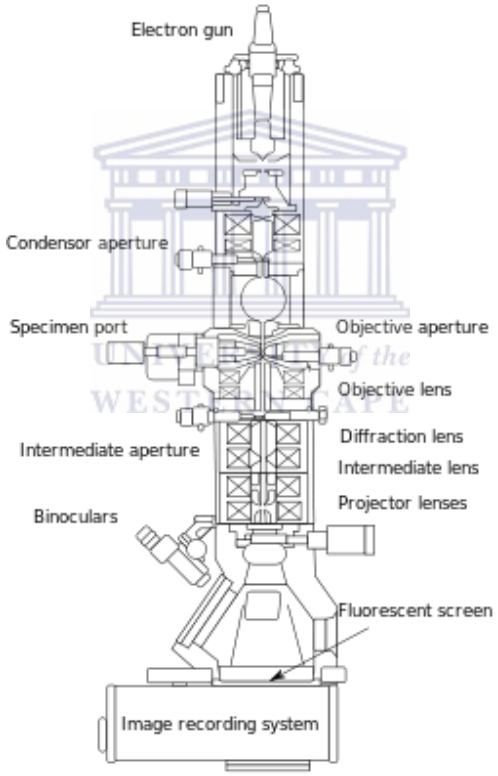

Fig2.5: A schematic representation of TEM

2.4.2 Scanning Electron Microscopy (SEM)

Scanning electron microscopy is a kind of electron microscope which produces an image of a sample by scanning it with a focused beam of electrons in a raster scan pattern. The electrons interact with electrons in the sample, signals are produced that can be detected and

contain information about the sample's surface topography, composition, and other properties such as electrical conductivity.

SEM produces various signals which are secondary electrons (SE), back-scattered electrons (BSE), X-rays, specimen current, cathodoluminescence (CL), and transmitted electrons. The signals result from interactions of the electron beam with atoms at or near the surface of the sample. The SEM can produce very high resolution images of a sample, revealing details less than 1nm in size.

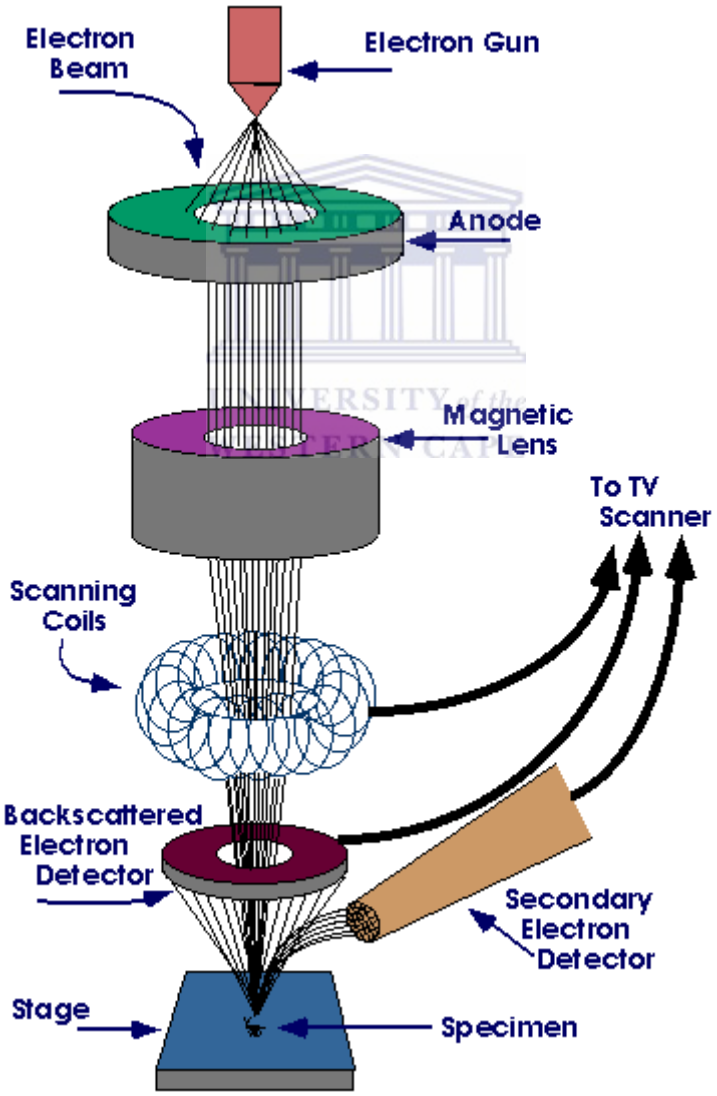

Fig 2.6: *A schematic representation of SEM.*

For conventional imaging in the SEM, specimens must be electrically conductive and electrically grounded to prevent the accumulation of electrostatic charge at the surface. Specimens that are non-conductive like polymers, coating with an electrically conductive material such as carbon and gold are used. The coating is done to prevent the accumulation of static electric charge on the specimen during electron irradiation and increases signals and surface resolution.

SEM is one of the most important instruments for the structural analysis of membranes, SEM results for polymeric membranes indicated that membranes were highly porous and asymmetric with sponge-like structures. Cross-sectional morphology showed that the membrane consist of two layers; a low porosity skin layer that serves as membrane support and porous upper layer. Recently SEM has also been used for studying the structure of the fouling layer at nano scale. SEM also provides the size and shape of foulants (Meng *et al., 2010).*

Energy dispersive X-ray spectroscopy known as EDS/EDX is an analytical tool used for the elemental analysis or chemical composition of a sample. It relies on the investigation of a sample through interactions between electromagnetic ration and matter, analyzing emitted X-rays by matter in response to being hit with charged particles. In stimulating the emission of characteristic X-rays from a specimen a high-energy beam of charged particles such as electrons, protons or beam of X-rays is focused into the sample.

2.5 Atomic Force Microscope

Scanning probe microscopy (SPM) describes a broad group of instruments used to image and measure properties of material, chemical and biological surfaces. The SPM images are obtained by scanning a sharp probe across the surface while examining and collecting the tip-

sample interactions to produce an image. SPM has two types of microscopes which are scanning tunnelling microscopy (STM) and atomic force microscopy (AFM)

AFM function by measuring force between a probe and the sample, the probe is usually a sharp tip. The image resolution is acquired; AFM measures the vertical and lateral deflections of the cantilever by using the optional lever. Forces between probing tip and sample ranges from 10^{-11} to 10^{-6} N. Two force regimes that are well-known: contact and non-contact mode. In non-contact mode at tip-sample separations of 10 to 100nm is operated, forces such as van der Waals, electrostatic, magnetic forces can be sensed and give information about surface topography, distribution of charges. In contact mode the probing tip is in contact with the sample, ionic repulsion forces allow the surface topography to be traced with high resolution.

In contact mode, the AFM tip is brought close to the surface of the sample, the scanner makes a final adjustment in tip-sample distance based on a set point determined by the user. The tip is in contact with the sample surface through any adsorbed gas layer, the tip scans across the sample under action of a piezoelectric actuator, either by moving the sample or the tip relative to the other. A laser beam aimed at the back of the cantilever-tip assembly reflects off the cantilever surface to a split photo diode, which deflects the smaller cantilever deflections. By maintaining a constant tip-sample separations and using Hooke's Law

$$F = -kx$$

Where F is force, k is the spring constant and x is the cantilever deflection, the force between the tip and the sample is calculated.

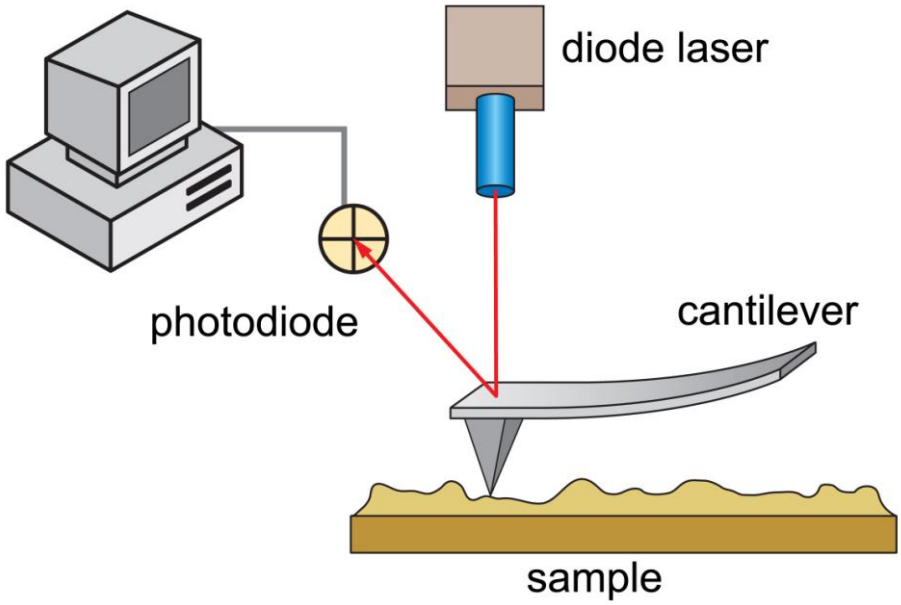

Fig 2.7: schematic representation of contact mode AFM

In non-contact mode, the tip of the cantilever does not contact the sample surface, but instead the cantilever is oscillated at either frequency modulation or above the amplitude modulation where the amplitude of oscillaton is a few nanometers down. The force (van der Waals) above the surface acts to decrease the resonance frequency of the cantilever. Measuring the tip to sample to sample distance at each (x,y) data point allows the scanning software to construct a topographic image of the sample surface.

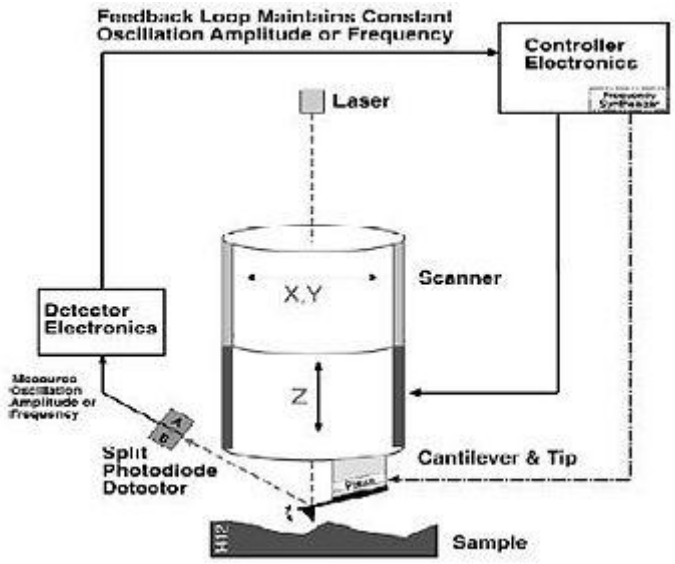

Fig2.8: A schematic representation of non-contact mode AFM

AFM has a number of advantages over the scanning electron microscope (SEM). Unlike the electron microscope which provides a two-dimensional projection or a two-dimensional image of a sample, the AFM provides a three-dimensional surface profile. In addition, samples viewed by AFM do not require any special treatments (such as metal/carbon coatings to enhance the sample's conductivity) that would irreversibly change or damage the sample, and does not typically suffer from charging artefacts in the final image. While an electron microscope needs an expensive vacuum environment for proper operation, most AFM modes can work perfectly well in ambient air or in a liquid environment (Geisse et al.,2009).

A disadvantage of AFM compared with SEM, is the single scan image size. In one pass, the SEM can image an area on the order of square millimeters with a depth of field on the order of millimeters, whereas the AFM can only image a maximum height on the order of 10-20 micrometers and a maximum scanning area of about 150×150 micrometers (Schitter *et al., 2008*). The scanning speed of an AFM is also a limitation. Traditionally, an AFM cannot scan images as fast as a SEM, requiring several minutes for a typical scan, while a SEM is capable of scanning at near real-time, although at relatively low quality. The relatively slow rate of scanning during AFM imaging often leads to thermal drift in the image making the AFM microscope less suited for measuring accurate distances between topographical features on the image (Lapshin 2007).

2.6 RAMAN Spectroscopy

Raman spectroscopy is a spectroscopic method used to monitor vibrational, rotational and low-frequency modes in a system. It relies on inelastic scattering or Raman scattering of monochromatic light, usually from laser in the visible, near ultraviolet range. The laser interacts with molecular vibrations phonons producing the energy of the laser photons being

shifted up or down. The energy shifts gives information about the vibrational modes in the system. The infrared spectroscopy yields similar, but complementary information.

The Raman effect occurs when light strikes upon a molecule and interacts with electron cloud and the bonds of that molecule. A photon will excite the molecule from the ground state to a virtual energy state, when the molecule relaxes it emits a photon and it returns to a different rotational or vibrational state known as the spontaneous Raman effect. The difference in energy between the original state and this new state leads to a shift in the emitted photon's frequency away from the excitation wavelength.

When a monochromatic radiation is incident upon a sample then this light will interact with the sample in some fashion. It is the scattering of the radiation that occurs which can tell information about the sample's molecular structure. The incident photons will thus interact with the present molecule, the amount of energy change by a photon is characteristic of the nature of each bond present.

The Stokes shift, is whereby the final vibrational state of the molecule is more energetic than the initial state, and then the emitted photon will be shifted to a lower frequency in order for the total energy of the system to remain balanced. Whereas in the case of the final vibrational state is less energetic than the initial state, then the emitted photon will be shifted to a higher frequency, this is known as the Anti-Stokes shift

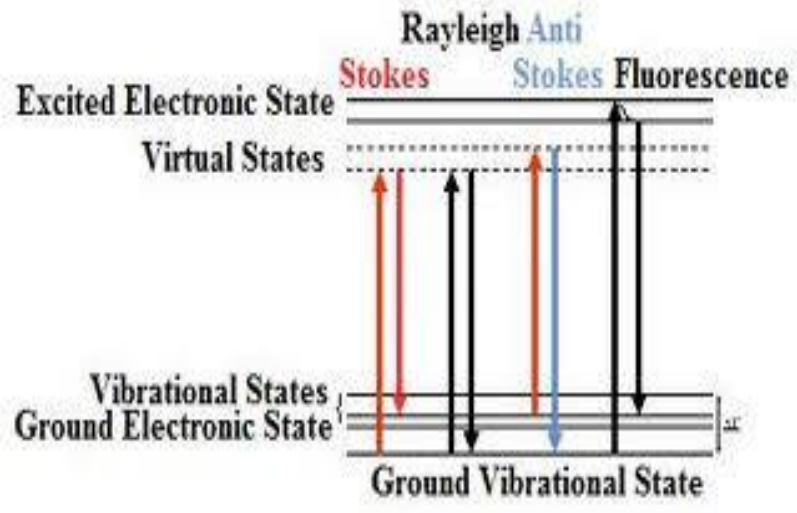

Fig2.9: A schematic representation of the Stokes and Anti-Stokes shift

2.7 Instrumentation

2.7.1 Electrochemical measurements

Electrochemical experiments carried out and recorded with a computer interface to a BAS/50W Epsilon integrated automated electrochemical workstation (Bioanalytical Systems Lafeyette, IN, USA). Cyclic voltammetry and the Square Wave voltammetry were carried out in a 10mL electrochemical cell, with Ag/AgCl (3 M NaCl) as a reference electrode and platinum wire as the auxiliary electrodes. The Pt electrode obtained from BAS was used as the working electrode. Alumina micropolish and polishing pads (Buehler, IL, USA) were used for polishing the electrodes. The PSF and modified PSF were dry coated unto the Pt electrode and studied as the working electrode. For fixed frequency impedance the measurement were carried out using VoltaLab instrument (Radiometer Analytical, France) and the dynamic impedance measurements were done using the Zahner IM6 electrochemical workstation (MeBtechnik).

2.7.2 Scanning Electron Microscopy (SEM)

The scanning electron measurements were carried out using the LEO 1450 scanning electron microscope and in the case where the image obtained in LEO 1450 was not good then the Zeiss Auriga, High resolution (fegsem) field emission gun scanning electron microscope was used. Each sample was coated with carbon, the carbon coating was done to enhance the conductivity of the membrane film.

2.7.3 Transmission Electron Microscope

Metal nanoparticles that were synthesized were analyzed with a Tecnai G2F20 X-Twin MAT 200 kV Field Emission Gun Transmission Electron microscope. Metal nanoparticle powder samples were dispersed in ethanol and 2µl of the well dispersed sample was drop coated onto a Cu grids.

2.7.4 Contact Angle Instrument

The Contact Angle instrument was used in this study to measure the contact angle of water on the prepared membrane films. The membrane films were prepared by casting the nanocomposite in the 0.5 M H_2SO_4 and left to dry. Using the sessile drop method, a drop of dH_2O with a volume of 10 µl was drop coated onto the membrane surface. The angle that the droplet makes with the surface of the membrane was measured using KRUSS Drop Shape Angle software. Four measurements were done for each material and the mean contact angle and standard deviation results were reported.

2.7.5 Raman Spectroscopy

Horiba Xplora Raman Spectrometer was used for the Raman spectroscopic analysis. The casting suspensions were drop coated onto a glass slide and left to dry.

2.7.6 Atomic Force Microscopy (AFM)

The Nanosurf easyScan2 AFM was used as to evaluate the roughness of the thin films. The PSF thin films were prepared as drop cast films of uncontrolled thickness. Unfortunately the AFM measurements were not successful due to the highly convoluted nature of the cast films, the probe tip was not able to function in close range since it became trapped in the material folds, resulting in cantilever breakage of AFM tip and the measurements were abandoned.

2.8 Reagents and Materials

All solutions prepared were analytical grade reagents and purified water from a Milli-pore Mill Q system and analytical grade Argon gas was used to purge the system. Polysulfone (Sigma Aldrich, 182443) was purchased as beads. The Cobalt (Sigma Aldrich, 255599, 98% purity) and Nickel (Sigma Aldrich, 339350, 98% purity) were purchased as the chloride salts, as well as $AgNO_3$ (Sigma Aldrich, 209139, 99% purity). N,N – dimethyl acetamide was purchased as solvent to dissolve the polysulfone, was also purchased at Sigma Aldrich (purity 99.5%).

These techniques will be used to study the morphology of the thin films and relate it to its hydrophobic nature. The spectroscopic techniques will be used to study the vibrational bands of the thin films under the Raman spectroscopy. The voltammetry will be used to evaluate where the organic pollutants will oxidizes and reduces. The fouling behaviour was studied using the impedance spectroscopy. The chemicals were used for preparing and synthesizing polysulfone nanocomposite thin films.

Chapter 3

This chapter discusses how the metal nanoparticles were synthesized and also the preparation of the Polysulfone thin films. The prepared nanoparticles were characterised using different instruments, the results are illustrated.

3.1 Preparation of PSF thin film

The preparation of 0.08g.m^{-1} Polysulfone membrane film was prepared by dissolving 4g of polysulfone in 50ml N, N-dimethyl acetamide and thereaction mixture was sonicated in a waterbath until a clear homogenous casting suspension was obtained. For a thin film, 2µl aliquot of the solution was drop coated onto a Pt electrode with a micropipette. Freestanding film was cast by swirling the solution in a glass beaker with 0.5 M H_2SO_4 and polysulfone solution to obtain a homogenous film. The film was then rinsed thoroughly with deionised water and left to dry for at 24hrs.

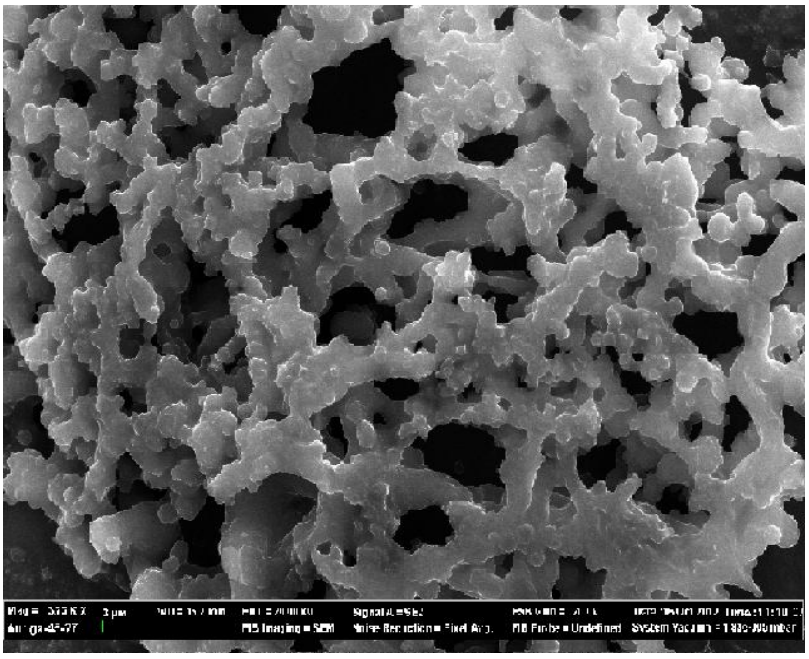

Fig3.1: SEM image of the polysulfone

The SEM image of the polysulfone shows highly branched network structures. The scanning electron microscopy was done to study the morphology and the elemental analysis of the polysulfone.

Fig3.2: EDS spectra of the polysulfone

The EDS sprectrum of the unmodified PSF shows an abundance of Sulfur which confirms the composition of the PSF.

3.2 Synthesis of nanoparticles

3.2.1 Synthesis of Co Nanoparticles

Cobalt salt ($CoCl_2.6H_2O$) was dissolved in ethanol to form a dark blue solution. A mixture of 5ml sodium borohydride and 2ml of sodium hydroxide was added to the 3ml of the dark solution. The reaction mixture was left for 24hrs to react. The resultant mixture was the centrifuged for 20min at 1400rpm and the pellets were thoroughly washed with dH_2O. After centrifuging for a further 20min the pellet was rinsed with ethanol and left to dry for 24hrs in

an oven. After the pellet was dry, it was grinded with a pestle and mortar until a fine powder was formed.

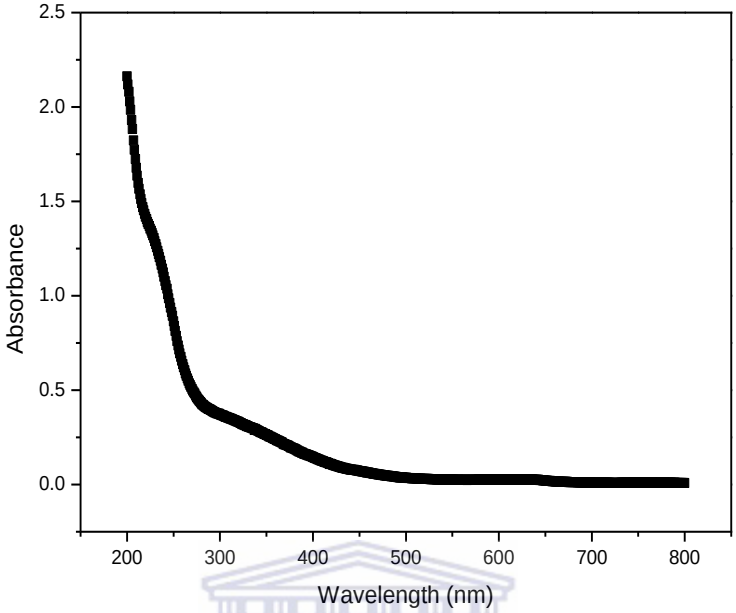

Fig 3.3: UV-vis spectra of Co nanoparticles

The UV-vis spectrum of the Co nanoparticles does not show an absorbance which can be due to an incomplete reduction of the $CoCl_2.6H_2O$ salt. In literature cobalt nanoparticles usually absorbs around 500nm. In 2008 Zhang and Lan, prepared cobalt nanoparticles using a laser beam method, the absorption of Co nanoparticles was at 510nm (J. Zhang, C.Q Lan *et al., 2009)*

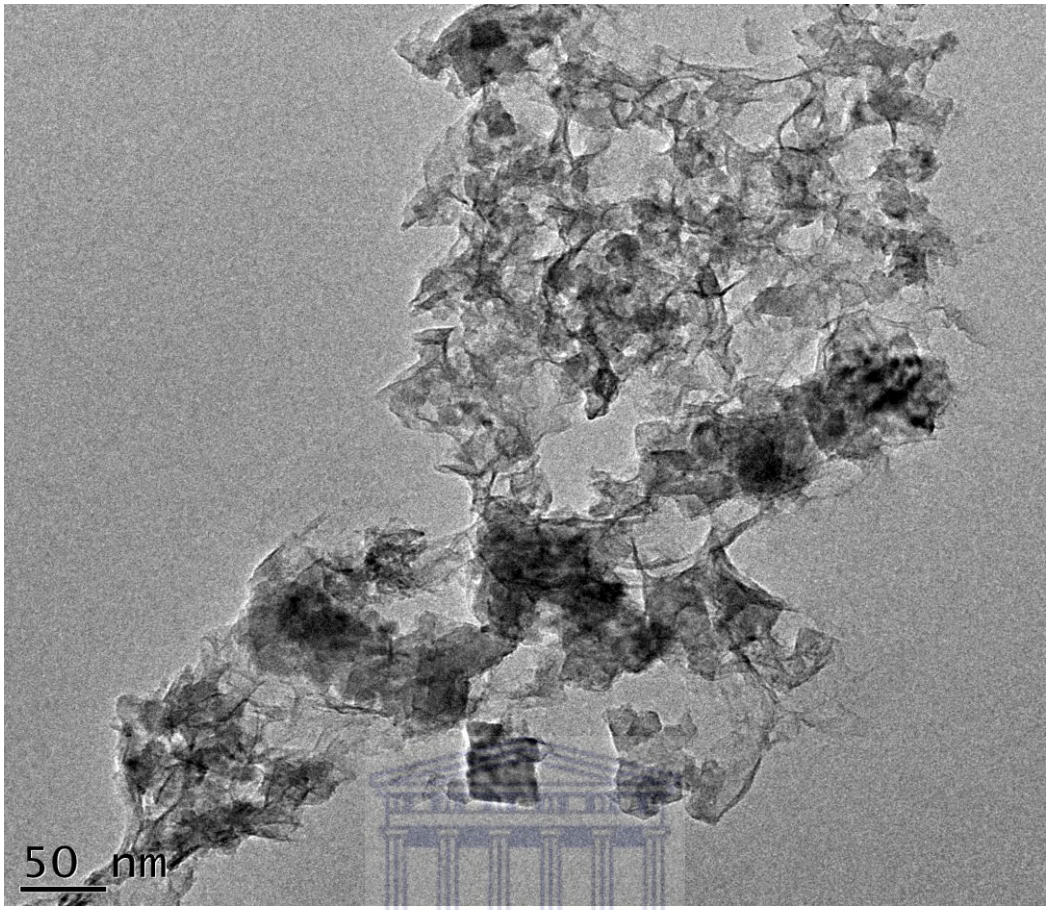

Fig3.4: HR-TEM image of the Co nanoparticles.

The Co salt was reduced with $NaBH_4$ to produce Co nanoparticles. The transmission electron microscope was done to evaluate the size and shape of the nanoparticles. The TEM image of the CoNPS shows that the nanoparticles do not exhibit any specific shape. The Co occurs in three valence states (0, +2 and +3). The Co is more stable as Co (II) than Co (III), the Co (0) is the metallic form which occurs in three allotropic forms, high-coercivity hcp-Co, pseudo-cubic Co, and symmetric low coercivity fcc-Co. We expect the Co to be present as Co^0 with diameter in the nanometer range. We observed from the SEM evidence of incomplete reaction and elucidating of Co nanoparticles. Cobalt nanoparticles were identified as hexagonal in shape.

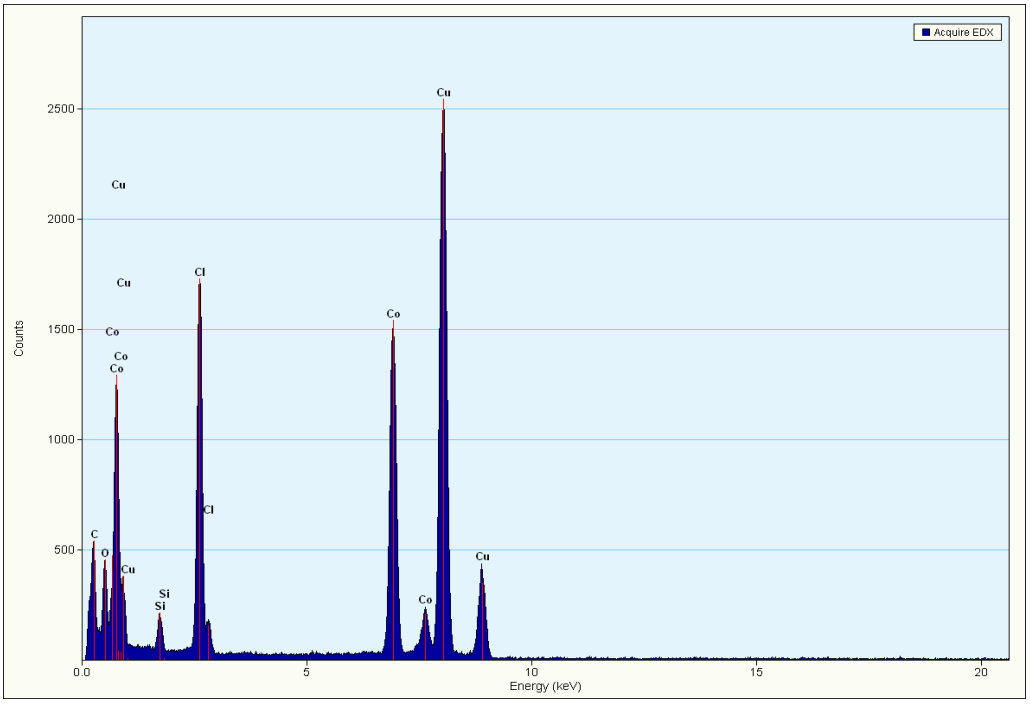

Fig3.5: EDX spectrum of the Co nanoparticles

The EDX spectrum of the Co, shows the presence of Co and the Cl, the presence of the Cl is from the $CoCl_2.6H_2O$ that was in the synthesis. The Cu present is due to the grid that was used to drop coat the Co nanoparticles onto.

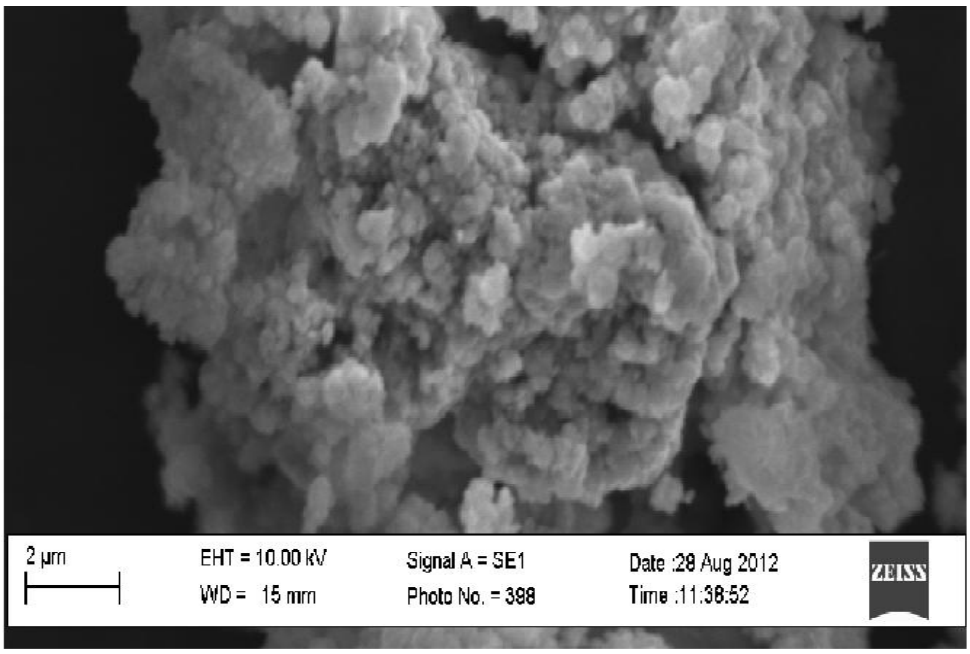

Fig3.6: SEM image of Cobalt nanoparticles

The SEM image of the Co nanoparticles showed that the nanoparticles are agglomerated and that the washing was not done properly since there are some traces of the starting material in the end product of the synthesis of the nanoparticles. Punte et al, reported that the large van der Waals forces and magnetic dipole interactions makes it hard to get isolated Co nanocrystals. The intensity of the applied megnetic field required to reduce the magnetization of sample to zero is known as coercivity. Coercivity measures the resistance of materials that are ferromagnetic to becoming demagnetized (Salazar-AlVarez *et al, 2007*)

3.2.2 Synthesis of Nickel nanoparticles

Nickel chloride ($NiCl_2.6H_2O$) weighed to be 0.1189g was dissolved in 50 mL ethanol to make a solution of 0.1M. The solution was stirred under magnetic stirrer. In the solution 0.025g of polyvinylpyrollidone (PVP) was added and the reaction mixture continued stirring. Both the sodium borohydride (0.0757g) and 0.3M sodium hydroxide were added to the reaction mixture and the reaction took 2hrs to be completed. The mixture was then centrifuged for 20min and the pellet was washed with distilled water. After centrifuging for another 20min the pellet was washed with ethanol and left to dry at 90^0C for 24hrs.

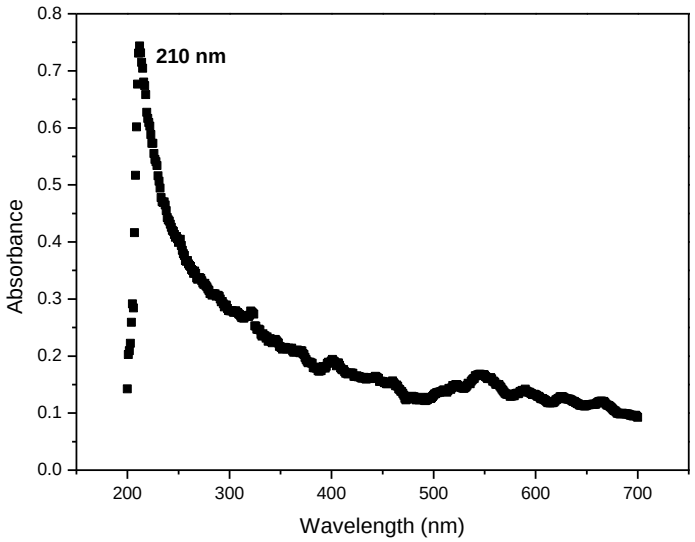

Fig 3.7: UV-VIS of Ni nanoparticles

The nickel nanoparticles showed absorbance at 210nm in the UV-vis spectrum. Meftah et al (2009) synthesized nickel nanoparticles by dissolving $NiCl_2$ salt in water and PVP was also added to the reaction mixture. The nickel nanoparticles showed absorbance at 395nm, the band is due to the electronic transitions from highly occupied electron orbital to the unoccupied electron orbital (Meftah *et al.,2009*).

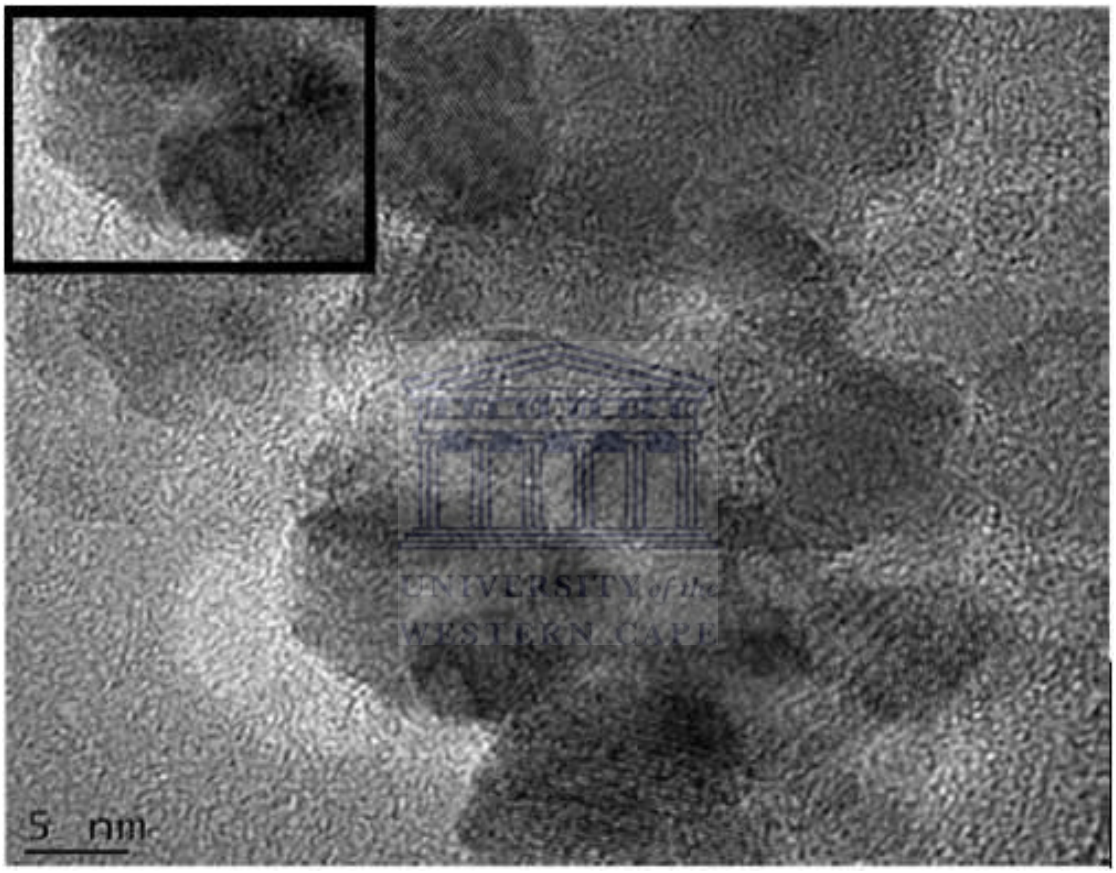

Fig3.8: HR-TEM image Ni nanoparticles

The Ni nanoparticle were synthesized using the $NaBH_4$ as the reducing agent and PVP as the capping agent. The Ni(II) forms complexes with three different geometries which tetrahedral, octahedral and square planar. Strong field ligands with Ni(II) forms square planar complexes and the weak ligands forms tetrahedral complexes. Ni nanoparticles are useful in catalysis, conducting inks and magnetic materials. The nanoparticles are known to exist in two

crystalline structures, fcc and hcp (Srisudha *et al, 2013*). The TEM image of the NiNPs confirms a cubic shape and particles size is 5nm.

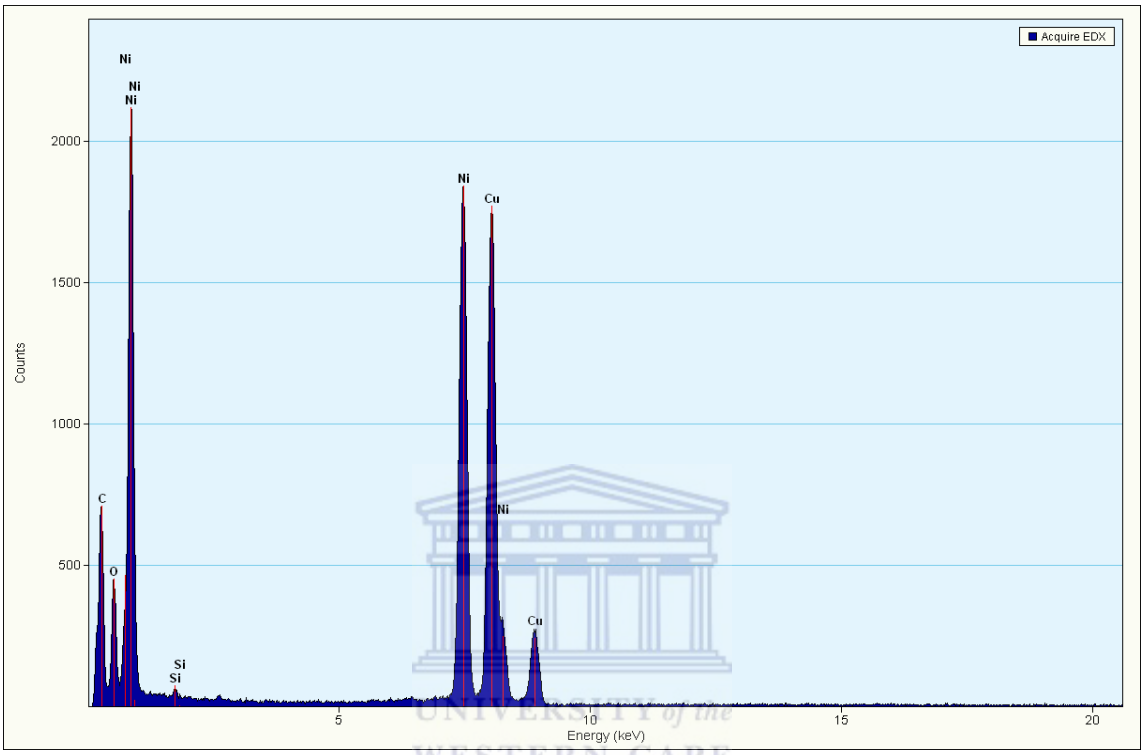

Fig3.9: EDX of the Nickel nanopartiles

The EDX spectrum of the Ni nanoparticles confirms the presence of nickel nanoparticles, with energy lines in the region of 8 – 9 kev which are the K lines and also in the region of 0.8 – 1 kev which are the L lines (Srisudha *et al, 2013*).

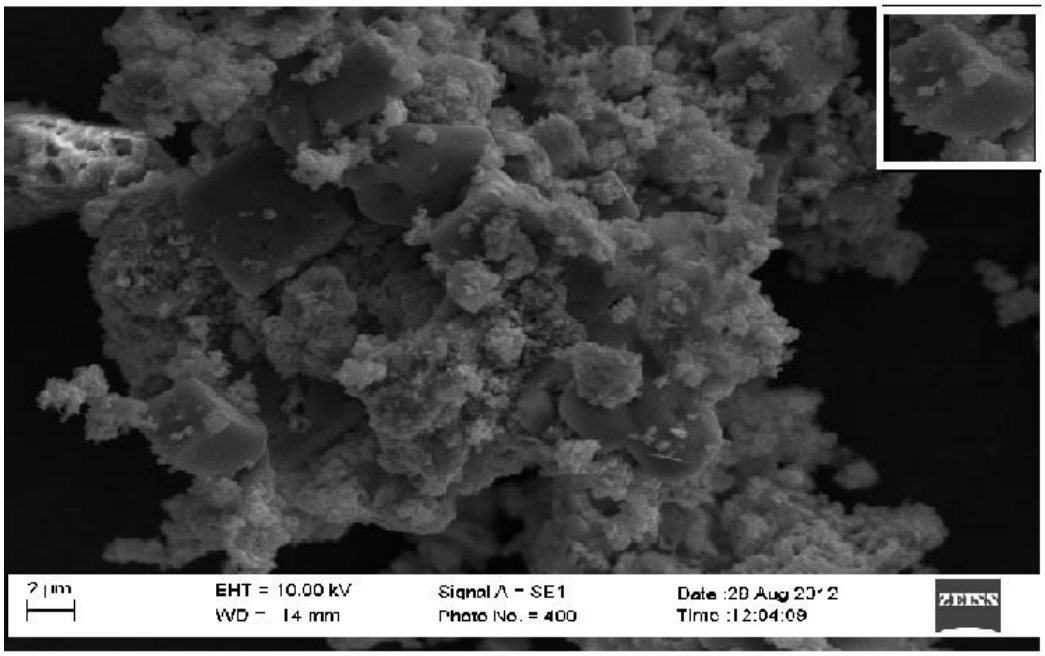

Fig3.10: SEM image of Ni nanoparticles. The insert shows cubic Ni nanoparticles.

The SEM image of the Ni nanoparticles, shows the particles to exhibit a cubic shape, however this was also observed in TEM of NiNPs. TEM also confirmed the dimensions of the cubic nanoparticles to be approximately 5 nm.

3.2.3. Synthesis of Silver nanoparticles

The synthesis of AgNp involved the reduction of the $AgNO_3$ with trisodium citrate. Briefly 50 mL of 1 mM $AgNO_3$ solution was heated to boiling using an Erlenmeyer flask. Into this solution, 5 mL of 1% $C_6H_5O_7Na_3$ was added dropwise. The solution was stirred vigorously by the use of a magnetic stirrer. The solution was heated until a pale yellow color was observed and the solution was removed from the heating surface and continued stirring until it cooled down to room temperature.

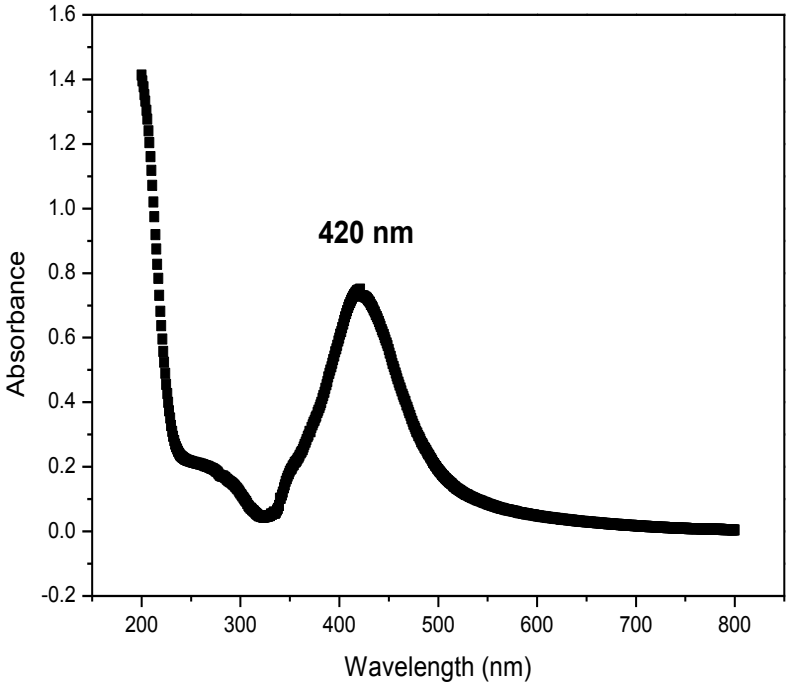

Fig 3.11: UV-VIS of AgNPs

After the synthesis of AgNPs the UV-vis characterisation was done and AgNPs absorbed at 420nm, A. Ahmad et al synthesized AgNPs and absorbed at 413nm. The shift in absorbance is due to the morphology of the nanoparticle and also the size plays a role in the absorbance of nanoparticles. Different shapes of silver nanocrystals possess a unique optical scattering response. Highly symmetric spherical particles exhibit single scattering peak, anisotropic shapes such as triangular, cubes and prisms exhibit multiple scattering peaks in the visible wavelength due to highly localized charge polarization (Yang *et al,2008*). The UV-VIS of metallic Ag^0 is in the range of 250nm to 330nm. From (fig 3.11) three absorption peaks were observed at 275nm, the other at 346nm and the last peak at 420nm and was the major peak. When the particle size is above 10nm the absorption band shifts to longer wavelength because of the high magnetic-dipole moment appear for larger radii particles (Baia *et al, 2007).*

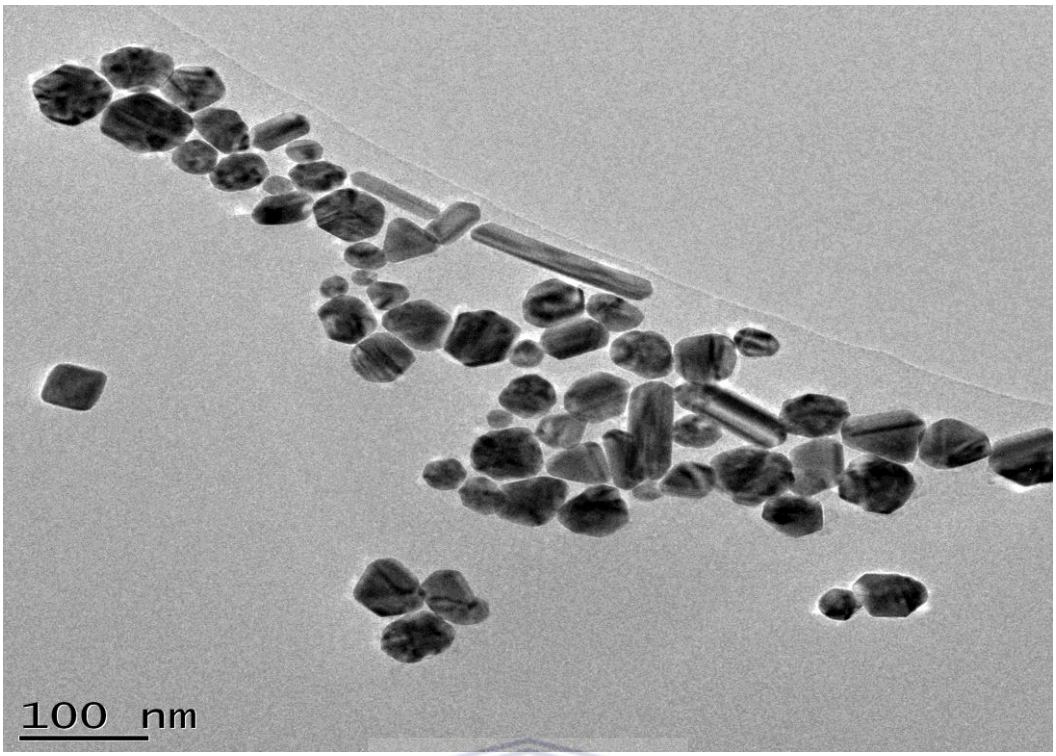

Fig3.12: HR-TEM image of the Ag nanoparticles which shows different shapes; spherical, cubic and hexagonal.

The size, shape and the crystalline properties of the nanoparticles were investigated using high resolution transmission microscopy. Nanoparticles produced were found to be well dispersed and non-agglomerated with an average diameter of 20-50 nm. Atomic lattice fringes were observed on the nanoparticles demonstrating the crystalline nature of the nanoparticles. The non-aggregation of the nanoparticles can be attributed to the electrostatic repulsion of negatively charged sodium citrate molecules which were adsorbed on the surface of the nanoparticles. The different shape distribution ranging from spherical, cubic, hexagonal and rods are evident in the TEM (fig3.12).

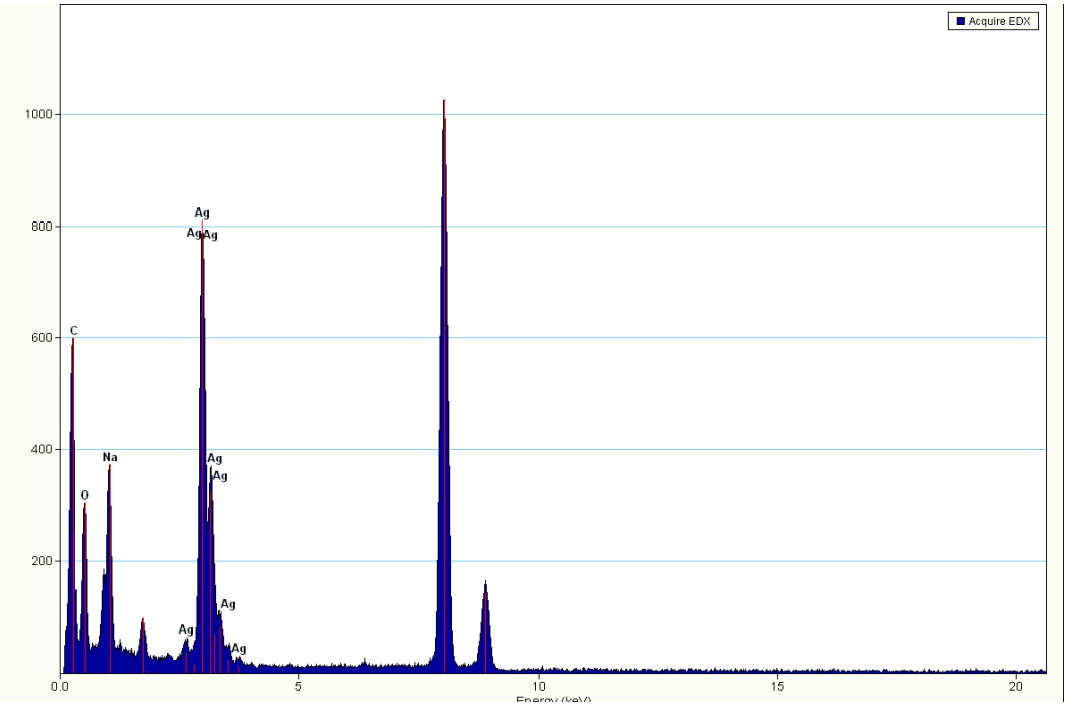

Fig3.13: EDX spectrum of the Ag nanoparticles

From the EDS spectrum Ag is present and Na which is from the reducing agent that was used to reduce $AgNO_3$ to AgNPs.

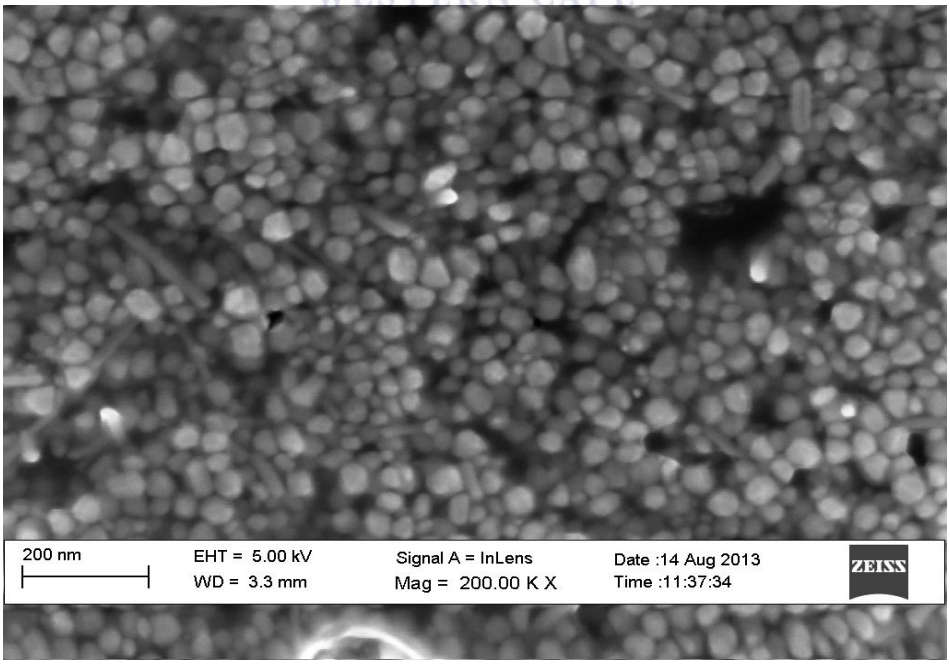

Fig 3.14: SEM image of Ag nanoparticles

The SEM image of the Ag nanoparticles showed different shapes ranging from spherical, cubic, hexagonal and rods. The size of the nanoparticles was in the range of 20-70nm.

3. 3 Preparation of nanocomposite thin films

3.3.1 Preparation of the nanocomposite films (Co, Ni, Ag nanoparticles)

Polysulfone was dissolved in N,N-dimethyl acetamide (DMAc) and the metal nanoparticle powder was added . The polysulfone was modified by measuring 5ml of the polysulfone into a small beaker, 10% the cobalt nanoparticles was added to the beaker and the mixture was sonicated until a uniform homogenous casting suspension was formed.

The same concentration of nickel nanoparticle solution (10%) was used when preparing a nickel nanocomposite solution

The 10% of the Ag nanoparticle suspension was drop coated onto 1 mL of polysulfone casting suspension. The dried polysulfone modified with Ag nanoparticle suspension was re-dissolved in 2 mL of N,N- dimethyl acetamide

For nanocomposite film, a 2 µl aliquot of the solution was drop coated onto the Pt working electrode surface. For the electrochemical characterisation of the thin film, 3 mL 0.1 M HCl was used as the electrolyte for the experiments.

All solutions that were prepared analytical grade reagents and purified water from a Milli-pore Mill Q system. The analytical grade argon gas was used to purge the system.

3.4 Characterisation of the prepared thin films

3.4.1 Scanning electron microscopy

Scanning electron microscopy of the chemically prepared membrane nanocomposites was done to observe the surface morphology of the materials. The sample in SEM is imaged by scanning the sample with a high-energy beam of electrons in a raster scan pattern. The electrons interact with the atoms that make up the sample producing signals that contain information about the sample's surface topography, composition and the morphology.

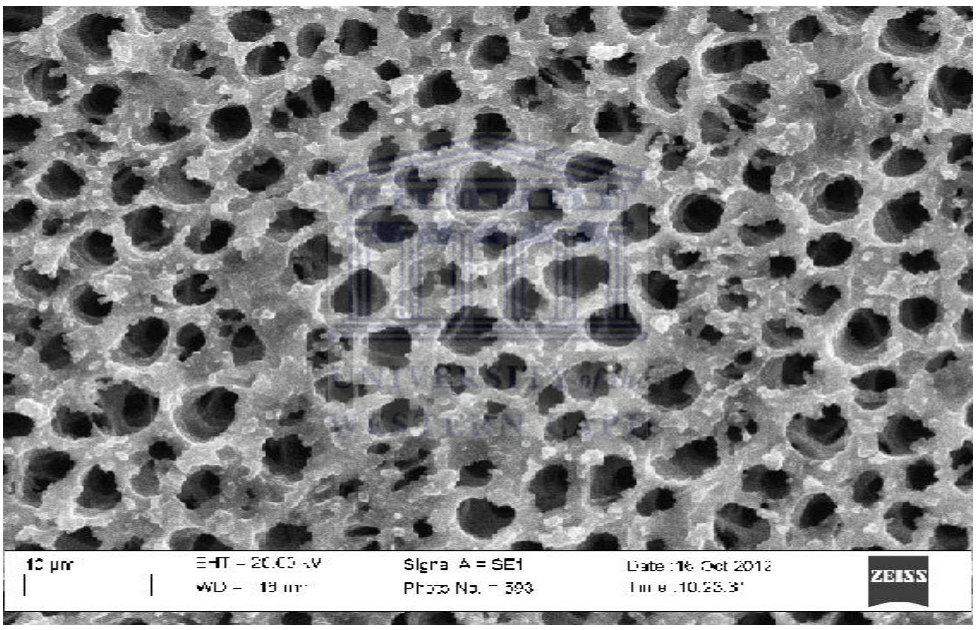

Fig3.15: SEM image of the Polysulfone modified with Cobalt nanoparticles

The SEM image of PSF/Co shows a uniformly distribution of pores, with an average of pore size ranging from 1.75 -7.88 µm. A 3D honey comb structure was observed for PSF/Co

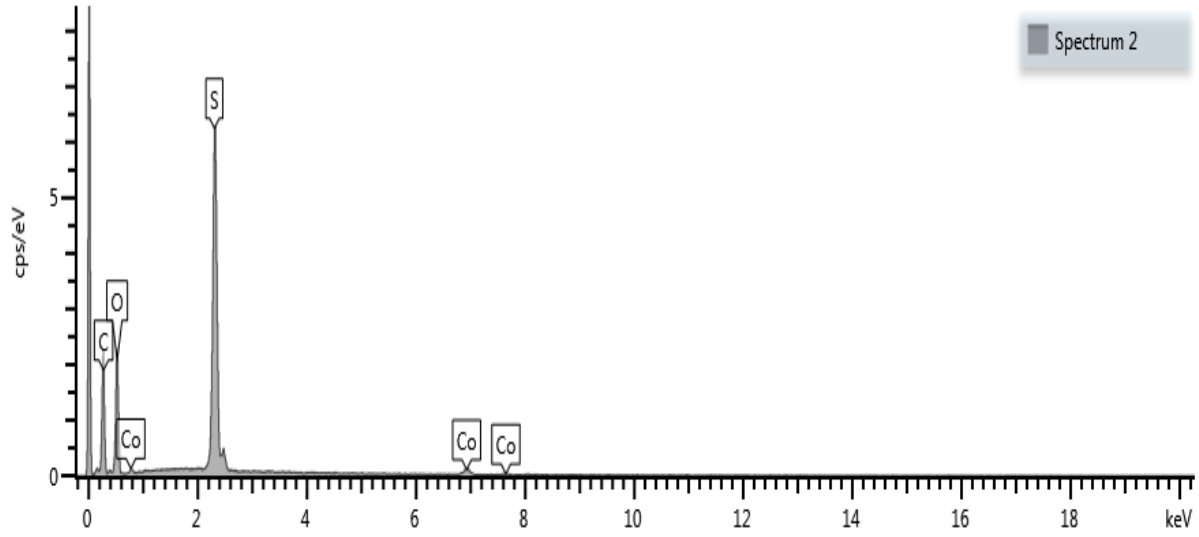

Fig3.16: EDS of PSF modified with Co nanoparticles

The SEM image of the PSF modified with the Co nanoparticles shows well organised pores. The EDS spectrum confirms that the Co nanoparticles are incorporated in the PSF casting suspension in the range of 6.8 keV to 7.6 keV.

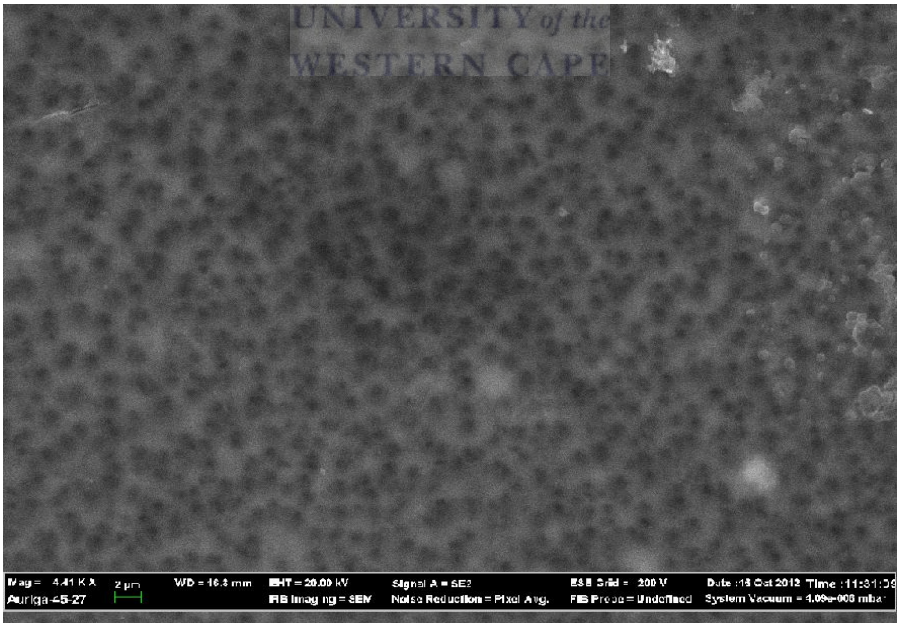

Fig3.17: SEM image of Polysulfone modified with Nickel nanoparticles

The SEM image of PSF/Ni small pores that are uniformly distributed were observed. Because of the size of the pores measuring the pore size was difficult to measure them. The pore size of the polysulfone modified with nickel nanoparticles was ranging from 0.4 – 1.5µm.

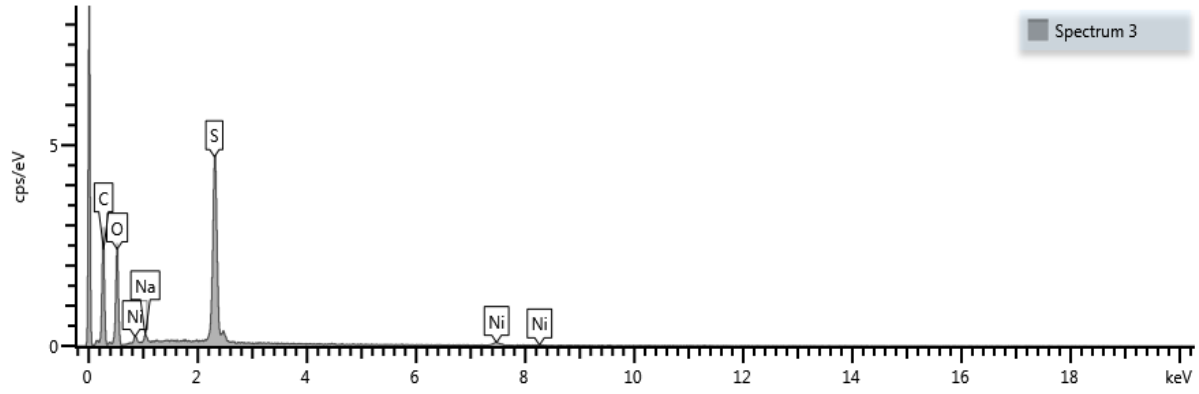

Fig3.18: EDS of Polysulfone modified with Nickel nanoparticles

The EDS spectrum for the PSF modified with the Ni nanoparticles confirms the incorporation of Ni in PSF. The Ni nanoparticles are in the range from 7.4 keV to 8.2 keV.

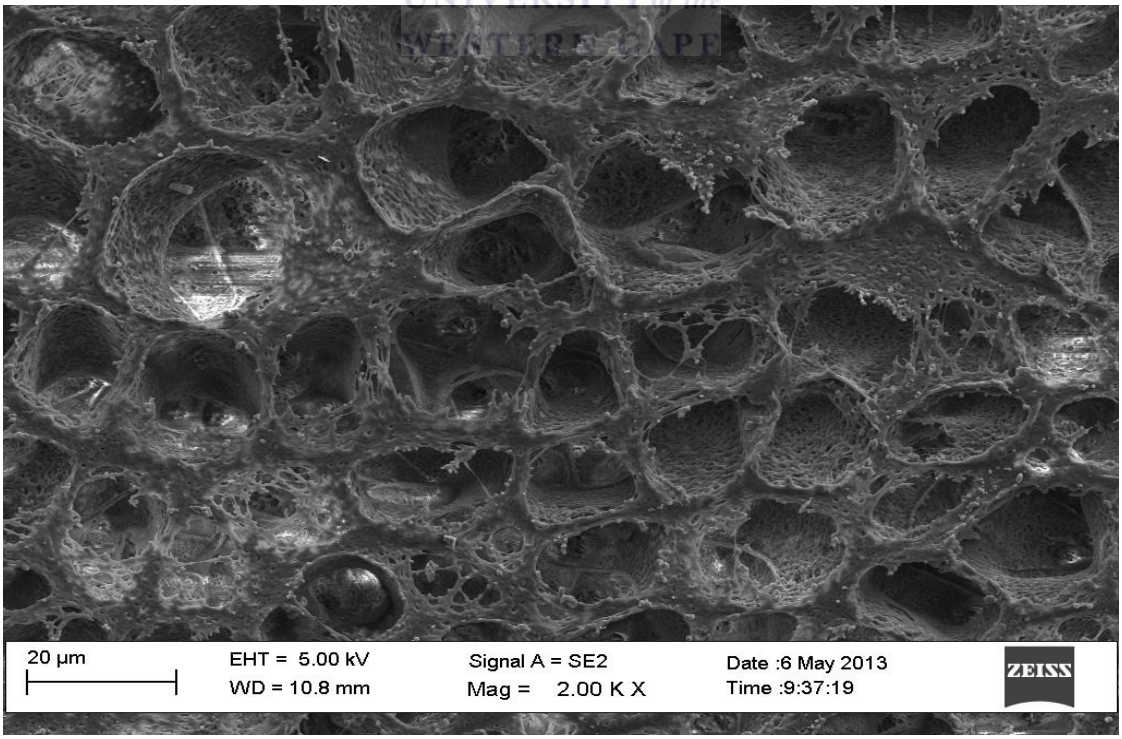

Fig3.19: SEM image of PSF modified with Ag nanoparticles

The SEM image of PSF/Ag shows a uniform distribution of pores, with the pore size of 10.73 – 15. 88 µm.

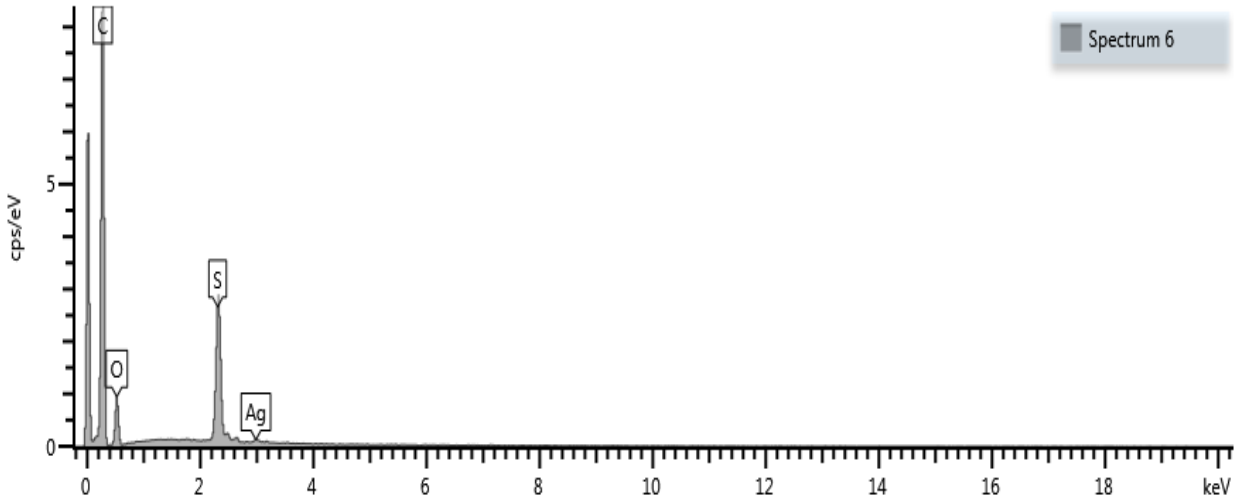

Fig3.20: EDS spectrum of PSF/Ag

EDS spectrum of PSF/Ag confirms the incorporation of AgNPs in the PSF casting solution

Both the PSF/Co and PSF/Ag showed to have larger pores than the PSF/Ni. PSF/Ag had larger pores, followed by PSF/Co and the last was PSF/Ni. The Ag nanoparticle are at 3keV.

Crystal lattice is a systematic arrangement of atoms that are found in crystals with the exception of amorphous solids and gases. A unit cell is the smallest component of the crystal lattice and illustrates the arrangement of atoms in a crystal. The unit cell is characterized by its lattice parameters which consist of the length of the cell edges and the angles between them. The lattice constant and also known as lattice paramet refers to the constant distance between unit cells in a crystal lattice. The lattices in three dimensions generally have three lattice constants: a, b, and c. In case of cubic crystal structures, all of the constants are equal and refered only as *a*. However, in case of hexagonal crystal structures, the a and b constants are equal, and only refered to as a and c constants (Yoshichiko Bandu *et al.*, 1986). Ni nanoparticles are known to favour a cubic close packed arrnagement (or fcc) whereas Co

nanoparticles favour a hexagonal closed packing (hcp) arrangement (Matveev *et al*., 2006). However the packing efficiency of both these packing arrangements are high (74%) with co-ordination number of 12. In a fcc unit cell the atoms touch along the face diagonals and the lattice parameter may be calculated from equation 1 as follows:

$$4r = a(2)^{½} \quad (1)$$

Where r, is the radius of Ni = 0.1246 nm

For the hcp close packing arrnagement the lattice paramters a (=b) and c may be calculated from the radius as follows using equoations 2 and 3:

$$a = 2r \quad (2)$$

and

$$2a = [(a / \sqrt{3})^2 + (c/2)^2]^{½} \quad (3)$$

where r is the radius of Co = 0.1253 nm

The lattice parameters for Co and Ni nanoparticles were calcuated based on unit cell dimensions identified from TEM measurements (Table 3.1)

Metal nanoparticle	Nanoparticle size (nm)	Membrane pore size (µm)	Lattice parameters a,b,c (Å)
Co	h = b = 50, l =100	2 – 8	$a = 2.506x10^{-11}$ $c = 8.32x10^{-12}$
Ni	l = 5	0.5 – 1.5	$a = 2.492x10^{-11}$
Ag	40 - 70	10 - 16	-

Table 3.1: *table showing the particle size of the metal nanoparticles, pore size of the modified membrane and also showing the lattice constant of the nanoparticle*

From the above table, it is clear that the metal nanoparticle size and close packing arrangement direct the shape and size of pore formation. Nickel nanoparticles with the smallest produced the smallest pore size in the modified polysulfone membrane, followed by Co nanoparticles. The irregular shape and size dsitribution observed for Ag nanoparticle formation, produced a membrane with very large pores.

Membrane Material	Contact angle (degrees)	Standard deviation (n = 4)
Polysulfone	87.5	25.2
Polysulfone/Co	31.7	7.68
Polysulfone/Ni	46.2	8.50
Polysulfone/Ag	49.5	3.77

Table 3.2: Contact angle measurements of the polysulfone membrane unmodified and the modified polysulfones and the standard deviation.

Contact angle measurements evaluate the angle between a water droplet and the flat membrane surface and provide an indication of the hydrophilicity (0-90°) or hydrophobicity (> 90°) of the membrane. The SEM in literature was used to indicate the pore size, membrane thickness and surface morphology. A decrease in contact angle of the surface with water was used as an indication of improvement in the hydrophilic property of the membrane. In contact angle for a hydrophilic membrane the contact angle should be 0 degrees, although the value is purely theoretical (J. Mulder, 1996).

The table shows PSF/Co to be the most hydrophilic membrane when compared to PSF/Ni and PSF/Ag, whereas the unmodified polysulfone membrane shows higher contact angle value. The modification of the polysulfone with metal nanoparticles shows improvement in hydrophobicity than the unmodified PSF.

3.5 AFM Results

Drop coating the polymers structures produced agglomerated clusters which had very uneven surface, which resulted in difficulty during probe approach and also loss of non-contact tips due to breakage. The surface roughness of the material on both the glass slide and the Pt working electrode made it difficult to perform AFM.

3.6 RAMAN Results

In preparing for the RAMAN measurements, the PSF casting solution was drop coated on a glass slide and left to dry. All the modified casting suspensions were prepared the same as the unmodified PSF.

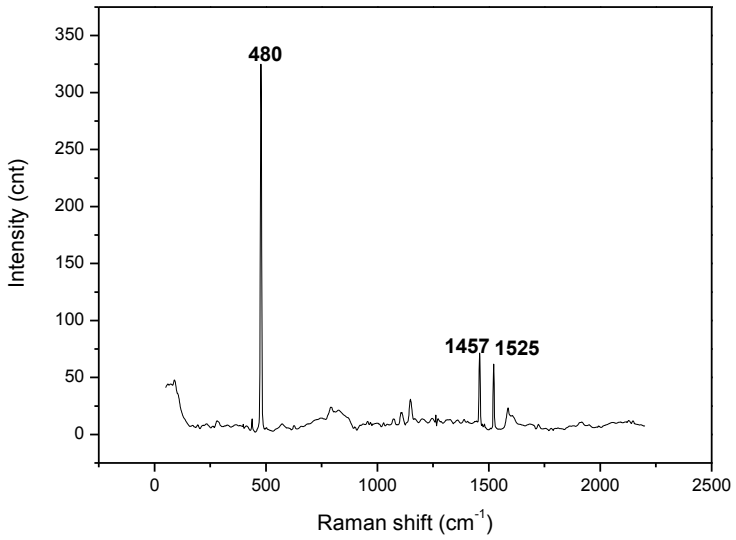

Fig.3.21: Raman spectrum of PSF

From (fig 3.21) the peak at 1457 cm^{-1} is an indicative of the aromatic ring. The peak at 1450cm^{-1} indicated an aromatic ring in the structure of the polysulfone.

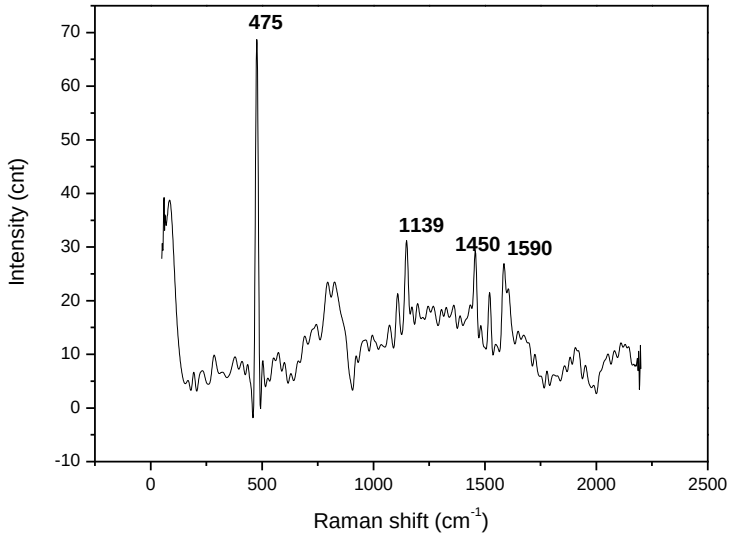

Fig.3.22: Raman spectrum of PSF/Co

The Raman spectrum of PSF/Co exhibit a new peak that was not observed in (fig 3.22) the peak at 1139 cm^{-1} was due to the symmetric C-O-C stretching mode, the peak at 1450cm^{-1} indicated an aromatic ring. The peak at 1590 cm^{-1} was due to the in-plane benzene ring vibration. Xu et al reported that CoNPs were used to coat the graphitic carbon (C-CoNPs). The Raman spectra of C-CoNPs, showed two major peaks centered at 1321 cm^{-1}(D peak) and the other peak at 1586 cm^{-1} (G peak). The signal is provided by the graphiticic layers that are present around the Co nanoparticles (Xu, *et al., 2008*). In 1996 Huang synthesized cobalt nanocrystals and coated onto a graphite carbon. Raman spectra of the prepared samples before and after acid titration were illustrated. Huang reported that there was a peak at 700 cm^{-1} that was observed in the spectrum which is due to uncoated cobalt nanoparticles. After months of the carbon coated cobalt nanoparticles in the acid, from the Raman a peak from 1582cm^{-1} -1603 cm^{-1} and the other from 1342cm^{-1} – 1320 cm^{-1} were observed to be broader. The peak intensities were reversed, indicating that the carbon shell surrounding cobalt

nanoparticles becomes more disorded instead of exhibiting the expected acid catalytic graphitization (Huang, *et al., 1998*)

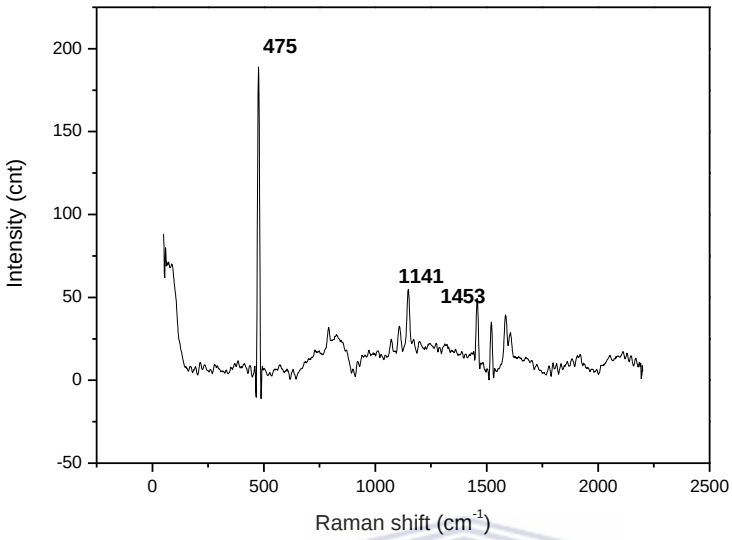

Fig3.23: Raman spectrum of PSF/Ni

The Raman spectrum of PSF/Ni exhibit a similar peak that was observed for PSF/Co at 1141cm^{-1} which indicates the symmetric C-O-C stretching mode and the in-plane benzene ring vibration peak at 1453cm^{-1}.

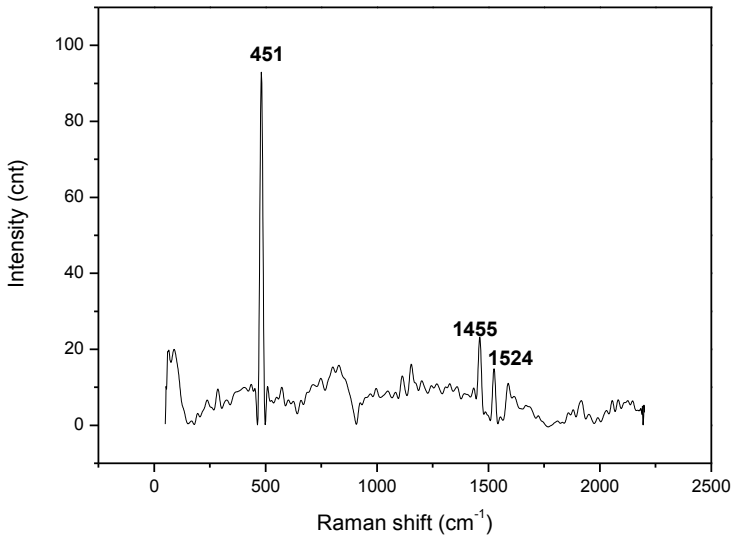

Fig3.24: Raman spectrum of PSF/Ag

The PSF/Ag behaved similar to the PSF having 3 peaks, the peak at 1455 cm^{-1} is an indicative of an aromatic ring and the in-plane benzene ring vibration peak at 1524 cm^{-1}.

The Raman spectra of the polysulfone modified with cobalt showed a new peak at 1139 cm^{-1} the peak was not observed for the unmodified polysulfone. The Raman spectrum of PSF/Ni exhibited a similar peak that was observed for PSF/Co at 1141cm^{-1} which indicates the symmetric C-O-C stretching mode. The Raman spectra of the PSF/Ag showed a shift in peaks one at 1455 cm^{-1} and the other at 1524 cm^{-1}.

3.7. Electrochemical Characterisation

3.7.1 Cyclic Voltammetry

The Cyclic voltammetry and the Square Wave voltammetry studies were done to study the electrochemistry of the PSF, PSF/Co, PSF/Ni and PSF/Ag and to be able to calculate the diffusion coefficient and the formal potential. The membrane materials were drop coated onto a Pt working electrode, Ag/AgCl in 3 M NaCl as the reference electrode and Pt wire as the counter electrode. The experiments were done using 3 mL of 0.1 M HCl as the electrolyte solution. The potential window was between -200mV to 1500 mV.

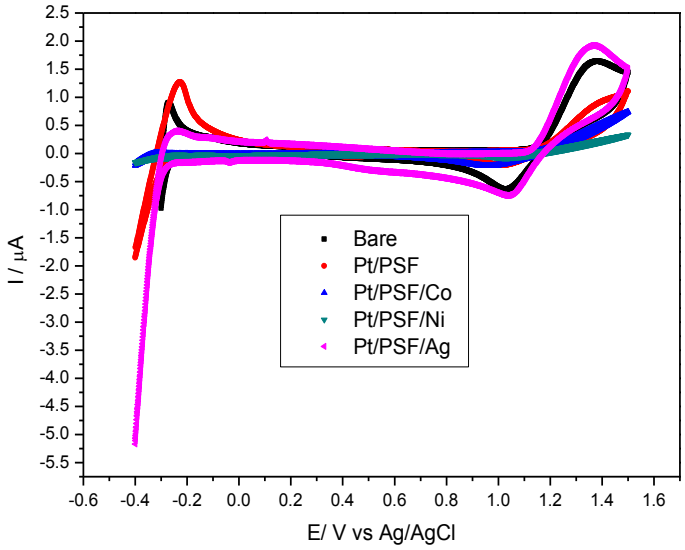

Fig3.25: CV of the polysulfone unmodified, modified polysulfone with metal nanoparticles and the Bare Pt electrode at 100mV/s

The CV of Pt modified with polysulfone membranes didn't show any additional peaks to the peaks that are due to the Pt bare electrode. However peak current response for the modified Pt electrode compared to bare electrode was distinctly different, the peak current was enhanced when the PSF was modified with Ag nanoparticles because silver is more conductive than Co and Ni. From the cyclic voltammetry the diffusion coefficient were calculated for each thin film prepared. Diffusivity or diffusion coefficient is related to the molar flux due to molecular diffusion and the gradient in the concentration of the species (or the driving force for diffusion) as a proportional constant. The diffusion coefficient is proportional to the squared velocity of the diffusing particles, which depends on the temperature, viscosity of the fluid and the size of the particles. In dilute aqueous solutions the diffusion coefficients of most ions are similar and have values that at room temperature are in the range of $0.6x10^{-9}$ to $2x10^{-9}$ m^2/s. For biological molecules the diffusion coefficients normally range from 10^{-11} to 10^{-10} m^2/s. The Randles-Sevčik equation was used to calculate the diffusion coefficient.

$$I_p = (2.69x10^5)An^{3/2}C_O D^{1/2}v^{1/2} \quad (4)$$

Membrane	Diffusion Coefficient (cm^2/s)	Formal Potential (V)
Polysulfone	$2.671x10^{-3}$	1.16
Polysulfone/CoNPs	$1.182x10^{-3}$	1.20
Polysulfone/NiNPs	$2.812x10^{-1}$	1.21
Polysulfone/AgNPs	$8.557x10^{-2}$	1.15

Table 3.3: Table of results showing the diffusion coefficient and the Formal potential of the unmodified PSF and modified PSF

The PSF/Ag showed to have smaller E^o than the other thin films in comparison of the Diffusion coefficient of the modified polysulfone membrane, PSF/Co shows to be the one with the lowest diffusion coefficient when compared to PSF/Ni and PSF/Ag. The PSF/Ni has the highest diffusion coefficient followed by the PSF/Ag. The unmodified PSF has the lowest diffusion coefficient than all the modified PSF thin films.

The metal nanoparticles were synthesised successfully and also were incorporation into the polysulfone membrane confirmed by the EDX and EDS. The SEM images of the modified polysulfone thin films showed that by modifying the polysulfone highly organised porous structures are formed. The contact confirmed that the modified thin films, the hydrophilicity were improved. From the CV, PSF unmodified in the presence of HCl showed high diffusion coefficient.

Chapter 4

Electrochemical analysis of the polysulfone thin films prepared at the presence of tannic acid and alginic acid using cyclic voltammetry and square wave voltammetry.

The electrochemistry of alginic acid and tannic acid showed measureable redox performance before onset fouling. This redox chemistry was evaluated using cyclic voltammetry and square wave voltammetry. Kinetics parameters associated with alginic acid and tannic acid was determined. The cyclic voltammetry studies of PSF, PSF-Co, PSF.-Ag and PSF-Ni were done at different concentration of the analyte to check the sensitivity of the electrode and whether the oxidation and reduction was taking place. Studies of different scan rates were also conducted to calculate the diffusion coefficient. Prepared materials were immobilised at a platinum electrode using the method of drop coating and 0.1 M of 3 mL HCl was the electrolyte used to conduct experiments. The Pt wire was used as the counter electrode and the Ag/AgCl in 3 M NaCl was used as the reference electrode. The modelling organic acids were introduced, the alginic acid (0.05 M) representing the class of polysaccharide and tannic acid (0.2 M) representing carbohydrates. The electrochemical window that was used was from -0.4V to 1.5V.

4.1 Cyclic Voltammetry of Polysulfone (PSF)

Cyclic voltammetry typically shows a single oxidation and reduction peak were symmetrically shaped irrespective of the scan rate associated with the formation of a PSF thin film at a Pt electrode. Linearity was observed for both peaks and the system shown to be diffusional controlled (Park S-Y, *et al 1999*). Tannic acid was chosen to represent the class of carbohydrates and the alginic acid represents the class of polysaccharides. Tannic acid (TA) is part of the group of the polyphenols. The polyphenol is oxidized to a

semiquinone during the oxidation process. When the semiquinone form of the polyphenol is generated another equivalent of Fe (III) can be reduced, simultaneously oxidizing the semiquinone to the quinone (Perron *et al., 2009*).

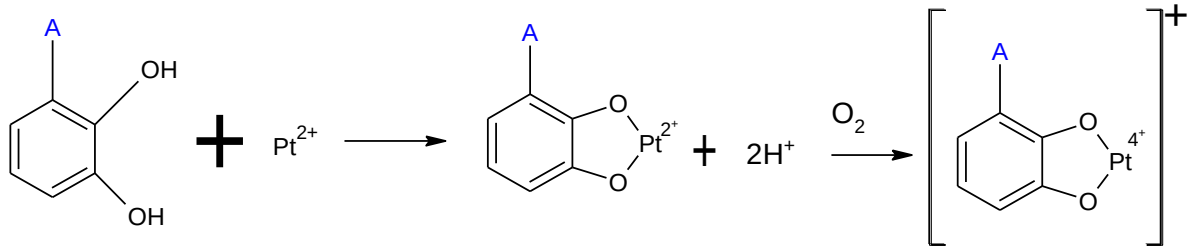

Fig 4.1: reaction mechanism of the Pt electrode with the polyphenol

The polyphenol in the reaction mechanism represents the tannic acid, the mechanism suggests a possible reaction that is taking place between the Pt electrode and the tannic acid.

For PSF films formed at a Pt electrode we observed three reduction peaks and one oxidation peak compared to bare Pt electrode which has two oxidation peaks and one reduction peak.

- CV of bare Pt and Pt/PSF in 0.1 M HCl

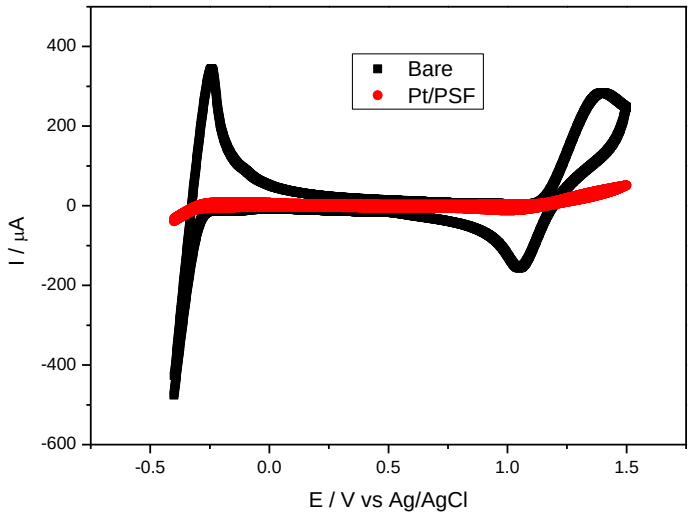

Fig4.2: CV of a bare Pt electrode (black) overlayed with Pt/PSF modified electrode (red).

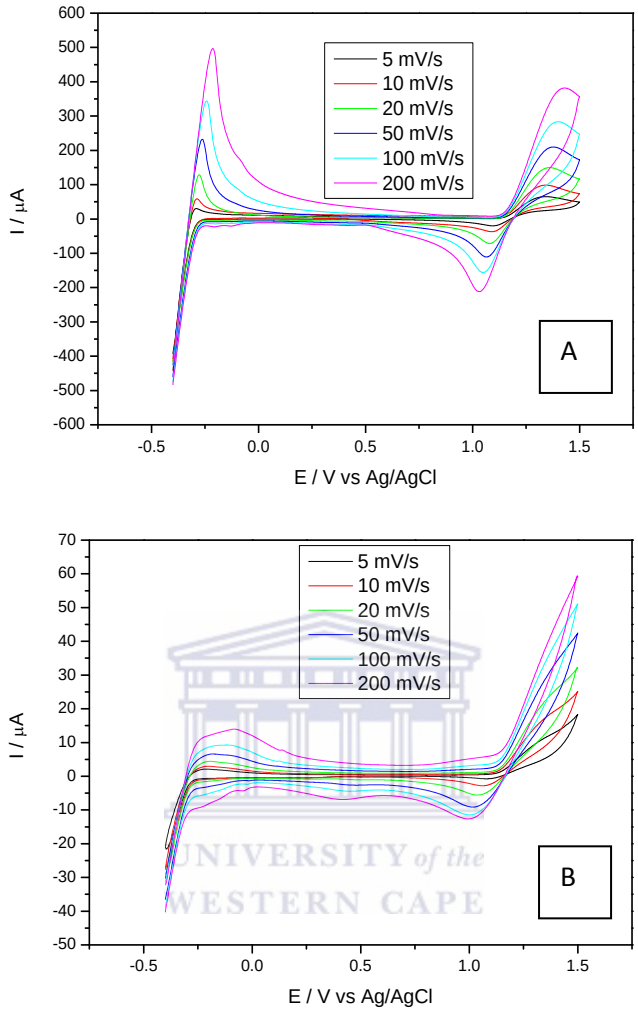

Fig4.3. Both studies are scan rate dependant studies (A) bare Pt and (B)Pt/PSF modified electrode

The linear regression for both the CVs where plotted and both curves shown to be linear suggesting that they are diffusional controlled. Both the studies are scan rate independent the current increased with the increasing scan rate. The diffusion coefficient of the Bare Pt electrode was found to be 1.02 $x10^{-2}$ cm^2 s^{-1} which was less than the diffusion coefficient of the Pt/PSF modified electrode which was 5.66 $x10^{-2}$ cm^2 s^{-1}.

4.2 Square Wave Voltammetry Results

Tannic acid and alginic acid were used as analytes both in CV and SWV. Polyphenols are plant secondary metabolites consisting of hydrolyzable and condensed forms.

The potential window that was used for the evaluation of tannic acid and alginic acid at different thin films prepared was from -400 to 1500 mV. The SWV was used to investigate further the peaks that were identified from the CV, because SWV is a high sensitive technique than the CV

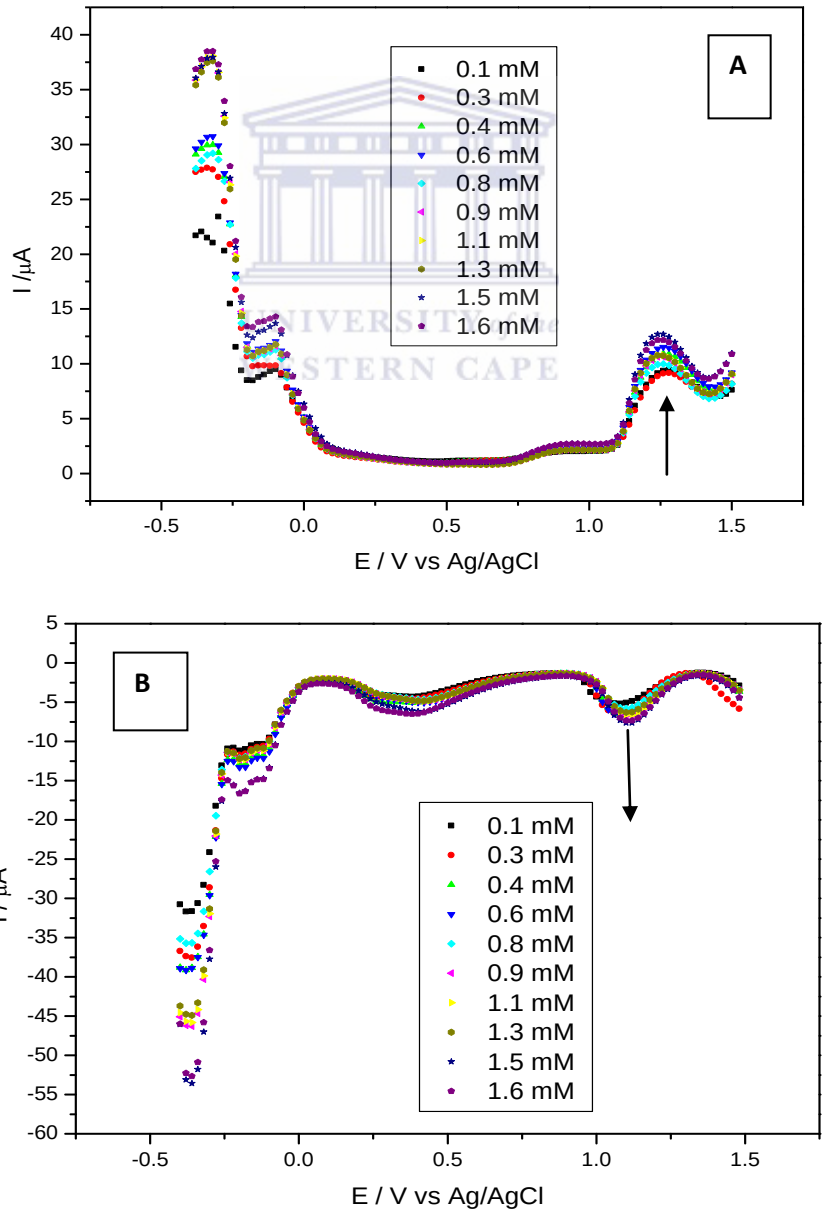

Fig.4.4:concentration dependant SWV of PSF in the presence of alginic acid , (a) oxidation SWV and (b) reduction SWV.

For unmodified PSF in HCl, two oxidation peaks at 0.89 V and 1.23 V were observed and two reduction peaks at 0.37 V and 1.19 V were also observed. The peak at 0.37 V was used to construct the calibration curve of Pt/PSF at different concentration of alginic acid (0.1mM – 1.6 mM), because it showed the change in current after every addition of alginic acid most clearly. However this peak was not observed to a have a reversible peak, therefore the formal potential for alginic acid at Pt/PSF was calculated for the reversible couple to be 1.16 V. The oxidation current was observed to be full catalytic as indicated by the increasing current with increasing concentration of alginic acid. The mechanism of the catalytic alginic acid involves a 2 step redox reaction as evidenced by the quasi reversible peak at 0.37 V and the reversible peak at 1.19 V. The oxidation product was observed to adsorb onto the Pt/PSF membrane since the reduction current in the reversible couple showed a decreasing trend.

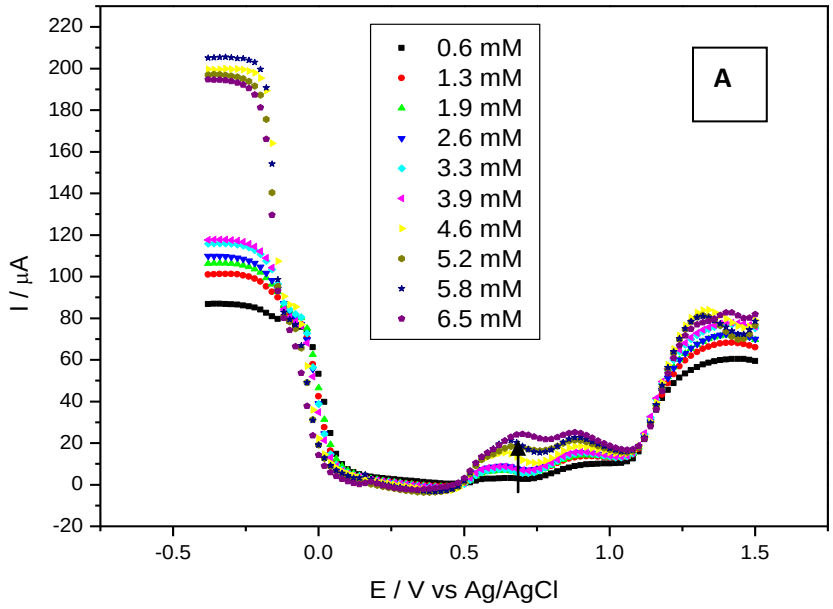

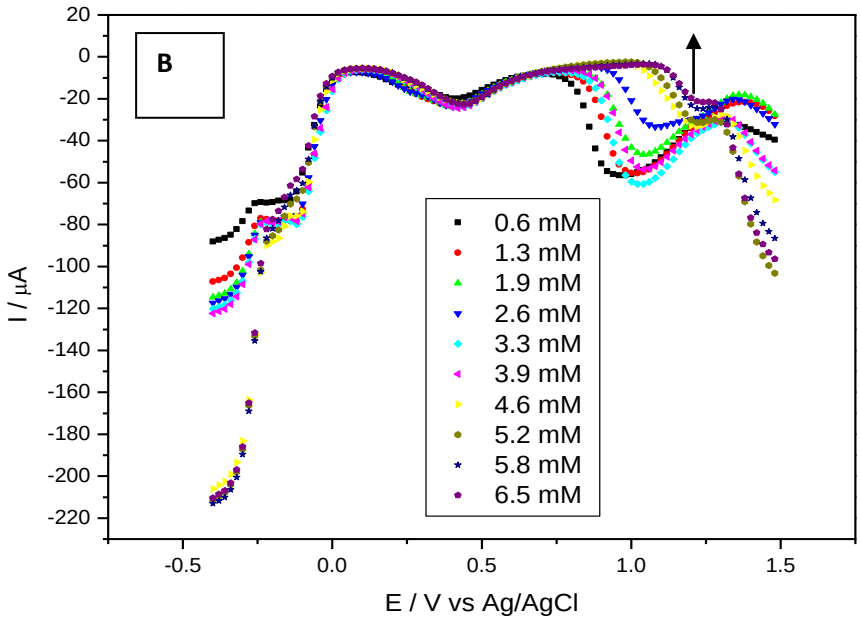

Fig.4.5: concentration dependant SWV of PSF in the presence of tannic acid (a) oxidation SWV and (b) reduction SWV

For the unmodified PSF membrane in HCl, three oxidation peaks at 0.58 V, 0.8V and 1.24 V were observed and two reduction peaks were also observed at 0.37V and 0.9 V. The peak at 0.58V was used to construct a calibration curve of Pt/PSF at different concentrations of tannic acid (0.6mM – 6.5 mM). The formal potential was calculated for reversible peaks to be 1.12 V and 0.47 V. The current response for the oxidation SWV at the PSF thin film with tannic acid showed to be catalytic as indicated by the increasing current with increasing concentration of tannic acid. The overlapping peaks indicate a 2 step coupled oxidation of tannic acid. The oxidation product was observed to adsorb onto the Pt/PSF membrane since the reduction current in the reversible couple showed a decreasing trend. The reduction peaks are well resolved.

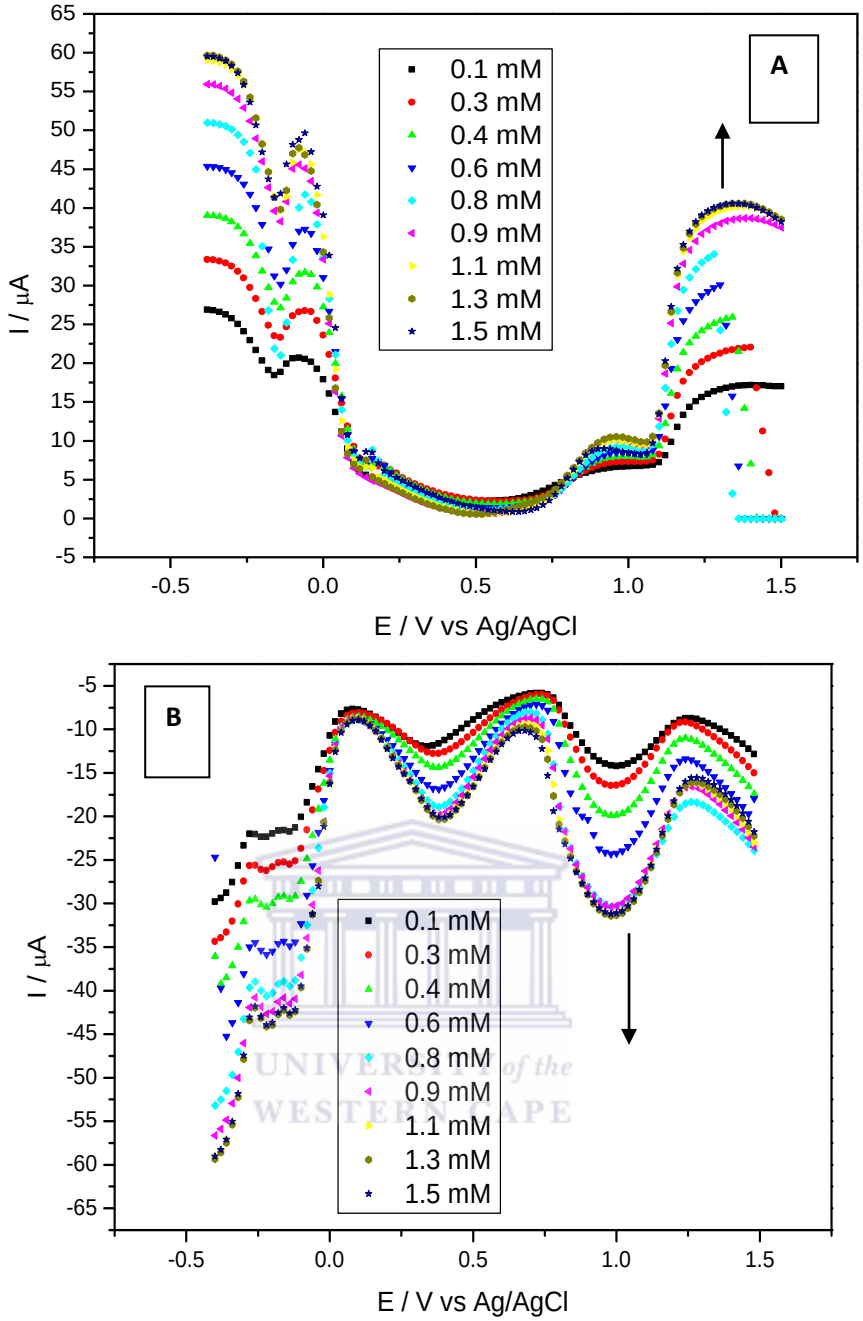

Fig.4.6: concentration dependant SWV of PSF/Co in the presence of alginic acid (a) oxidation SWV and (b) reduction SWV

For PSF modified membrane with Co nanoparticle in HCl, one oxidation peaks at 0.89 V was observed and two reduction peaks at 0.37 V and 1.19 V were also observed. The peak at 0.37 V showed the change in current after every addition of alginic acid most clearly and was used to construct the calibration curve of Pt/PSF/Co at different concentrations of alginic acid (0.1mM – 1.6 mM). However this peak was not observed to

a have a reversible peak, therefore the formal potential for alginic acid at Pt/PSF was calculated for the reversible couple to be 1.12 V. The oxidation current was observed to be full catalytic as indicated by the increasing current with increasing concentration of alginic acid. The oxidation product was observed to adsorb onto the Pt/PSF membrane since the reduction current in the reversible couple showed a decreasing trend.

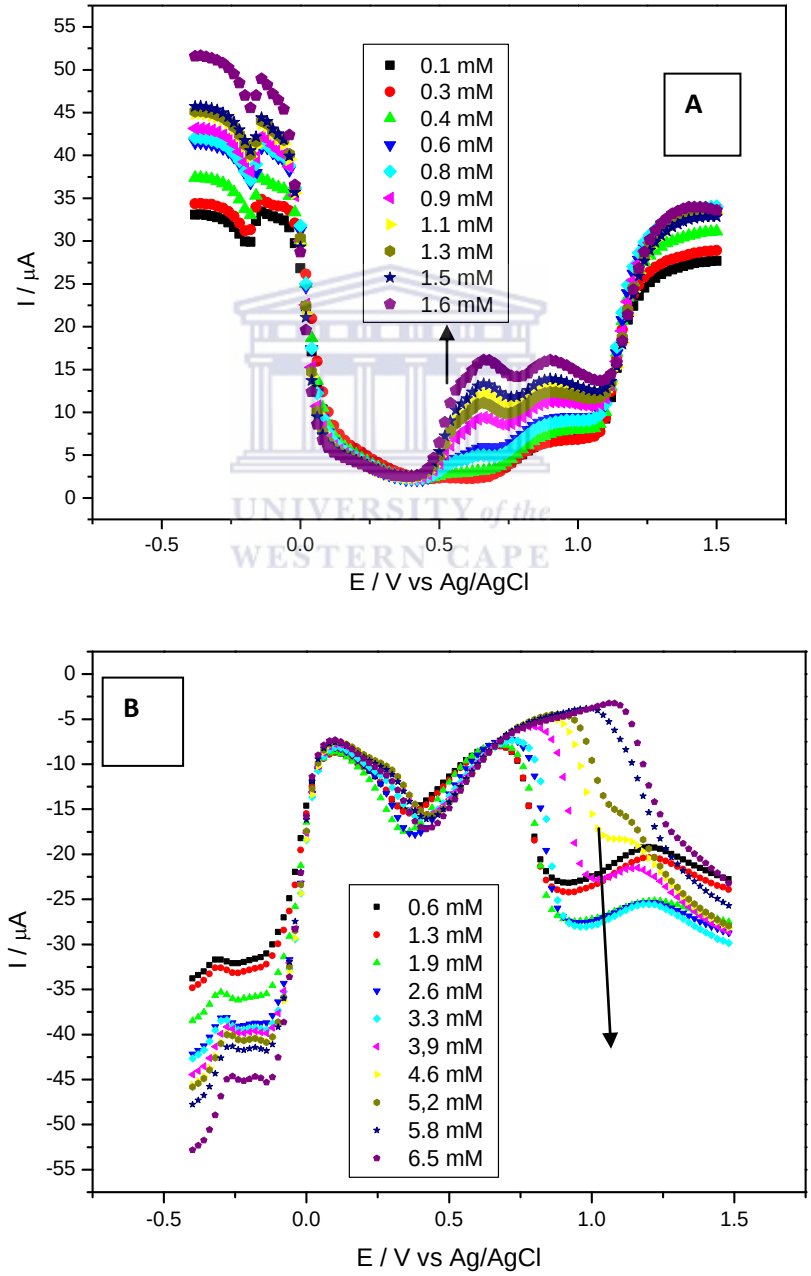

Fig.4.7: concentration dependant SWV of PSF/Co in the presence of tannic acid, (a) oxidation SWV and (b) reduction SWV

For the modified PSF with Co nanoparticles in HCl, two oxidation peaks at 0.58 V and 0.8 V were observed and two reduction peaks were also observed at 0.37 V and 0.84 V. The peak at 0.58V was used to construct a calibration curve of Pt/PSF/Co at different concentrations of tannic acid (0.6 – 6.5 mM). The current response for the oxidation SWV at the PSF/Co thin film with tannic acid showed to be catalytic as indicated by the increasing current with increasing concentration of tannic acid. The overlapping peaks indicate a 2 step coupled oxidation of tannic acid. The oxidation product was observed to adsorb onto the Pt/PSF/Co membrane since the reduction current in the reversible couple showed a decreasing trend. The reduction peaks are well resolved.

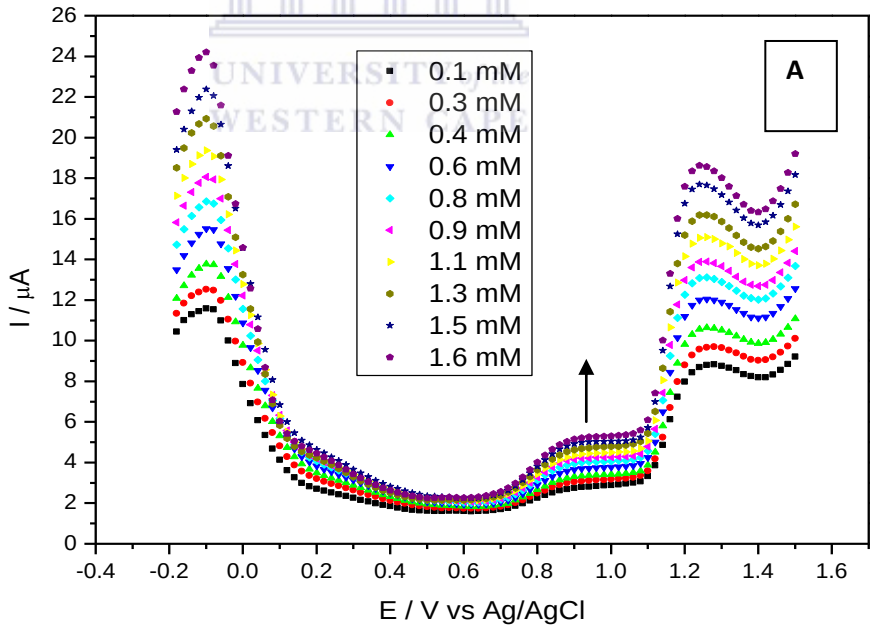

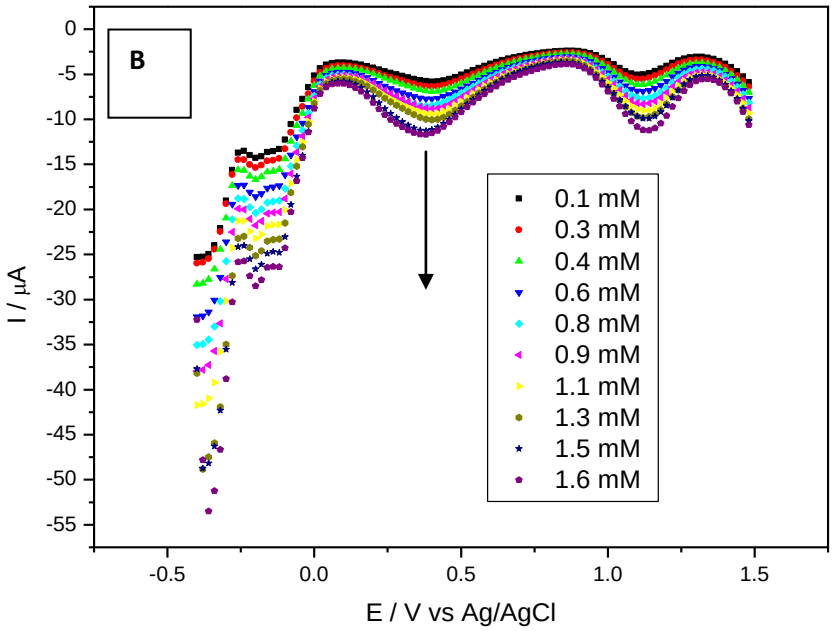

Fig.4.8: concentration dependant SWV of PSF/Ni in the presence of alginic acid

For PSF modified membrane with Ni nanoparticle in HCl, two oxidation peaks at 0.9 V and 1.23 V were observed and two reduction peaks at 0.37 V and 1.2 V were also observed. The peak at 0.37 V was used to construct the calibration curve of Pt/PSF/Ni at different concentration of alginic acid (0.1mM – 1.6 mM), because it showed a change in current after every addition of alginic acid most clearly. However this peak was not observed to a have a reversible peak, therefore the formal potential for alginic acid at Pt/PSF was calculated for the reversible couple to be 1.19 V. The oxidation current was observed to be full catalytic as indicated by the increasing current with increasing concentration of alginic acid. The mechanism of the catalytic alginic acid involves a 2 step redox reaction as evidenced by the quasi reversible peak at 0.37 V and the reversible peak at 1.2V. The oxidation product was observed to adsorb onto the Pt/PSF membrane since the reduction current in the reversible couple showed a decreasing trend.

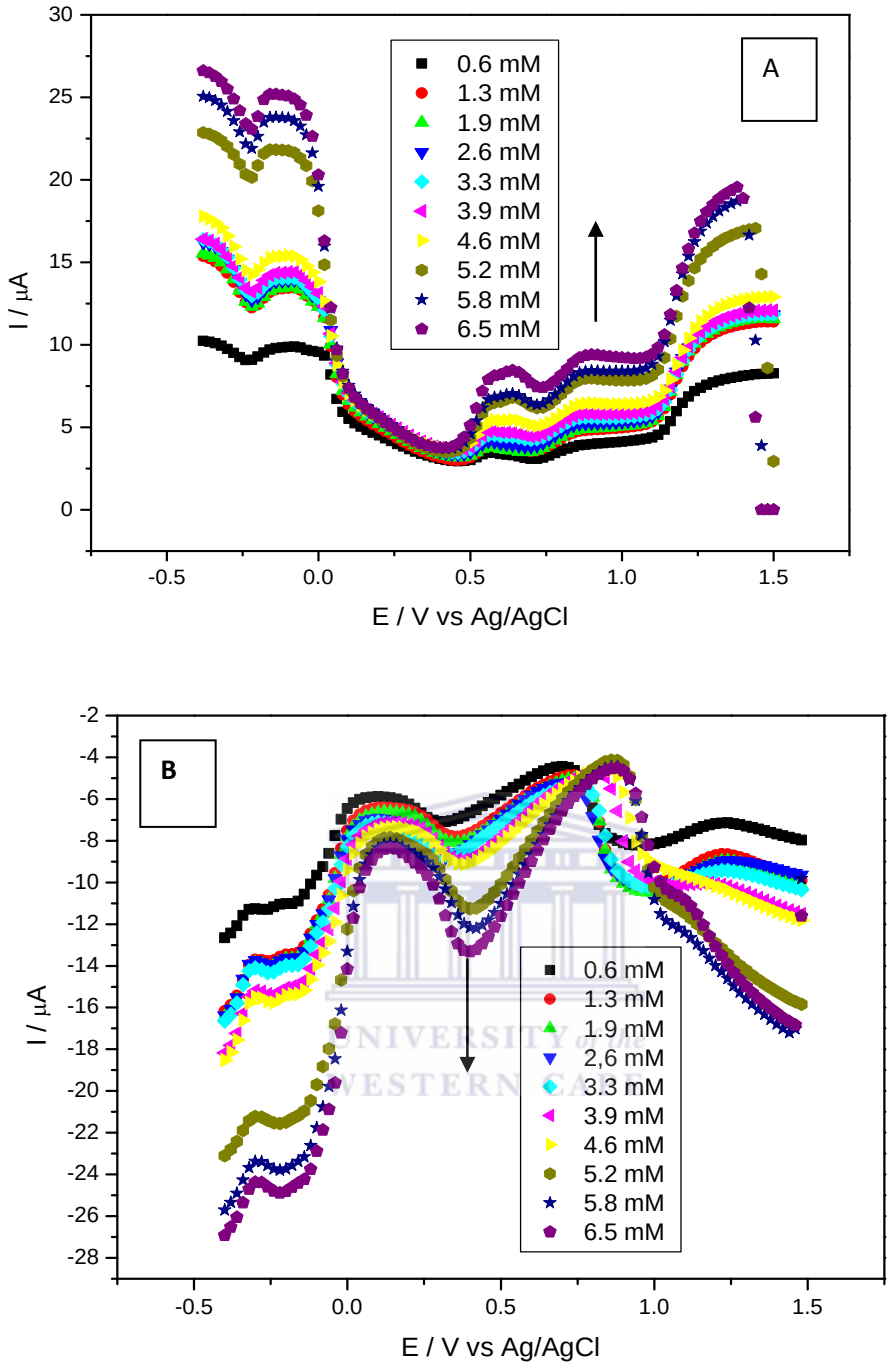

Fig.4.9: concentration dependant SWV of PSF/Ni in the presence of tannic acid, (a) oxidation SWV and (b) reduction SWV

For the modified PSF with Co nanoparticles in HCl, two oxidation peaks at 0.58 V and 0.8 V were observed and two reduction peaks were also observed at 0.37 V and 0.84 V. The peak at 0.58V was used to construct a calibration curve of Pt/PSF/Co at different concentrations of tannic acid (0.6mM – 6.5 mM). The current response for the oxidation SWV at the PSF/Co

thin film with tannic acid showed to be catalytic as indicated by the increasing current with increasing concentration of tannic acid. The overlapping peaks indicate a 2 step coupled oxidation of tannic acid. The oxidation product was observed to adsorb onto the Pt/PSF/Co membrane since the reduction current in the reversible couple showed a decreasing trend. The reduction peaks are well resolved.

.

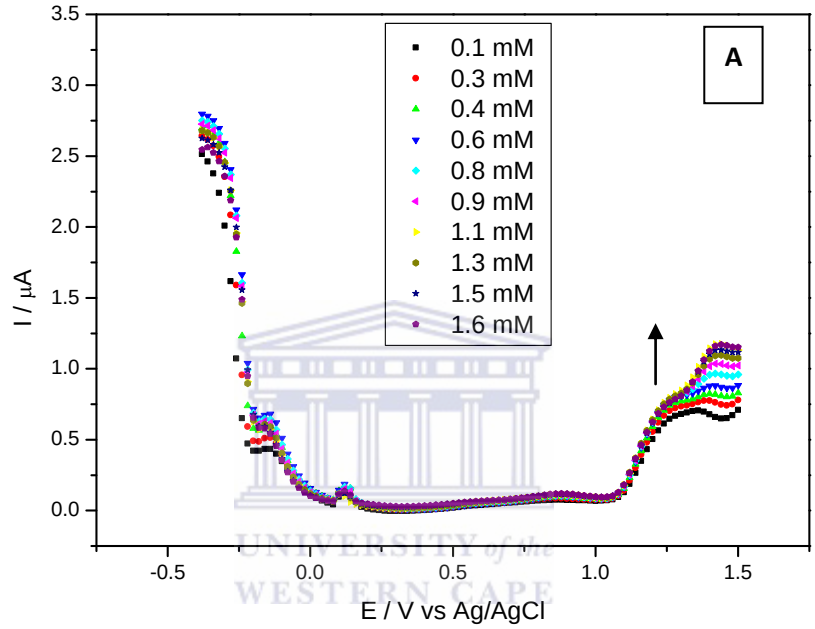

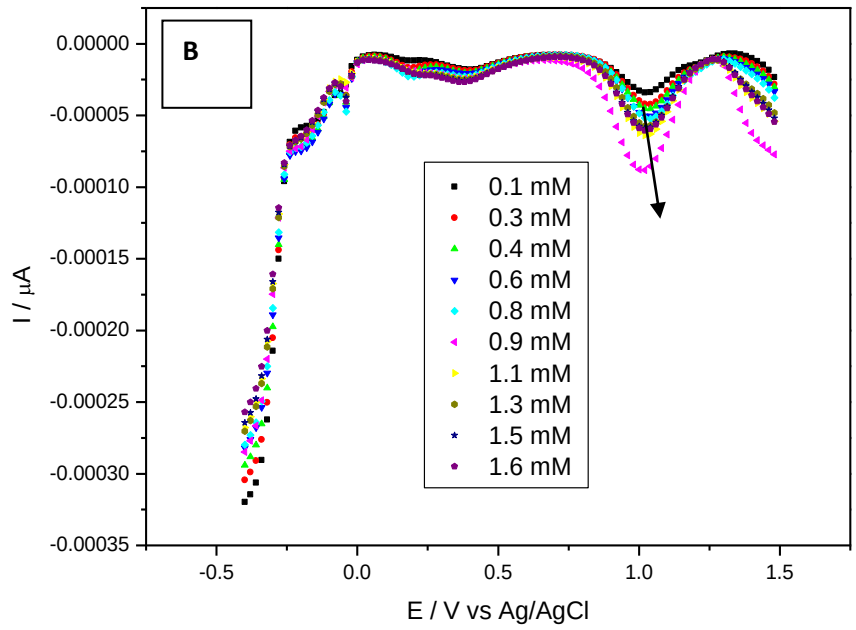

Fig.4.10:concentration dependant SWV of PSF/Ag in the presence of alginic acid, (a)oxidation SWV and (b) reduction SWV.

For PSF modified membrane with Ag nanoparticles in HCl, one oxidation peaks at 1.23 V were observed and two reduction peaks at 0.43V and 1.1 V were also observed. The peak at 1.1 V was used to construct the calibration curve of Pt/PSF/Ag at different concentration of alginic acid (0.1 – 1.6 mM), because it showed the change in current after every addition of alginic acid most clearly. However this peak was not observed to a have a reversible peak, therefore the formal potential for alginic acid at Pt/PSF was calculated for the reversible couple to be 1.21 V. The oxidation current was observed to be full catalytic as indicated by the increasing current with increasing concentration of alginic acid. The oxidation product was observed to adsorb onto the Pt/PSF membrane since the reduction current in the reversible couple showed a decreasing trend.

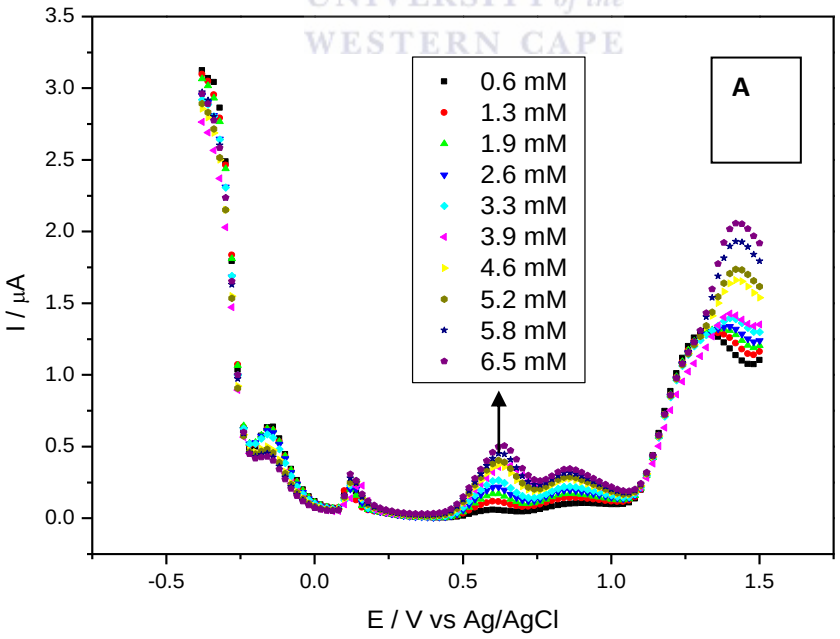

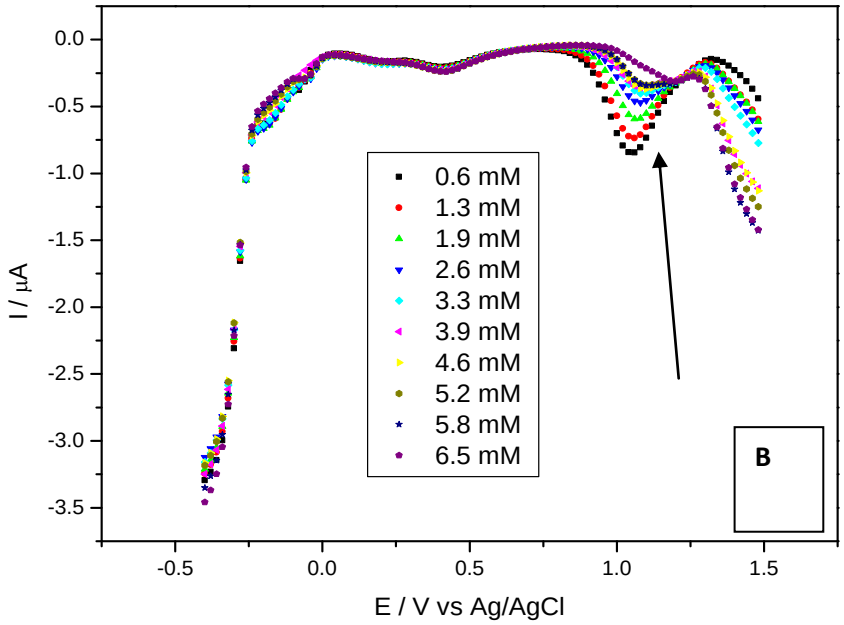

Fig.4.11: concentration dependant SWV of PSF/Ag in the presence of tannic acid

For the modified PSF with Ag nanoparticles in HCl, three oxidation peaks at 0.58 V, 0.8V and 1.25 V were observed and two reduction peaks were also observed at 0.43V and 0.98 V. The peak at 0.58V was used to construct a calibration curve of Pt/PSF/Ag at different concentrations of tannic acid (0.6mM – 6.5 mM). The current response for the oxidation SWV at the PSF/Ag thin film with tannic acid showed to be catalytic as indicated by the increasing current with increasing concentration of tannic acid. The overlapping peaks indicate a 2 step coupled oxidation of tannic acid. The oxidation product was observed to adsorb onto the Pt/PSF/Ag membrane since the reduction current in the reversible couple showed a decreasing trend. The reduction peaks are well resolved.

.

Thin film	Diffusion coefficient (cm^2/s)	Formal Potential
PSF	tannic acid = $2.671x10^{-3}$ alginic acid = $2.496x10^{-3}$	1.12 V 1.16 V
PSF/Co	tannic acid = $2.846x10^{-3}$ alginic acid = $1.288x10^{-3}$	1.26 V 1.12 V
PSF/Ni	tannic acid = $2.552x10^{-3}$ alginic acid = $3.199x10^{-3}$	0.96 V 1.19 V
PSF/Ag	tannic acid = $3.432x10^{-3}$ alginic acid = $4.629x10^{-3}$	1.22 V 1.21 V

Table 4.1: *Diffusion Coefficients of PSF, PSF/Co, PSF/Ni and PSF/Ag in alginic acid and tannic acid*

The PSF/Ag at tannic acid and alginic acid has the highest diffusion coefficient, meaning that the analyte moves faster to reach the thin film surface. The PSF/Ni has the 2nd highest diffusion coefficient in the presence of alginic acid, while the PSF/Co has the 2nd diffusion coefficient in the presence of tannic acid. The PSF/Ni showed to have a lower formal potential followed by the PSF. The standard deviation was calculated using the Formal potential value of the 4 thin films for tannic acid and alginic acid. The standard deviation for tannic acid was 0.13V/mM and for the alginic acid was 0.033 V/ mM.

The electrochemistry of the polyphenols (tannic acid and alginic acid) was evaluated. The polysulfone modified with Ag nanoparticles had the largest pores and also the highest diffusion coefficient however it showed to have the 3rd lowest contact angle when compared to polysulfone modified with nickel and polysulfone modified with cobalt nanoparticles. The polysulfone modified with nickel nanoparticles had the smallest pores, 2nd highest diffusion coefficient and the 2nd lowest contact angle. However the polysulfone modified with cobalt nanoparticles had the lowest contact angle, the least diffusion coefficient and the 2nd highest pore size.

4.3 Calibration curves

Concentration studies of the Pt/PSF, Pt/PSF/Co, Pt/PSF/Ag and Pt/PSF/Ni modified electrode was done to check the sensitivity of the electrode at different concentrations of the analytes. Calibration curves were constructed based the response from the CV

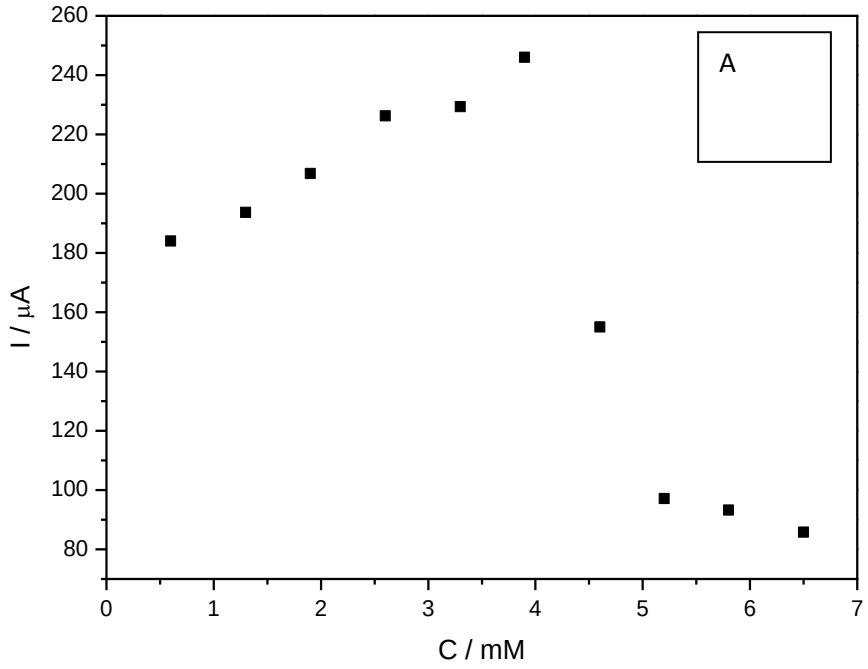

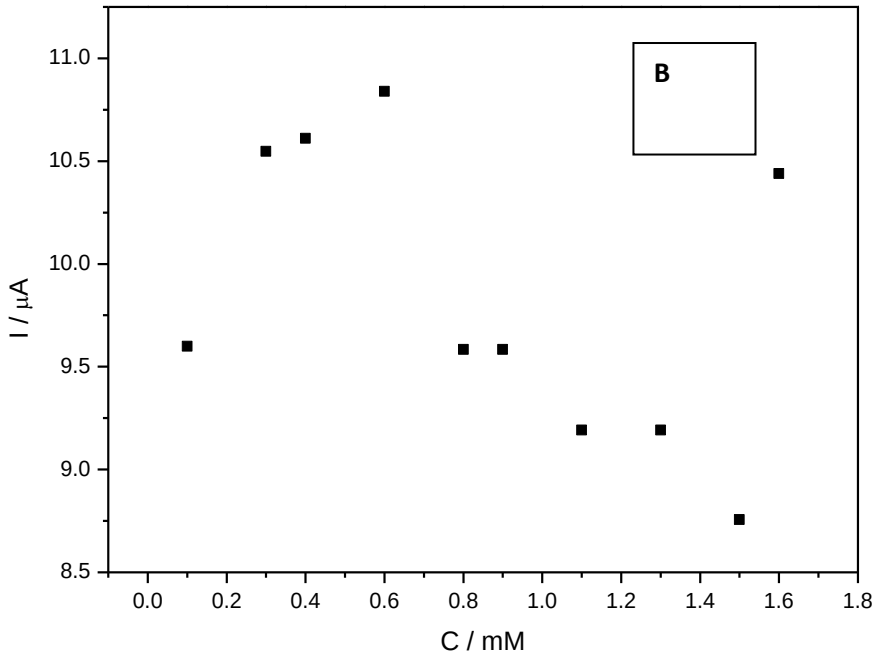

Fig.4.12: calibration curves (A) Pt/PSF at different concentrations of tannic acid, (B) Pt/PSF at different concentration of alginic acid

The polysulfone at tannic acid showed better sensitivity as evidenced by the higher slope than the PSF at alginic acid

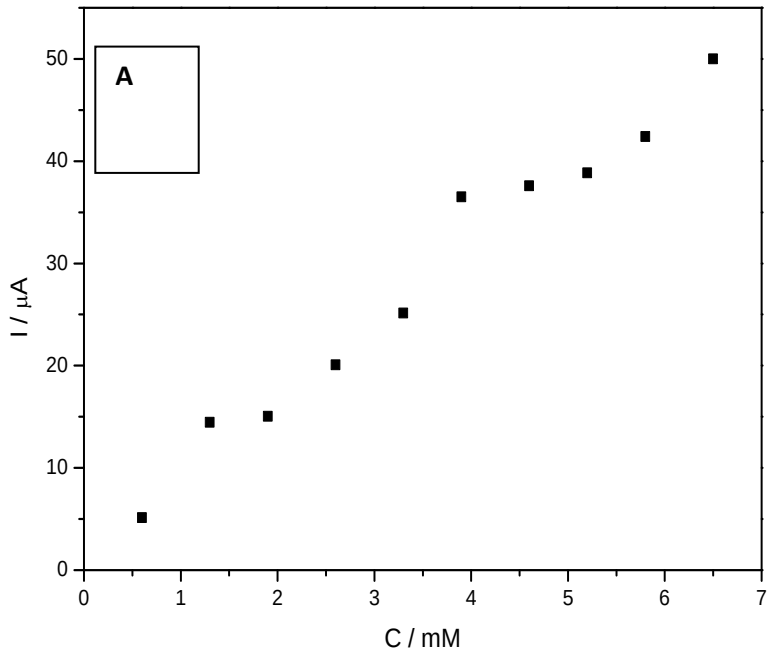

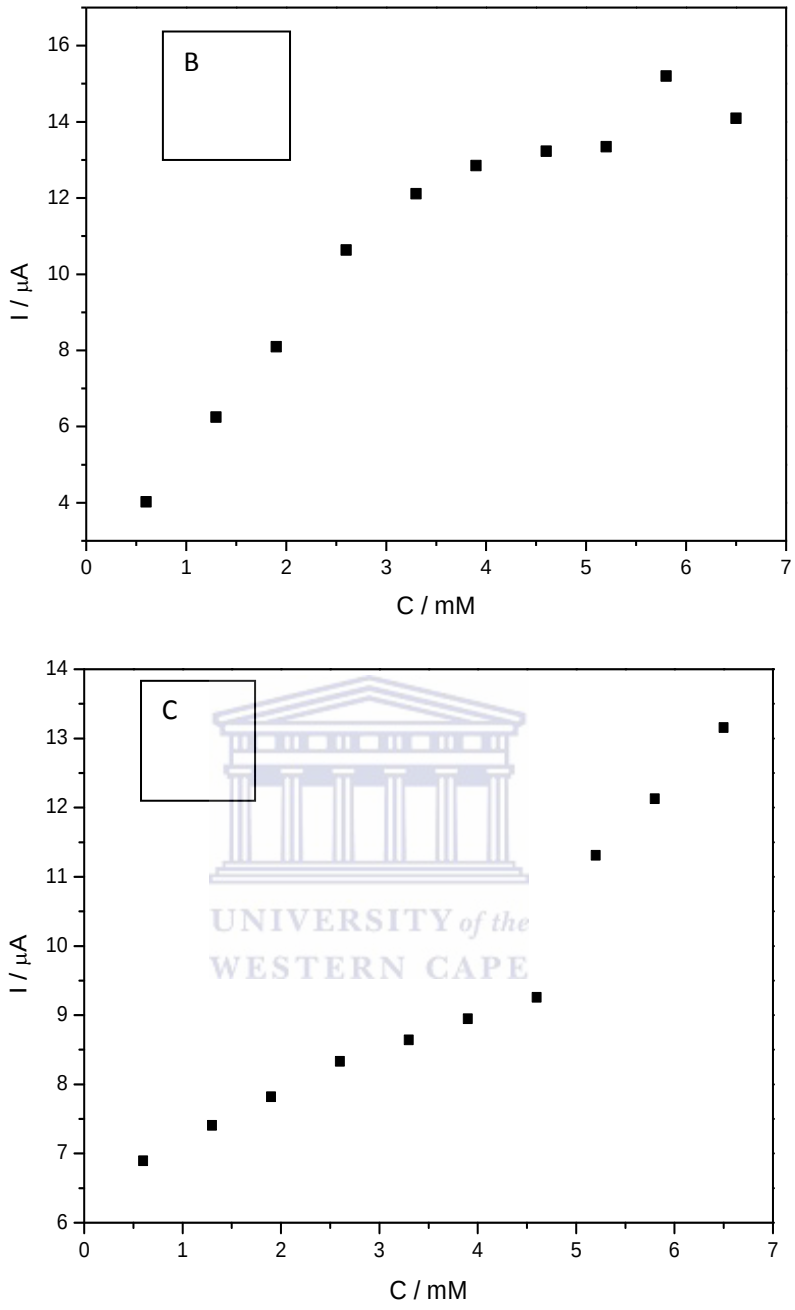

Fig 4.13: Calibration Curves; (a) Pt/PSF/Ag, (b) Pt/PSF/Co (c) Pt/PSF/Ni in the presence of tannic acid.

The PSF/Co showed better sensitivity because of the higher slope when compared to the PSF/Ni and PSF/Ag. PSF/Ni showed better quantitative detection because of the linear dynamic range of 0.6mM to 4.6 mM.

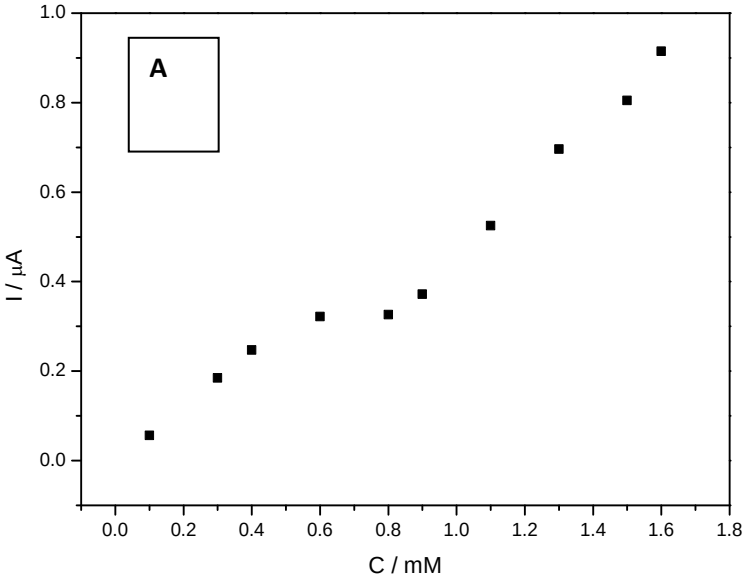

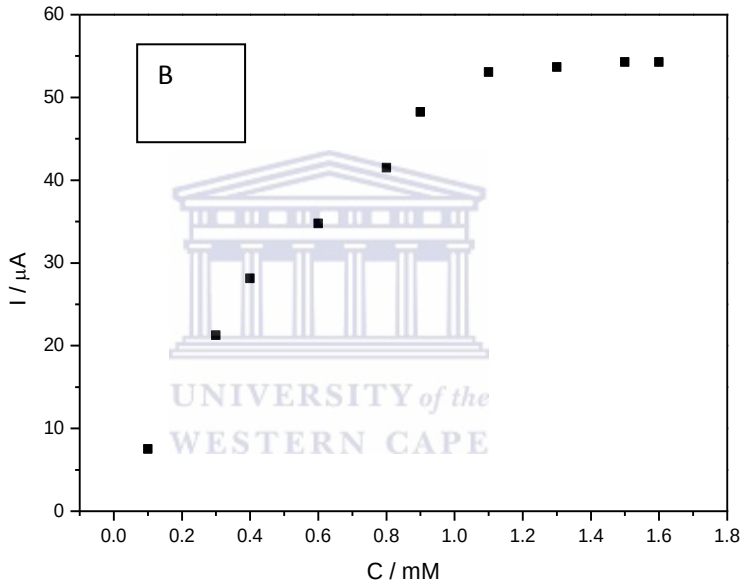

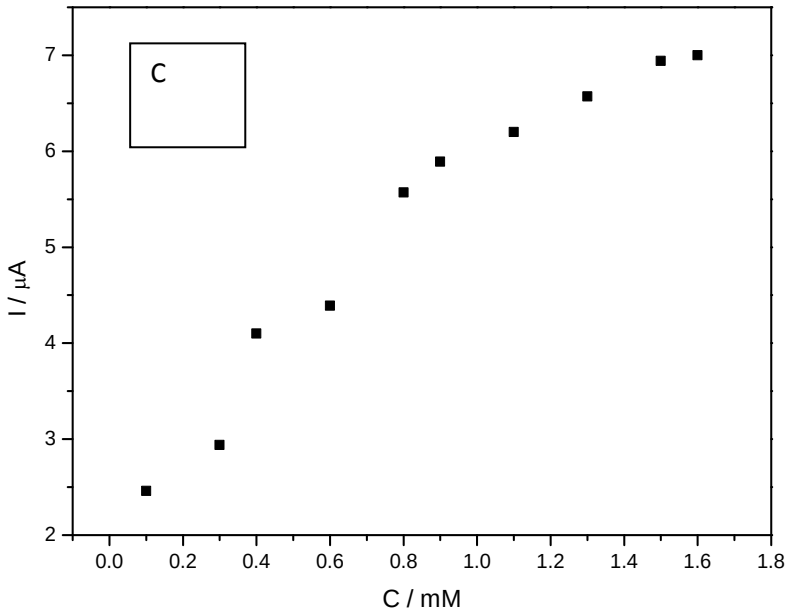

Fig.4.14: Calibration Curves; (a) Pt/PSF/Ag (b) Pt/PSF/Co (c) Pt/PSF/Ni in the presence of alginic acid

The PSF/Ni (0.1mM-1.1 mM) shows the best performance for the quantitative detection than both the PSF/Ag and PSF/Co, followed by the PSF/Ag (0.1mM-0.9mM). PSF/Co showed better sensitivity. The reason for the non-linearity may be due to the fact that the unmodified polysulfone membrane takes the shortest time to foul when compared to the modified polysulfone with metal nanoparticles. The polysulfone modified with Ni nanoparticles showed to have the longest cut-off time suggesting that it takes PSF/Ni longer to foul than other polysulfone composite membranes. The unmodified polysulfone membranes had the least sensitivity for both the alginic acid and tannic acid. The polysulfone modified with Ni nanoparticles showed highest sensitivity in tannic acid and polysulfone modified with Co nanoparticles to have highest sensitivity in alginic acid.

	Tannic Acid (mM)	Alginic Acid (mM)	Sensitivity (µA/ mM)
Pt/PSF	0.6 – 2.6	0.1 – 0.6	T. A= $1.83x10^{-5}$ A. A= $2.41x10^{-6}$
Pt/PSF/Co	0.6 – 3.3	0.1 – 0.8	T.A= $3.06x10^{-5}$ A.A = $4.46x10^{-5}$
Pt/PSF/Ni	0.6 – 4.6	0.1 – 1.1	T. A = $4.01x10^{-6}$ A. A = $3.03x10^{-5}$
PSF/Ag	0.6 – 4.6	0.1 – 0.9	T. A = $1.09x10^{-5}$ A. A = $1.22x10^{-5}$

Table 4.2: *Dynamic linear range of tannic acid and alginic acid at PSF, PSF/Co, PSF/Ag and PSF/Ni*

The PSF/Ni shows the best performance for the quantitative detection of the alginic acid and tannic acid as indicated by their respective dynamic linear range followed by the PSF/Ag. PSF/Co shows better sensitivity as indicated by the higher slope of the calibration curves for PSF/Co with tannic acid $3.06x10^{-5}$ A/mM and alginic acid $4.46x10^{-5}$ A/mM.

The tannic acid showed to be fully catalytic at the prepared thin films in the oxidation SWV, whereas the opposite was observed for the reduction SWV, the oxidation product was observed to adsorb onto the prepared thin film. The alginic acid at the different thin films

behaved the same as that was observed for the tannic acid was also observed for alginic acid, the oxidation SWV was observed to be fully catalytic and its product was observed to adsorb onto the surface of the prepared thin films. The concentration dependant studies the PSF/Co thin film to be the most sensitive thin film when compared with the PSF/Ni and PSF/Ag because of the higher slope of the calibration curve. The PSF/Ni showed better response for quantitative detection of both tannic and alginic acid, followed by the PSF/Ag.

CHAPTER 5

The extent and degree of fouling was investigated by measuring the impedance of each thin film at the presence of alginic acid and tannic acid.

5.1 Electrochemical impedance spectroscopy Results

To evaluate the fouling behaviour of tannic acid and alginic acid, fixed frequency impedance was used to assess the onset fouling, in the absence of redox parameters. Redox processes were minimised by limiting the applied potential for impedance studies to below 50 mV vs Ag/AgCl. Impedance studies were done at a fixed frequency of 10 Hz in the presence of fixed concentration (0.11 M) of tannic acid and alginic acid since they are the model organic acid which causes fouling of the membranes, and HCl was used as the electrolyte. The Pt electrode was modified with 2 µL of the thin film and 3 mL of the HCl was transferred onto the electrochemical cell.

The low frequency range was chosen to represent the area where diffusion behaviour could be best observed and the low potentials were chosen to avoid electrochemical induced analytic behaviour.

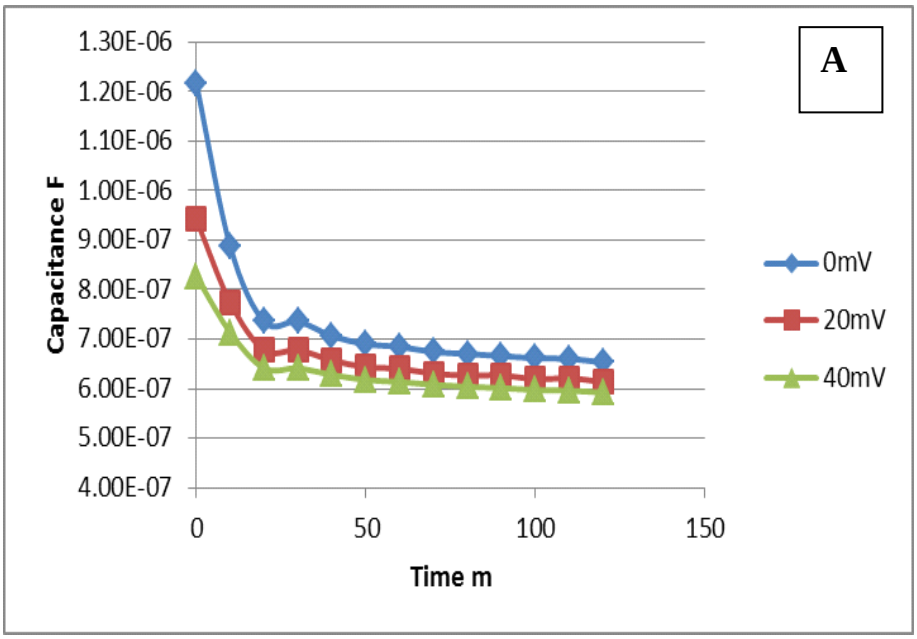

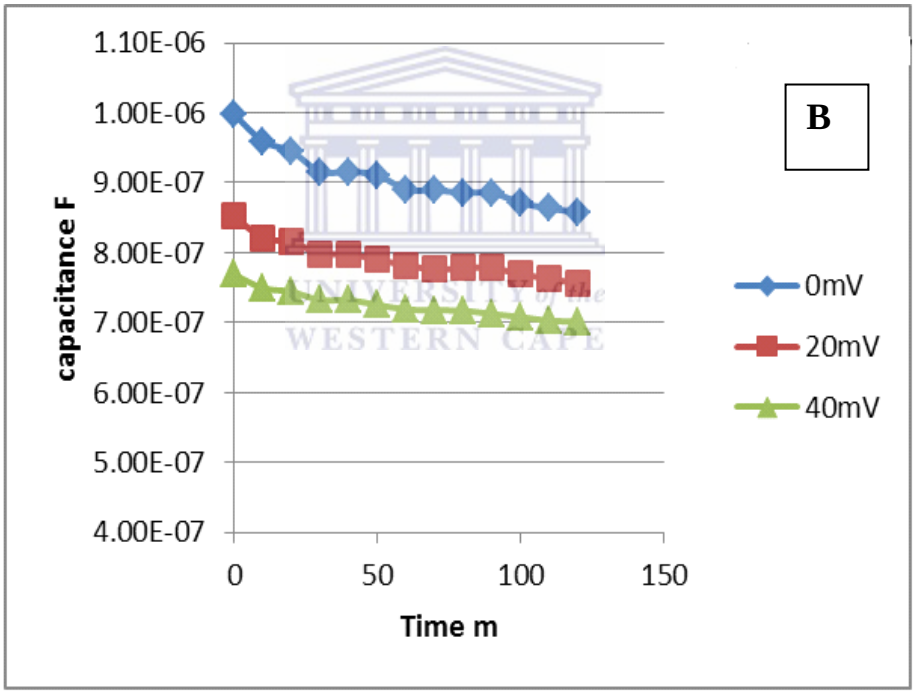

Fig5.1: Fixed frequency EIS studies for Pt/PSF in the presence of 0.11 M alginic acid and 0.11 M tannic acid

The capacitance response range for PSF was measured as 0.7µF to 1,2 µF Farads. An initial fast decrease in capacitance was observed which slowed down at cut off time at 35mins for

tannic acid and for alginic acid the cut off time was 20min. This cut off time was interpreted as the time for the thin film membrane to become saturated (fouled) with analyte molecule under diffusion controlled. The average slope for the alginic acid at PSF was calculated to be 3.25 x10^{-9} F/m and the standard deviation of the 3 slopes was 5.86 x10-^{9} F/m. For the tannic acid the slope was 6.31 x10^{-9} F/m and the STD was 1.80 10^{-9} F/m.

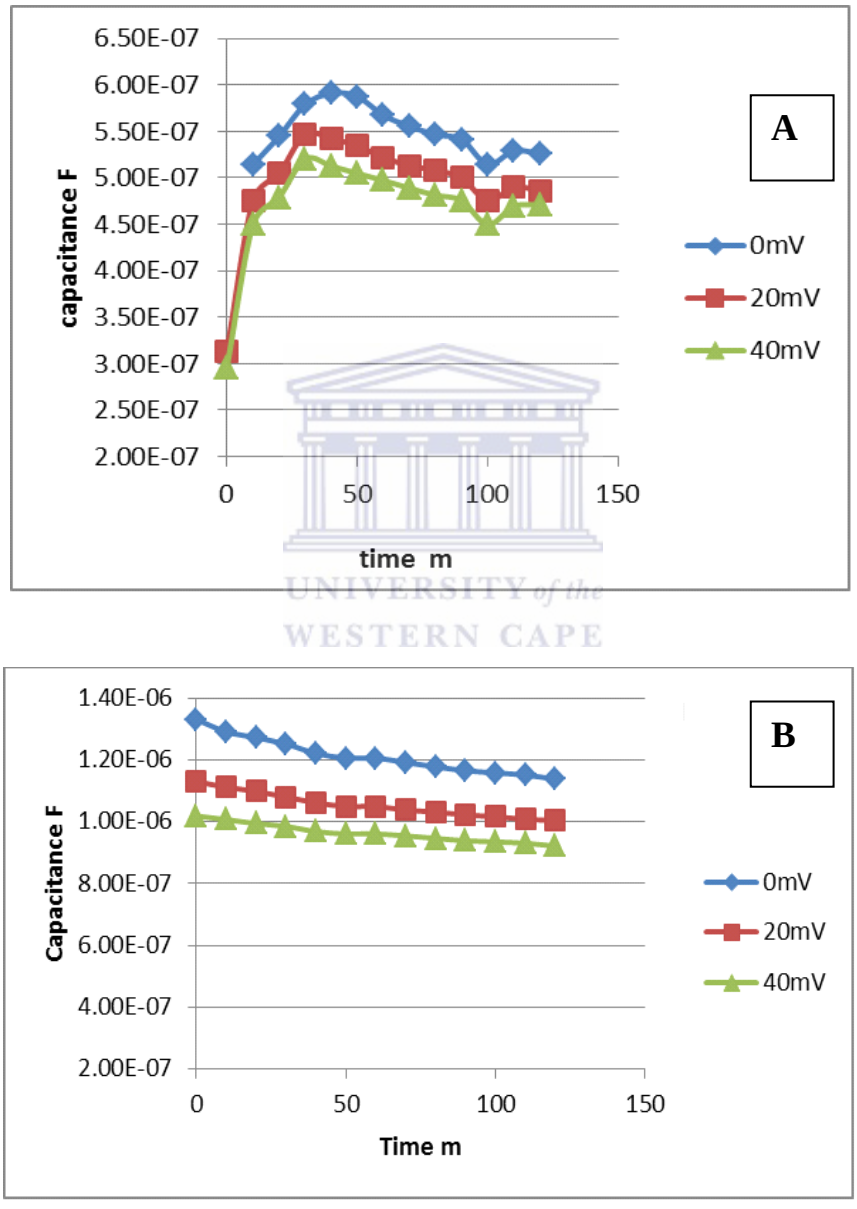

Fig5.2 Fixed frequency EIS studies for PSF/Co in the presence of alginic acid and tannic acid

The capacitance response range for PSF/Co thin film was observed to be in the range of 1 to 4 µ F for tannic acid and 0.3 – 0.6 µF for alginic acid. The initial rate of decrease was slower. The cut off time for Pt/PSF/Co in the presence of alginic acid and tannic acid was 45min for both analytes. The average slope of the alginic acid was 1.80 $x10^{-9}$ F/m and the standard deviation of the three slopes was 4.32 $x10^{-9}$ F/m. The tannic acid slope was 2.07 $x10^{-8}$ F/m and the standard deviation was 1.93 $x10^{-8}$ F/m. The mechanism of interaction between PSF/Co and alginic acid resulted in an initial increase in capacitance which may be attributed to the approach of the alginic acid molecules to the PSF/Co. The higher surface are due to organised pore structures induced by cobalt nanoparticles as indicated by the SEM image, may be the reason behind the change in capacitance behaviour observed like a match between pore size and analyte molecule would allow for penetration of molecule into the PSF/Co porous network and result in a different adsorptic profile. The initial slope showed high sensitivity to alginic acid.

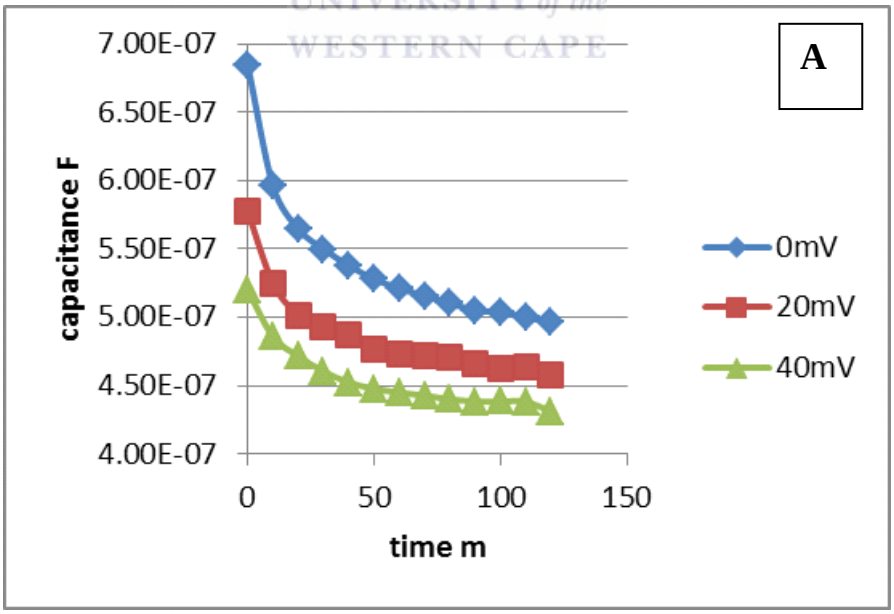

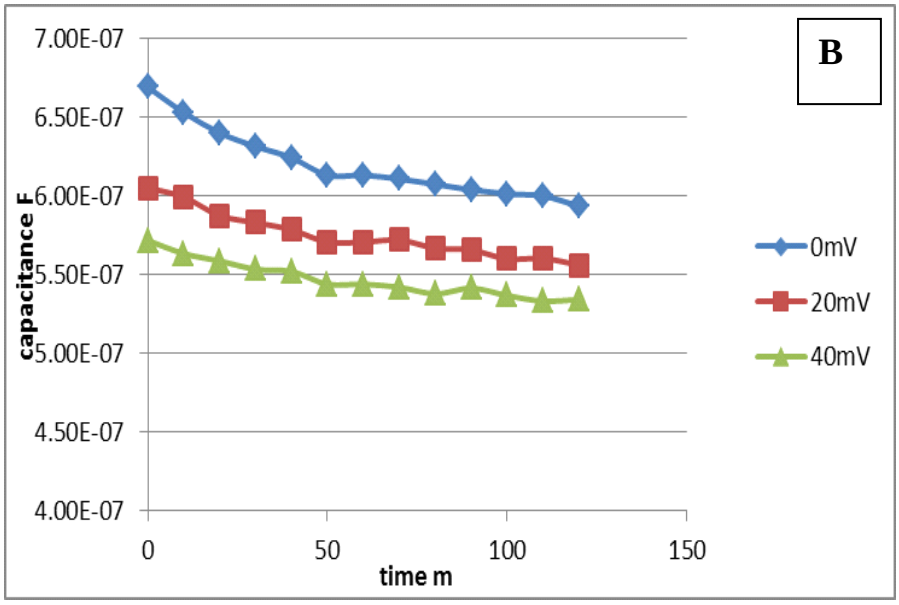

Fig5.3: Fixed frequency EIS studies for PSF/Ni in the presence of (A) alginic acid and (B) tannic acid

The capacitance response was observed in the range from 0.5 to 0.7 F/m for both the tannic acid and alginic acid. The slope of the alginic acid at the thin film was calculated to be 7.53 $x10^{-10}$ F/m and the standard deviation was 2.2 $x10^{-9}$ F/m. For tannic acid the average slope was 3.49 $x10^{-9}$ F/m and the standard deviation was 1.55 $x10^{-8}$ F/m. The decrease in capacitance was observed at cut off time of 50 min for the tannic acid and for alginic acid the cut off time was 45 min.

When comparing the results obtained (fig 5.1 – fig 5.3) and the calibration curves in chapter 4 there is a correlation in results. The unmodified polysulfone membrane showed to be non-linear, lowest sensitivity, lowest limit of detection (LOD) and the shortest cut-off time. For the modified polysulfone with metal nanoparticles showed linearity, improved sensitivity, highest LOD and longer cut-off time than the unmodified polysulfone. Unmodified polysulfone membrane takes the shortest time to fouls which is due to its hydrophobic nature and the contact angle suggested that the unmodified polysulfone is hydrophobic because of the highest contact angle value obtained (87°). The modification of the polysulfone with

metal nanoparticles improved the hydrophilicity of the polysulfone because of the high sensitivity, longer cut-off time and also the low contact angle values obtained.

Material	Slope (F/m)	Standard Deviation (F/m)	Cut-off time (m)
Polysulfone	Alginic acid 3.25×10^{-9}	5.68×10^{-9}	20
	Tannic acid 6.31×10^{-9}	1.80×10^{-9}	35
Polysulfone/Co	Alginic acid 1.80×10^{-9}	4.32×10^{-9}	45
	Tannic acid 2.07×10^{-9}	1.93×10^{-9}	45
Polysulfone/Ni	Alginic acid 7.53×10^{-9}	2.2×10^{-9}	40
	Tannic acid 3.49×10^{-9}	1.55×10^{-8}	50

Table5.1: Table of results of the polysulfone thin films prepared in the presence of tannic acid and alginic

These times indicate that polysulfone ummodified fouls in the shortest time and hence PSF/Co and PSF/Ni shows an improvement in performance because of higher hydrophilicity.

For the dynamic EIS studies the potential was fixed at 0.58V which represents the formal potential for tannic acid oxidation at these thin films. For alginic acid the potential was fixed at 0.37 V which represents the formal potential for alginic acid reduction. The frequency range used was from 100 mHz – 1KHz. The Randles circuit was used to model the data, where Rs represent the solution resistance, Rct represent charge transfer resistance. The CPE was used instead of pure capacitor to model the capacitance.

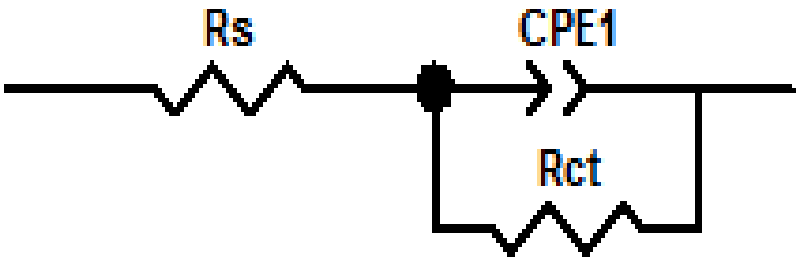

Fig5.4: Randles circuit

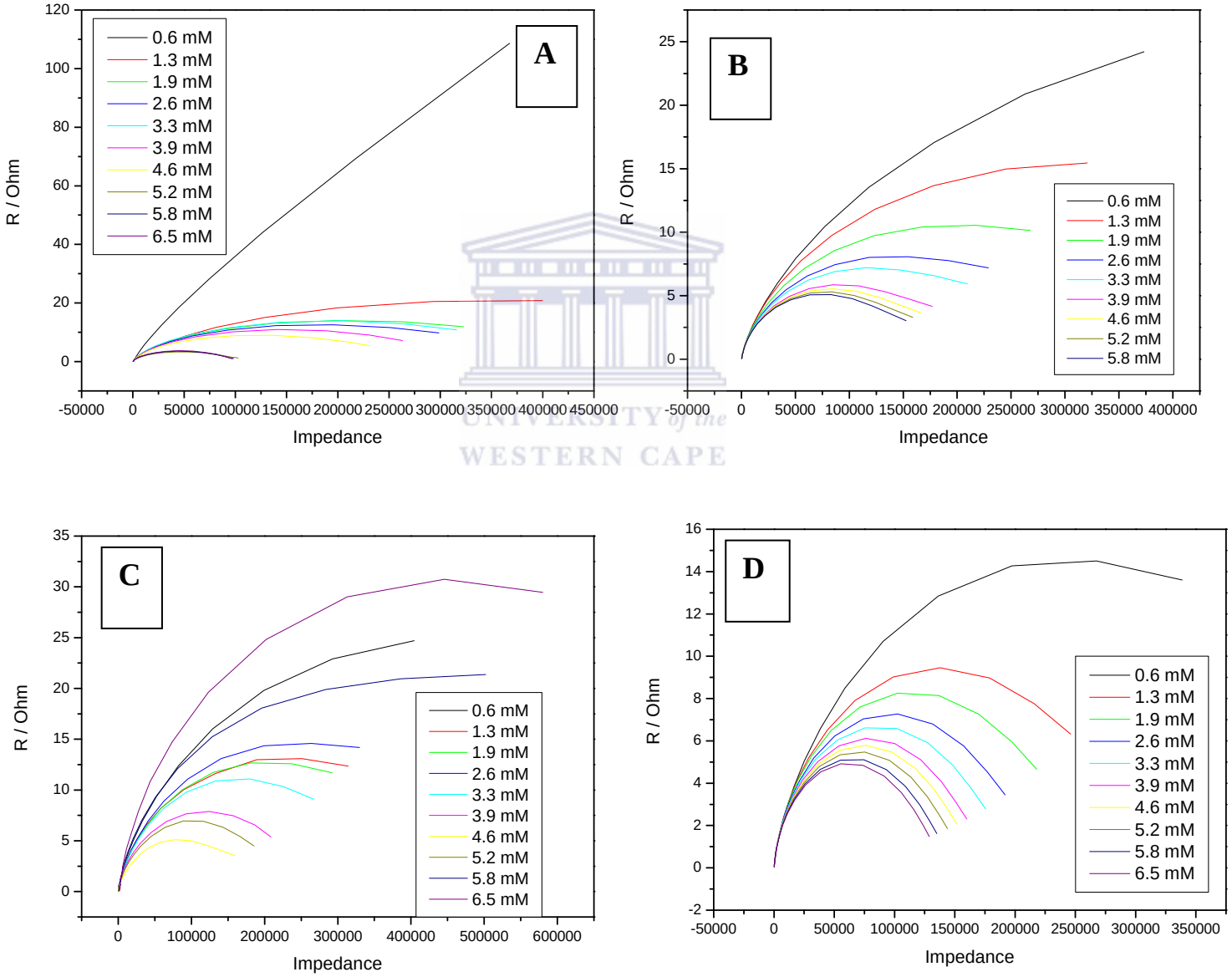

Fig5.5: EIS plot of (A) PSF,(B) PSF/Co,(C) PSF/Ni and (D) PSF/Ag in the presence of tannic acid

Tannic acid at fixed potential of 0.58 V and over a frequency of 100 mHz to 1 KHz was evaluated as concentration dependent response. The electrocatalysis of TA followed typical diffusion control kinetics as evidenced by semi circle at low frequency in the concentration range evaluated and was modelled as Randles circuit using CPE to model non-homogenous adsorptic at the interface.

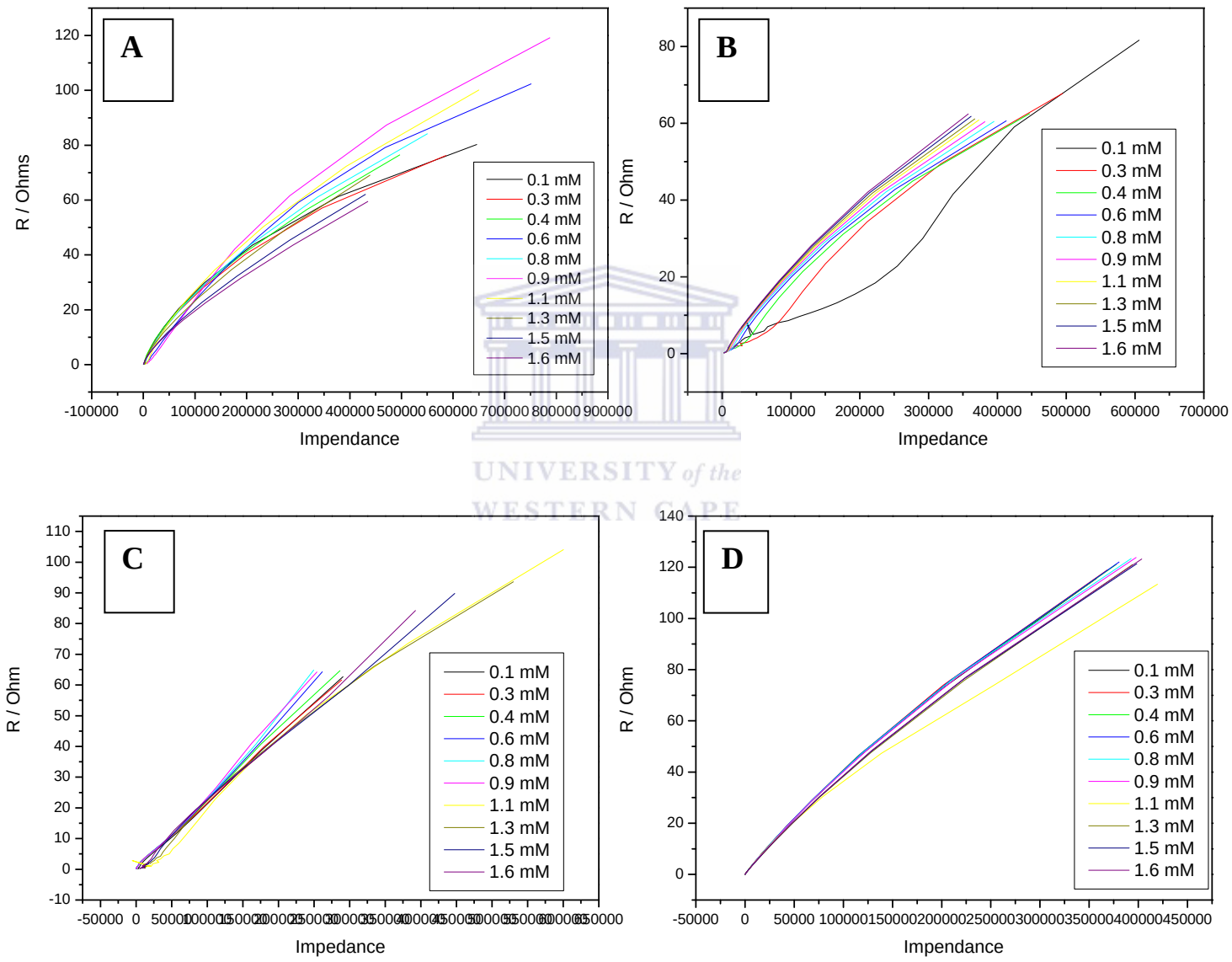

Fig5.6: EIS plot of (A) PSF, (B) PSF/Co, (C) PSF/Ni and (D) PSF/Ag in the presence of alginic acid

Alginic acid electrocatalysis at fixed potential of 0.37 V and over a frequency range of 100 mHz to 1 KHz was evaluated as a concentration dependent response. Alginic acid electrocatalysis appeared to be influenced by passivating infinite diffusive behaviour as evidenced by unresolved low frequency impedance arcs. This type of data should best be modelled as infinite Warburg discussion, but for consistency in data interpretation, the same RCT circuit was used as for tannic acid.

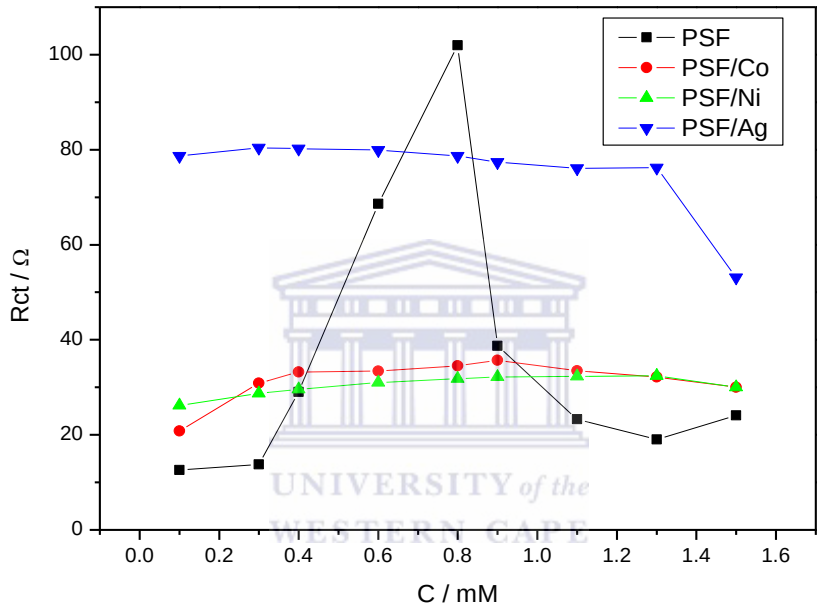

Fig5.7: Rct plot of alginic acid at the polysulfone thin films

The PSF/Ag appeared to be insensitive to alginic acid whereas PSF/Co displayed the highest sensitivity towards alginic acid as evidenced by initial slope. The PSF unmodified was inconsistent in its response to alginic acid and may require further controlled evaluation. However the same inconsistency in concentration response was also observed in voltammetric evaluation (CV, SWV).

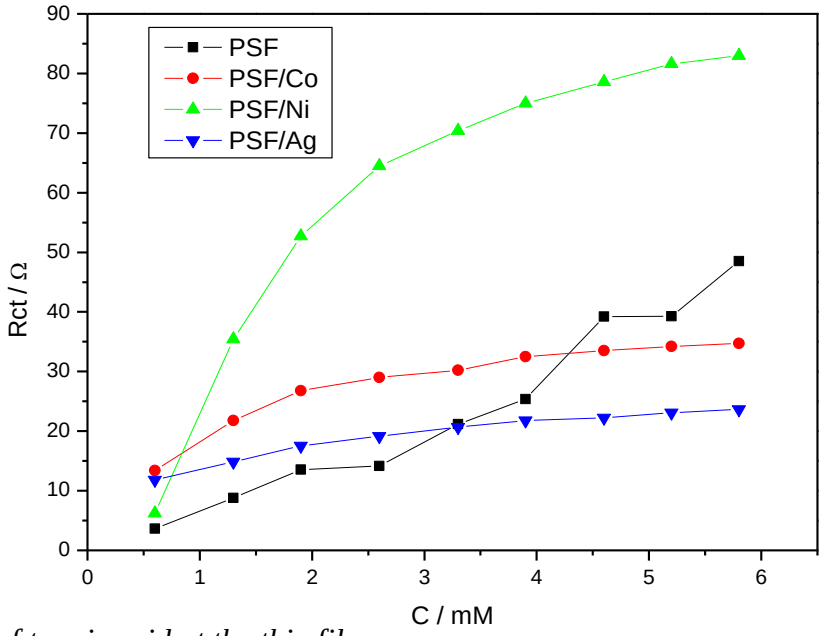

Fig5.8: Rct plot of tannic acid at the thin films

The adsorptive behaviour of tannic acid at the different polysulfone films was evaluated under electrochemical stimulation to induce catalysis. The PSF/Ni films showed the best quantitative response indicated by the limit of detection which was 2.6 mM when compared to PSF/Ag and PSF/Co, and highest sensitivity towards tannic acid indicated by the highest slope which was found to be 2.91 $x10^{-6}$ Ω / mM. However all films showed a tendency towards fouling above 2 mM of tannic acid added.

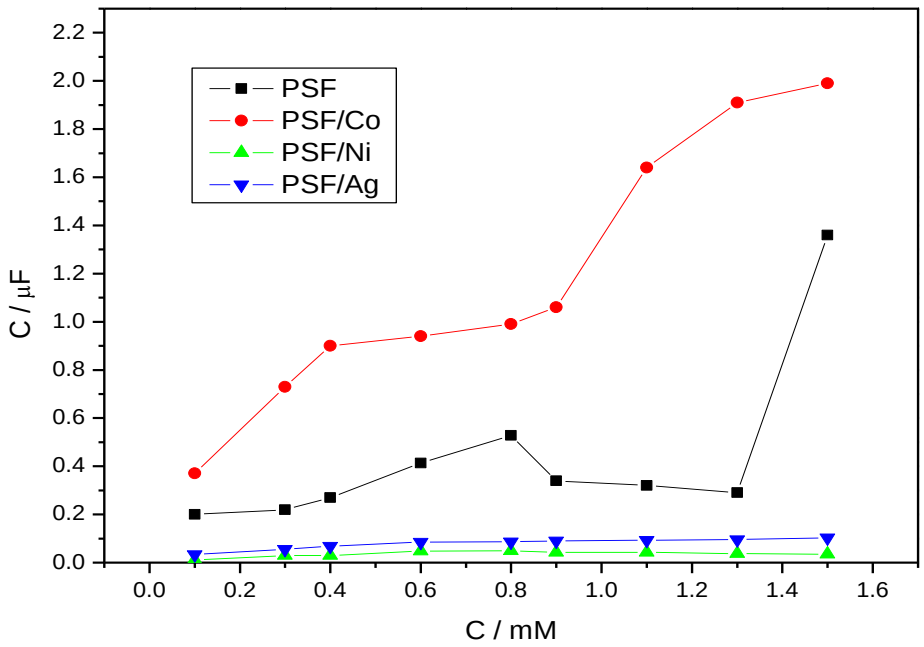

.

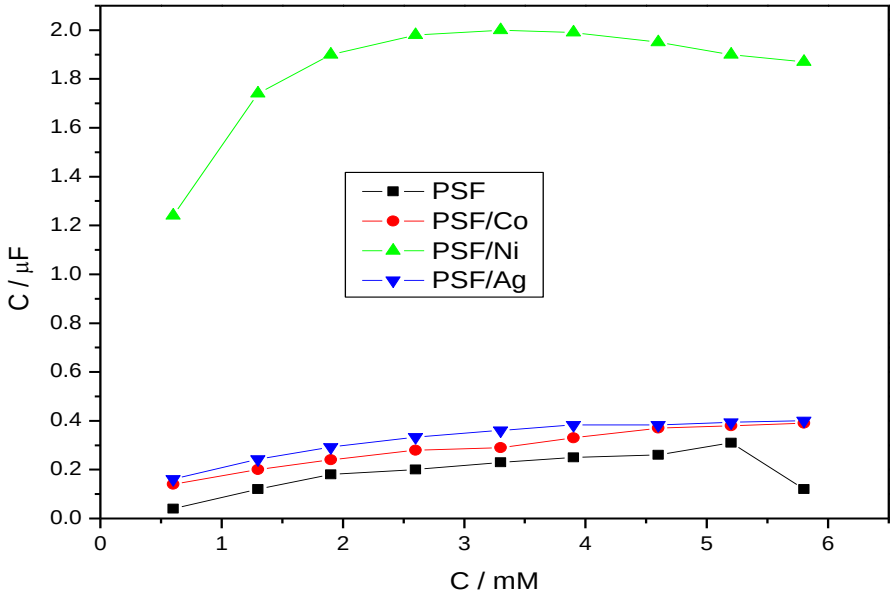

Fig5.9: Caps plot of PSF, PSF/Co, PSF/Ni and PSF/Ag in the presence of (A) alginic acid and (B) tannic acid

The capacitance response range for the PSF and modified thin films were consistently in the range of 1.0µF to 0.1µF as previously detailed by the fixed frequency impedance. However, further analysis of capacitance under electrochemically was not attempted here since this would represent capacitance electrochemically induced catalytic control, which is not relevant to membrane fouling

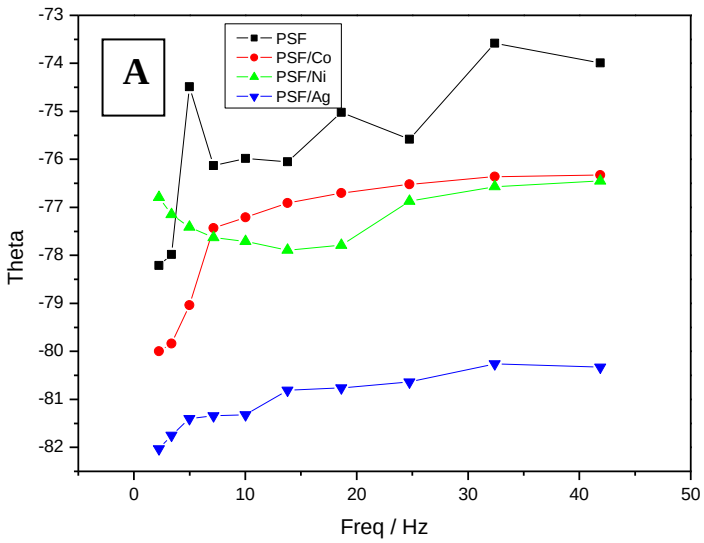

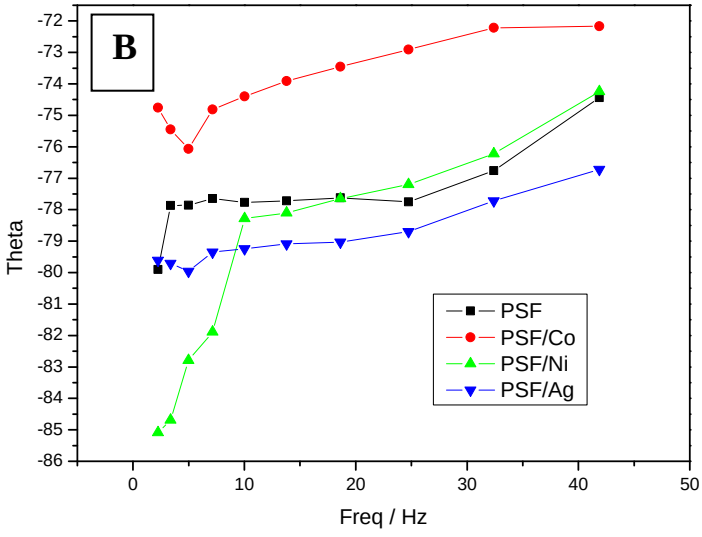

Fig5.10: Phase angle plot of PSF, PSF/Co, PSF/Ni and PSF/Ag in the presence of (A) alginic acid and (B) tannic acid

Evaluating the above plot, phase angle change during the catalysis events confirmed that the PSF and modified PSF thin films retained their semiconducting nature and hence fouling was dominated by interfacial film properties such as surface area and analyte loading.

From the fixed frequency, the PSF/Ni showed to have the longest slope of 7.53 x10-9. The Rct result shows that PSF/Ni films showed the best quantitative response and highest sensitivity towards tannic acid.

Chapter 6

This chapter draws the conclusion of the whole work that was done and also the future work.

6.1 Conclusion

Briefly in this study three metal nanoparticles were successfully synthesized by the chemical reduction method. Three nanocomposites of polysulfone thin films were prepared and characterized by means of cyclic voltammetry, square wave voltammetry, electrochemical impedance spectroscopy, contact angle and scanning electron microscope.

The SEM, TEM and EDS confirmed the synthesis of nanoparticles. The SEM images of both Ni and Co nanoparticles were agglomerated, the agglomeration of the nanoparticles may be to incomplete reaction or the metal salts were not fully reduced by the reducing agent that was used. The TEM image of Ag nanoparticles showed the nanoparticles to be well dispersed and non-agglomerated with the average size of 20 – 50 µm. The nanoparticles showed different shapes like cubic, rods and spherical. In comparing the SEM images of the unmodified polysulfone membrane with the metal modified polysulfone, the PSF/Ag nanocomposite showed have larger pores than the PSF/Co and PSF/Ni, followed by the PSF/Co and the PSF/Ni showed small pores. The unmodified polysulfone membrane didn't show pores. The EDS of the modified polysulfone membrane confirmed the incorporation of the metal nanoparticles into the polysulfone.

The contact angle measurements were done to study the hydrophilicity of the modified and unmodified polysulfone membrane. From the results obtained in contact angle confirmed that when the polysulfone is modified with metal nanoparticles the hydrophilicity of the unmodified polysulfone was improved. The contact angle of the unmodified polysulfone

membrane was 87.5° and when the PSF was modified with metal nanoparticles the conctact decreased, the PSF/Co showed to be the most hydrophilic (31.7°) when compared with PSF/Ni and PSF/Ag. The PSF/Ni showed to be the second most hydrophilic PSF nanocomposite with the PSF/Ag being the least hydrophilic PSF membrane.

The electrochemical characterisation of the PSF unmodified and PSF modified was done in the presence of an analyte (alginic acid and tannic acid), to study the fouling behaviour of the prepared polysulfone thin films. Cyclic voltammetry studies of the different thin films that were prepared were done at the presence of the electrolyte which was the HCl. The polysulfone unmodified thin film showed to have the highest diffusion coefficient followed by the polysulfone modified with Ni nanoparticles. From the cyclic voltammetry showed that both analytes behaves differently at the membrane thin films prepared, the tannic acid showed an oxidation peak at 0.58 V where as the alginic acid had a reduction peak at 0.37 V.

Calibration curves were constructed using the peak measurements for the analytes from the square wave voltammetry results. The PSF/Co showed to be the most sensitive polysulfone nanocomposite in the presence of both the alginic acid and tannic acid because of the highest slope when compared with the PSF/Ni and PSF/Ag. The PSF/Ni showed better performance for quantitative detection studies in the presence of both analytes.

From the fixed frequency, unmodified polysulfone thin films had the longest cut off time when compared to the PSF/Co and PSF/Ni, indicating that modification with metal nanoparticles into the polysulfone improved the cut off time because of the hydrophilic membranes. The Rct result shows that PSF/Ni films showed the best quantitative response and highest sensitivity towards tannic acid. The phase angle of the prepared polysulfone thin films was observed to be 75° - 86°, indicating that the thin films retained their

semiconducting nature and hence the fouling was dominated by the interfacial film properties such as surface area and analyte loaching.

6.2 Future Work

For future work:

- For this research the EIS was used to evaluate the fouling mechanisms of the prepared thin films of polysulfone, the other method that can be used to study the fouling mechanism of the thin films is the rotating disk electrode. The results obtained for EIS can be compared with the RDE results.

- Two model organic acids were chosen to study the fouling caused by them in ultrafiltration membranes. The other model organic acid to be used is the humic acid to study the fouling it causes to membranes of water treatment. A solution of humic acid will be prepared and the fouling behaviour will be tested using impedance spectroscopy.

- The fixed frequency EIS of PSF/Ag in the presence of both tannic acid and alginic acid will be done for full comparison of the unmodified polysulfone and the modified polysulfone membrane. The experiment will be done by drop-coating the PSF/Ag onto a Pt electrode, fixing the frequency at 10 mHz – 1 KHz and using the both tannic acid and alginic acid as analytes.

References

Absar Ahmada, Priyabrata Mukherjee, Satyajyoti Senapati, Deendayal Mandal, M. Islam Khanb, Rajiv Kumar, Murali Sastry , 2003, Colloids and Surfaces B: Biointerfaces 28, 313–318

Adou, A.F.Y., Muhandiki, V.S., Shimizu, Y., Matsui, S., 2001, Water Science and Technology 43, 1–7.

Alam J, Dass L.A, Alhoshan M.S, Ghasemi M, Mohammad A.W, (2012), Applied Water Science 2, 37-46

Allen J. Bard, Larry R. Faulkner, 2002, Electrochemical Methods: Fundamentals and Applications, 2nd edition, John Wiley & Sons, New York, USA

Aryanti P.T.P, Wenten G.I, Khoiruddin, 2013, Journal of Water Sustainability 3, 85-96

Ayse Asatekin a, Seoktae Kangb, Menachem Elimelech b, Anne M. Mayesc, 2007, Journal of Membrane Science 298, 136–146

Baker R.W, Membrane Technology and Applications, JohnWiley, Chichester, 2004.

Boksoon Kwon, H.K. Shon, Jaeweon Cho, 2009, Desalination and Water Treatment 8, 177–187

Byoung-Yong Chang and Su-Moon Park, 2010, Anal. Chem. 3, 207–29

Castro E.F Vidaurre, C.A. Acheteb, F. Gallob, D. Garciac, R. Simãob A.C. Habertc, 2002, Materials Research 5, 37-41

Choong Jeon , Young Je Yoo , Wolfgang H. Hoell, 2005, Bioresource Technology 96, 15–19.

Choong Jeon, Jae Yeon Park, Young Je Yoo, 2002, Biochemical Engineering Journal 11, 159–166

Chowdhury S.R., 2001, Separation/ Purification Technology 24271-282

Combe C., E. Molisa, P. Lucasa, R. Riley, M.M., Clark, 1999, Journal of Membrane Science 154, 73-87

D.A. Skoog, F.J. Holler, T.A. Nieman, *Principles of Instrumental Analysis*, Brooks/Cole Publishing Co., 5th edition, 1997,chapter 25.

Derek A. Long. *The Raman Effect*. John Wiley & Sons, New York, 2002.

Ehsan Saljoughi, Toraj Mohammadi, 2009, Desalination 249, 850–854

Geisse, Nicholas A. (July-August 2009). *Materials Today* 12, 40–45

Giessibl, Franz J., 2003, *Reviews of Modern Physics* 75: 949

Goosen M.F.A, S.S. Sablani, H. Ai-Hinai, S. Ai-Obeidani, R. Al-Belushi, D. Jackson, 2004 Sci. Technol. 39, 2261–2297.

Gordeyev S. A., G. Yu. Nikolaeva, K. A. Prokhorov, R. Withnall, I. R. Dunkin, S. J. Shilton, and P. P. Pashinin, 2001 , Laser Physics 11, 82–85.

Guezguez, I., Mrabet, B. Ferjani, E., 2013, Desalination 313, 208-211

Hamid N.A.A, A.F. Ismail , T. Matsuura , A.W. Zularisam , W.J. Lau, E. Yuliwati , M.S. AbdullahN.A.A. Hamid, 2011, Desalination 273, 85–92

http://www.jtbaker.com/msds/englishhtml/t0065.htm (12/04/2012)

Jae Weon Cho, Gary Amy, John Pellegrino, Yeomin Yoon, 1998, Desalination 118, 101-108

Jeon, C., Park, J, Y. and Yoo Y.J., *Immobilization of Alginic Acid Using PVA for Lead Adsorption*, 216th ACS National Meeting, Boston, August 21-28 (1998).

Kabsch-Korbutowicz M., 1994, Sep. Sci. Technol 29, 2345.

Kim J and Van der Bruggen B., 2010, Environmental Pollution 158, 2335-2349.

Kim K.S., 2002, Journal of Membrane Science 199, 135–145

Kim, James H. Herman J. Gibb, Paul D, Concise international chemical assessment document; 69

Lang, K.M.; D. A. Hite, R. W. Simmonds, R. McDermott, D. P. Pappas, and John M. Martinis, (2004), Review of Scientific Instruments 75, 2726–2731

Lee J, Ahn W and Lee C. (2001), Water Research 35, 2435-2445.

Lowe J., Hossain Md.M, (2008), Desalination (218), 343–354

Lucian Baia and Simion Simon, (2007), *UV-VIS and TEM assessment of morphological features of silver nanoparticles from phosphate glass matrices*, Modern Research and Educational Topics in Microscopy.

Macdonald J. Ross, 1992, Annals of Biomedical Engineering 20, 289-305

Madaeni S.S. & Akbarzadeh Arbatan T., 2010, Iran. J. Chem. Chem. Eng 29, 105-111

Matveev V.V. et al., (2006) , Chemical Physics Letters 422, 402–405

Maximous N, Nakhla G, Wan W and Wong K, 2010, Journal of Membrane Science 352, 222-230.

Mulder J, "*Basic Principles of Membrane Technology*," 2nd Edition, Kluwer Academic Publishers, Dordrecht, 1996, p. 584.

N.B. Colthup, L.H. Daly, S.E. Wiberley. *Introduction to Infrared and Raman Spectroscopy*.(Third Edition) Academic Press, 1990.

Odegaard, H., Eikebrokk, B., Storhaug, R., 1999, Water Science and Technology 40, 37–46.

Perron R.N, Brumaghim J.L, 2009, Cell Biochem Biophys 53, 75-100

Puntesa Victor F., Kannan Krishnanb and A. Paul Alivisatosa, *2002,Topics in Catalysis 19,*

Rahimpour A., Madaeni S.S. (2007), Journal of Membrane Science 305, 299–312

Rama Chemnnamsetty, Isabel Escobar, Xinglong Xu, (2006), Desalinisation 188, 203-212

Reckhow, D.A., Singer, P.C., Malcolm, R.L., (1990), Environmental Science and Technology 24,1655–1664.

Rong Guan, Hua Zou , Deping Lu, Chunli Gong, Yanfang Liu, 2005, European Polymer Journal 41, 1554–1560

Sabine Vico, Barbara Palys, and Claudine Buess-Herman, 2003, Langmuir 19, 3282-3287

Salazar-AlVarez, 2007 , Chem. Mater 19, 4957-4963

Sangyoup Lee and Menachem Elimelech, 2006, Environ. Sci. Technol 40, 980-987

Schafer, A.I., Fane, A.G., Waite, T.D., 2005. Nanofiltration: Principle and Application. Ed, Elsevier Ltd, Oxford.

Selby Maphutha, Kapil Moothi1, M. Meyyappan, & Sunny E. Iyuke, (2013) *A carbon nanotube-infused polysulfone membrane with polyvinyl alcohol layer for treating oil-containing waste water,*

Sheppard Patrick, *Preparation and Characterization of composite PES/Nanoparticle Membrane,*

Srisudha M, K. Karthik and S. Ponnuswamy, 2013, Nano Vision, Vol.3 (1), 37-43

Stevenson, F.J., 1994. Humus Chemistry: Genesis, Composition, Reactions, second ed. John Wiley & Sons, New York.

Summers G.J., M.P. Ndawuni, C.A. Summers, 2001, Polymer 42, 397–402

Sutton, A., Harrison, B. E., Carr, T. E., and Barltrop, D.*(* 1971) Int.J.Radiat.Biol.Relat Stud.Phys.Chem.Med. 19, 79-85.

Suzuki, E. (2002), *Journal of Microscopy* 208 (3): 153–157.

Weber A (Editor). *Raman Spectroscopy of Gases and Liquids*. Topics in Current Physics. John Springer-Verlag, Berlin, 1979.

Weber, J.H., 1988. *Binding and transport of metals by humic materials. In Humic Substances and Their Role in the Environment*: Frimmel, F.H., Christman, R.F. (Eds.*)*, John Wiley & Sons, Chichester.

Yamaguchi, H., Higasida, R., Higuchi, M., Sakata, I., 1992, J. Appl. Polym. Sci. 45, 1463–1472.

Yoshichiko Bandu and Takahito Terashima, 1986 , Bull. Chem. Soc, Japan 59, 607-612,

Yoshichiko Bandu and Takahito Terashima, Preparation and Coercivity of Cobalt ultrafine particles by reduction of multilayered CoO-SiO films, Bull. Chem. Soc, Japan, 59, 607-612, 1986

Yuehua Deng, Lin Wang, Xiaobin Hu, Benzhi Liu, Zhongbo Wei, Shaogui Yang, Cheng Sun, 2012, Chemical Engineering Journal 181– 182, 300– 30

Yunan Zhou , Xin-Hui Xing, Zehua Liu , Liwen Cui b, Anfeng Yu , Quan Feng a, Haijun Yang, 2008, Chemosphere 72, 290–298

Zhao C. et al. 2004, Desalination 170, 263-270

Zhao Lijun, Liang Xiaoming, *Room-temperature synthesis of air-stable cobalt nanoparticles and their high-efficient adsorption ability for Congo red*, Electronic Supplementary Material (ESI) for RSC Advances, 2012